# NEW METHODS TO STUDY COMPOSITION AND PROCESSES OF ATMOSPHERIC ORGANICS IN THE GAS AND THE CONDENSED PHASE

**Joseph Timkovsky**

Joseph Timkovsky
Institute of Marine and Atmospheric Research Utrecht (IMAU)
Atmospheric Chemistry and Physics Group
Utrecht University

Address:
Princetonplein 5, 3584 CC, Utrecht, the Netherlands
timkovsky@yahoo.com

ISBN: 978-90-5335-986-0
Printing: RidderPrint BV

# NEW METHODS TO STUDY COMPOSITION AND PROCESSES OF ATMOSPHERIC ORGANICS IN THE GAS AND THE CONDENSED PHASE

**Nieuwe methoden om de samenstelling en de processen van atmosferische organische stoffen in de gas fase en in fijnstof te onderzoeken**

(met een samenvatting in het Nederlands)

Proefschrift

ter verkrijging van de graad van doctor aan de Universiteit Utrecht op gezag van de rector magnificus, prof.dr. G.J. van der Zwaan, ingevolge het besluit van het college voor promoties in het openbaar te verdedigen op maandag 12 januari 2015 des ochtends te 10.30 uur

door

IOSIF TSIMKOUSKI

geboren op 5 juli 1987

te Minsk, Wit-Rusland

Promotor: Prof.dr. T.Röckmann

Copromotor: Dr. R.Holzinger

‘Plans are useless but planning is indispensable.’

(Dwight David Eisenhower)

Моим родителям посвящается

# Table of Contents

# Summary

Volatile organic compounds (VOCs) and organic aerosols (OA) play an important role in the Earth's atmosphere due to their influence on human health and climate. To be able to control amounts of VOCs and OA in the atmosphere, one has to understand the main sources of them and the effect of external factors on these sources. While many studies on the main VOC source (i.e. emission from plants) have been performed, there has been only a limited number of studies on how external factors such as environmental pollution effect plant emissions. Historically, OA is measured as bulk organic carbon. Measuring the chemical composition of OA is more challenging but nevertheless essential to fully understand secondary sources and climate effects of aerosols. The first part of this work (Chapter 2) describes the development of a setup that is capable of characterizing how plant VOC emissions change under influence of various pollutants. The second part (Chapter 3) describes the development an offline tool of measuring OA composition, and the third part (Chapter 4) further characterize the OA composition measurements by an existing in situ tool.

The presence of VOCs and nitrogen oxides ($NO_x$) in the atmosphere leads to ozone formation. Ozone is a poisonous gas harmful to human beings and plants. Ozone is also a greenhouse gas contributing to the increase of the Earth's surface temperature and climate change. The oxidation of VOCs in the atmosphere leads to the formation of secondary organic aerosol (SOA) to which important climate feedbacks have been linked. Plant emissions comprise 90% of the annual VOC emissions in the atmosphere (Guenther et al., 1995). Possible mechanisms on how pollution may influence this huge natural source of VOCs are poorly studied. In Chapter 2, I describe the setup we built in our laboratory in order to study the effect of pollution on VOCs emitted by plants. Various pollutants such as ozone, complex mixture produced by oxidation of plant emissions and representing the real atmosphere conditions, and nitrogen dioxide can be applied in the setup. The system consists of two plant chambers, one reaction chamber and proton-transfer-reaction time-of-flight mass spectrometer (PTR-TOF-MS) as a detection unit coupled to a gas chromatograph aided by cryogenic trapping. The setup allows for in situ detailed measurements of changes in plant emissions and allows distinguishing isomeric compounds (e.g., monoterpenes) emitted by plants in normal conditions as well as under stress. The ability to distinguish isomeric compounds is a substantial advantage of the system, since different monoterpenes have a different potential to form SOA, they may play different roles in

plant-to-plant communication patterns. The setup has been tested based on experiments with birch seedlings: their emissions were measured, oxidized and the oxidation products were measured as well in the reaction chamber. A reasonable agreement with literature data was observed. Additionally, an ozonolysis experiment with β-pinene was performed (by applying ozone to the reaction chamber containing β-pinene) and the main oxidation products reported in the literature were observed at comparable levels.

An additional feature of the setup is its flexibility: e.g., plant chambers can be easily exchanged. This gave us a possibility to perform measurements with plant chambers of smaller size and with a quartz lid, so that in situ changes in plant emissions under the UV light irradiation could be observed. As a result, substantially increased emissions of acetic acid were observed from 4-hour UV-treated Arabidopsis plants.

The oxidation of VOCs leads to the formation of poisonous greenhouse gas ozone and SOA. When inhaled aerosols penetrate into human lungs, which is the cause of significant health risks. Aerosol exposure is estimated to be responsible for more than 500,000 deaths every year (Nel, 2005). Recent studies indicated that high concentrations of aerosols in air might even lead to an increased occurrence of autism amongst population (Volk et al., 2013). From the climate change point of view, aerosol particles adsorb and scatter incoming solar radiation and increase clouds lifetime. The overall effect of this is that less solar radiation reaches the ground. Thus, aerosol particles offset global warming caused by the presence of greenhouse gases in the atmosphere. OA typically comprises a substantial part of the total aerosol mass (20 to 90%) (Kanakidou et al., 2005). Thus, the importance of OA in the atmosphere creates a need to understand their sources and production pathways to be able ultimately to control their amounts in the atmosphere. In order to understand sources and production pathways, the detailed chemical composition of OA has to be known, and multiple techniques have been applied so far to study it. However, many of them do not provide very detailed information on the chemical composition and characterize it in bulk terms. Other techniques, such as thermal-desorption proton-transfer-reaction mass-spectrometry (TD-PTR-MS), are capable of providing detailed chemical composition, but they are too expensive to allow for widespread deployment. I developed a laboratory based setup called offline TD-PTR-MS, which allows for detailed and relatively cheap measurements of OA composition based on filter samples which can be collected in a broad range of locations. The setup has been tested based on the inter-comparison with the in situ proven technique (in situ TD-PTR-MS) (e.g., Holzinger et al., 2010) and in

general a good agreement between the two techniques was confirmed. However, it was found that for the filters sampled for one day, positive sampling artifacts caused by the adsorption of semivolatile organic species on the filters were high, which is in accordance with previous findings described in the literature. For the filters sampled for two and three days slight negative artifacts were observed likely caused by not complete desorption of aerosols off the filters at temperatures up to 350 ˚C and potential chemical degradation of aerosols on the filters. In short, the developed setup creates a possibility to study chemical composition of aerosol in detail from a wide range of locations with suggested filter sampling times longer than one day.

Whereas detailed offline measurements of OA composition are very useful, the corresponding in situ measurements are capable of observing changes in OA concentrations and composition on a smaller timescale. Thus, with the in situ data one can separate potential different sources of OA more precisely. In Chapter 4 I briefly describe the in situ TD-PTR-MS technique and show the ability of the technique to reasonably measure total OA mass concentrations as well as speciated organics with a time resolution of 0.5 hour. The former is shown based on the comparison with aerosol mass spectrometer (AMS) measurements. The latter is done based on the inter-comparison with two-dimensional gas chromatography with a time-of-flight mass spectrometer (GC×GC/TOF-MS) technique. We found that species with mass concentrations above 2 ng $m^{-3}$, as measured by GC×GC/TOF-MS, were reasonably detected with the in situ TD-PTR-MS technique. All three measurements were performed during the CalNex 2010 field campaign in Pasadena, California during which more than 40 research groups participated aiming to characterize VOCs, aerosols and other constituents of the atmosphere.

# Samenvatting

Vluchtige organische stoffen (VOS) en organisch fijnstof (OF) spelen een belangrijke rol in de atmosfeer van de aarde vanwege hun invloed op de gezondheid van de mens, en het klimaat. Om de hoeveelheden VOS en OF in de atmosfeer te controleren, is het essentieel om hun belangrijkste bronnen en het effect van externe factoren op die bronnen te begrijpen. Terwijl veel onderzoek naar de belangrijkste VOS bron (plantenemissies) is verricht, is slechts een beperkt aantal studies naar het effect van externe factoren zoals milieuvervuiling op plantenemissies gedaan. Historisch wordt OF gemeten als hoeveelheid organisch koolstof. Metingen van chemische samenstelling van OF is meer uitdagend, maar dit is essentieel om de secundaire bronnen en klimaateffecten van fijnstof te begrijpen. Het eerste deel van deze thesis (hoofdstuk 2) beschrijft de ontwikkeling van het meetsysteem dat de verandering in plant VOF emissies onder de invloed van verschillende vervuilers kan karakteriseren. In hoofdstuk 3 wordt de ontwikkeling van een offline meetinstrument voor de OF samenstelling beschreven, en in het derde deel (hoofdstuk 4) wordt de OF-samenstelling gekarakteriseerd door middel van metingen met een bestaand in-situ instrument.

De aanwezigheid van VOS en stikstofoxides ($NO_x$) in de atmosfeer leidt tot ozonvorming. Ozon is een giftig gas schadelijk voor de mens en voor planten. Ozon is ook een broeikasgas dat bijdraagt aan de opwarming van de aarde en de klimaatverandering. Oxidatie van VOS in de atmosfeer leidt tot vorming van secundair organisch fijnstof (SOF), wat een belangrijke rol heeft in essentiële klimaatterugkoppelingen.

90% van de VOS-emissies in de atmosfeer bestaan uit plantenemissies (Guenther et al., 1995). Mogelijke mechanismes achter de rol van vervuilende stoffen op deze kolossale natuurlijke bron van VOS zijn echter nog niet goed begrepen. In hoofdstuk 2 beschrijf ik de ontwikkeling van het meetsysteem in ons laboratorium waarmee het effect van vervuiling op de VOS plantenemissies bestudeerd wordt. Diverse vervuilende stoffen zoals ozon; complexe mengsels, geproduceerd door oxidatie van plantenemissies voorstelde echte atmosferische condities; en stikstofdioxide kunnen worden gebruikt in het meetsysteem. Het system bestaat uit twee plantenkamers, een reactiekamer en een zogenaamde ‘proton-transfer-reaction time-of-flight mass spectrometer’ (PTR-TOF-MS) als detectie-eenheid gekoppeld aan een gaschromatograaf met cryogene trapping. Het meetsysteem kan gedetailleerde in situ metingen doen van de veranderingen in de

plantenemissies en kan isomeren (zoals monoterpenen, die uitgestoten door planten in normale condities en onder stress) onderscheiden. Het vermogen om isomeren te onderscheiden is het wezenlijke voordeel van het systeem: verschillende monoterpenen hebben verschillend potentieel om SOF te vormen, en ze spelen mogelijk een rol in plant-tot-plant communicatie. Het meetsysteem is getest met behulp van experimenten met berkzaailingen: de emissies zijn gemeten, daarna geoxideerd en de oxidatieproducten in de reactiekamer zijn ook gemeten. De meetresultaten kwamen redelijk overeen met in de literatuur vermelde waarden. We hebben ook ozonolyse experimenten met β–pineen uitgevoerd (ozon werd toegevoegd aan de reactiekamer met β–pineen) en de belangrijkste oxydatieproducten zoals vermeld in de literatuur zijn gemeten op vergelijkbare niveaus.

Een extra functie van het meetsysteem is de flexibiliteit: plantenkamers kunnen bijvoorbeeld makkelijk worden vervangen. Dit gaf ons de mogelijkheid om metingen met kleinere plantenkamers en met een deksel van kwarts uit te voeren, zodat in situ veranderingen in plantenkamers onder UV-lichtradiatie kunnen worden gemeten. Zo konden aanzienlijk toegenomen emissies van azijnzuur worden gemeten van Arabidopsis planten, die 4 uur met UV belicht werden.

Oxidatie van VOS leidt tot de formatie van het giftige broeikasgas ozon en SOF. Fijnstof dringt diep door in de menselijke longen als het wordt geïnhaleerd, en dat vormt een significant gezondheidrisico. Fijnstof-blootstelling is mogelijk verantwoordelijk voor meer dan 500,000 doden per jaar in de wereld (Nel, 2005). Recente studies geven aan dat hoge concentraties van fijnstof in de lucht kunnen leiden tot verhoogde frequentie van autisme onder de bevolking (Volk et al., 2013). Vanuit klimaatverandering oogpunt absorberen en verstrooien fijnstofdeeltjes de zonnestraling en bovendien laten ze de wolkslevensduur toenemen. Het totale effect daarvan is dat minder zonnestraling het oppervlak van de aarde bereikt. Fijnstofdeeltjes compenseren dus deels de mondiale opwarming, die veroorzaakt wordt door de toename van broeikasgassen in de atmosfeer. Organisch fijnstof is een wezenlijk deel van totale fijnstof massa (20 to 90%) (Kanakidou et al., 2005). Het belang van OF in de atmosfeer creëert een noodzaak om de bronnen en productiewegen te begrijpen om uiteindelijk de hoeveelheden in de atmosfeer te controleren. Om bronnen en productiewegen te begrijpen moet de chemische samenstelling van OF tot in detail bekend zijn, en meervoudige technieken zijn gebruikt om het te bestuderen. Echter, veel daarvan geven geen gedetailleerde informatie over de chemische samenstelling, maar karakteriseren het in grote lijnen. Andere technieken, zoals ‘thermal-desorption

proton-transfer-reaction mass-spectrometry' (TD-PTR-MS) kunnen gedetailleerde informatie over de chemische samenstelling geven, maar die zijn te duur om wijdverspreide toepassing te kunnen krijgen. Ik heb het offline TD-PTR-MS-meetsysteem in het laboratorium ontwikkeld (beschreven in hoofdstuk 3), waarmee gedetailleerde en behoorlijk goedkope metingen van OF samenstelling gedaan worden met gebruik van filtermonsters die kunnen worden verzameld op allerlei verschillende locaties. Het meetsysteem is getest door het vergelijken met een in situ bewezen techniek (in situ TD-PTR-MS) (e.g., Holzinger et al., 2010), en over het algemeen was er een goede overeenkomst tussen die twee technieken. Echter, voor OF dat gedurende één dag was verzameld op filters, werd een positief bemonsteringsartefact gevonden. Dat is vanwege de grote adsorptie van semivluchtige organische stoffen op filters, en dat is ook beschreven in de literatuur. Voor de filters die gedurende twee en drie dagen fijnstof verzamelden waren kleine negatieve artefacten opgemerkt, die waarschijnlijk veroorzaakt werden door niet complete desorptie van het fijnstof van de filters op temperaturen tot 350 ˚C en de potentiele chemische degradatie van fijnstof op de filters. In het kort, het ontwikkelde meetsystem creëert het mogelijkheid om gedetailleerde chemische samenstelling van fijnstof te bestuderen van diverse locaties met geadviseerde filter bemonstering voor tijden langer dan een dag.

Terwijl gedetailleerde offline metingen van OF samenstelling heel nuttig zijn, kunnen overeenkomstige in situ metingen de veranderingen in OF concentraties en samenstelling waarnemen op een kleinere tijdschaal. Daardoor is het mogelijk om met in situ data verschillende bronnen van OF beter te scheiden. In hoofdstuk 4 beschrijf ik de in situ TD-PTR-MS techniek en laat ik zien dat totale OF concentraties en organische stoffen goed te meten zijn met een tijdsresolutie van een half uur. Het eerste is aangetoond gebaseerd op de vergelijking met de 'aerosol mass spectrometer' (AMS) metingen. Het tweede is gedaan gebaseerd op de vergelijking met de 'two-dimensional gas chromatography with a time-of-flight mass spectrometer' (GC×GC/TOF-MS) techniek. We ontdekten dat stoffen met concentraties boven 2 ng $m^{-3}$, gemeten door GC×GC/TOF-MS redelijk gedetecteerd werden met de in situ TD-PTR-MS techniek. Alle drie de metingen waren uitgevoerd tijdens de CalNex 2010 verldcampagne in Pasadena, California, waar meer dan 40 onderzoeksgroepen deelnamen aan om VOS, fijnstof en andere bestanddelen van de atmosfeer te karakteriseren.

## Краткое содержание

Летучие органические соединения (ЛОС) и органический аэрозоль (ОА) играют важную роль в атмосфере Земли из-за влияния на здоровье людей и на климат. Для того чтобы контролировать количества ЛОС и ОА в атмосфере, необходимо знать их основные источники, а также влияние внешних факторов на эти источники. В то время как было проведено большое количество исследований основного источника ЛОС (растительность), только небольшое количество исследований было посвящено вопросу как внешние факторы, такие как загрязнители окружающей среды, влияют на эмиссии растений. Исторически состав ОА измеряется как общее содержание органического углерода. Детальное измерение состава ОА намного сложнее, но критично для глубокого понимания вторичных источников и климатических эффектов аэрозолей. Первая часть данной работы (глава 2) описывает установку, позволяющую анализировать, как ЛОС эмиссии растений меняются под воздействием различных загрязнителей. Вторая часть (глава 3) описывает разработанный мною оффлайн инструмент по измерению состава ОА, и третья часть (глава 4) более глубоко характеризует измерения состава ОА уже используемым in situ инструментом.

Присутствие ЛОС и оксидов азота ($NO_x$) в атмосфере приводит к образования озона. Озон является ядовитым газом для людей и растений. Также, озон – парниковый газ, вносящий вклад в увеличение температуры поверхности Земли и изменение климата. Окисление ЛОС в атмосфере приводит к образованию вторичного органического аэрозоля (ВОА), с которым связаны важные климатические фидбэки. Эмиссии растений составляют 90% суммарных ЛОС эмиссий в атмосферу (Guenther et al., 1995). Возможные механизмы влияния загрязнений на этот значительный источник ЛОС в настоящий момент мало изучены. В главе 2 я описываю установку, которую мы построили в нашей лаборатории для того чтобы изучать эффект загрязнения на эмитируемые растениями ЛОС. Различные загрязнители такие как озон, сложная смесь, полученная путем окисления эмиссий растений и представляющая реальные атмосферные условия, а также диоксид азота могут быть использованы в установке. Установка состоит из двух камер с растениями, одной реакционной камеры и масс-спетрометра с переносом протона (PTR-TOF-MS) в качестве измерительной установки, соединенной с газовым хроматографом и криогенной ловушкой. Установка

позволяет проводить детальные in situ измерения изменений в эмиссиях растений, а также позволяет разделение изомерных соединений (например, монотерпенов) эмитируемых растениями в нормальных и стрессовых условиях. Способность разделения изомеров является значительным преимуществом системы, поскольку различные монотерпены имеют разный потенциал образования ВОА, а также могут играть различные роли в коммуникации между растениями. Установка была протестирована с помощью экспериментов с саженцами березы. Их эмиссии были измерены, окислены, и продукты окисления были измерены в реакционной камере. Мы наблюдали допустимую согласованность с описанными в литературе научными данными. Кроме того, был проведен озонолиз с β–пиненом (путем добавления озона в реакционную камеру, содержащую β–пинен). При этом наблюдались основные продукты окисления, описанные в научной литературе, со сравнительными выходами.

Дополнительный плюс данной установки заключается в её гибкости: так, камеры с растениями могут быть легко заменены. Это позволило нам провести измерения с камерами меньшего размера и с крышкой из кварца, что позволило наблюдать in situ изменения в эмиссиях растений под воздействием УФ излучения. В результате, растения арабидопсис, облученные в течение 4 часов УФ, эмитировали значительно большие количества уксусной кислоты, чем необлученные соответствующие растения.

Окисление ЛОС приводит к образованию ядовитого парникового газа озон и ВОА. Аэрозоль при вдыхании попадает в легкие, что является причиной значительных рисков для здоровья. Эффект воздействия аэрозоля оценивается в более чем 500,000 смертей ежегодно (Nel, 2005). Недавние исследования показали, что высокие концентрации аэрозолей приводят к увеличению количества людей с аутизмом (Volk et al., 2013). С точки зрения изменения климата, аэрозольные частицы адсорбируют и рассеивают падающее солнечное излучение и увеличивают время жизни облаков. Суммарным эффектом этого является то, что меньшее количество солнечного излучения достигает поверхности земли. Таким образом, аэрозольные частицы задерживают глобальное потепление, вызванное присутствием парниковых газов в атмосфере. ОА имеет, как правило, значительную массовую долю в общей массе аэрозольных частиц (от 20 до 90%) (Kanakidou et al., 2005). Таким образом, важность ОА в атмосфере создает необходимость понимания источников и путей образования ОА для того чтобы можно было контролировать его количества в атмосфере. Для

понимания источников и путей образования аэрозоля необходимо детально знать химический состав ОА. Многочисленные методики используются для изучения химического состава ОА. Однако, многие из этих методик не позволяют получать детальную информацию о химическом составе и характеризуют его в общих чертах. Другие методики, такие как термодесорбционная масс-спектрометрия с переносом протона (TD-PTR-MS), способны измерять детальный химический состав, но являются слишком дорогими для того, чтобы получить относительно широкое распространение. Я разработал лабораторный метод под названием оффлайн TD-PTR-MS, который позволяет детальные и относительно недорогие измерения химического состава ОА на основании образцов фильтров, которые могу быть получены из разных географических мест. Установка была протестирована путем сравнения с уже используемой и достоверной in situ-методикой (in situ TD-PTR-MS) (e.g., Holzinger et al., 2010) и, в целом, наблюдалась высокая корреляция между двумя методами. Однако, на образцах фильтров, собранных в течение одного дня, наблюдались положительные артефакты, связанные с получением фильтров. Эти артефакты объясняются высокой адсорбцией семи-летучих соединений на фильтрах, что подтверждает ранее опубликованные в научной литературе исследования. Небольшие негативные артефакты наблюдались на фильтрах, собранных в течение двух и трех дней. Это, вероятно, вызвано неполной десорбцией аэрозолей с фильтров при температурах до 350 ˚C и возможным химическим разложением аэрозолей на фильтрах. В целом, разработанный метод позволяет изучать химический состав ОА в разных географических местах. При этом, рекомендуется собирать фильтры дольше, чем один день.

В то время как детальные оффлайн измерения состава ОА несомненно очень полезны, соответствующие in situ измерения позволяют наблюдать изменения в концентрациях и составе ОА в более коротком временном масштабе. Таким образом, при наличии in situ данных можно более точно разделять источники ОА. В главе 4 я кратко описываю in situ TD-PTR-MS методику и показываю способность данной методики хорошо измерять как суммарную концентрацию ОА, так и концентрации отдельных органических соединений, составляющих ОА, с временным разрешением 0.5 часа. Первое показано на основании сравнения с измерениями с помощью аэрозольного масс-спектрометра (AMS). Второе показано на основании сравнения с измерениями с помощью двухмерной газовой хроматографии с использованием время-пролётного масс-спектрометра (GC×GC/TOF-MS).

Мы наблюдали, что соединения с концентрацией выше 2 нг $м^{-3}$, измеренной с помощью GC×GC/TOF-MS, успешно детектировались с помощью in situ TD-PTR-MS методики. Все три серии измерений были проведены в ходе CalNex 2010 полевой кампании в Пазадене, Калифорния, в которой участвовали более 40 научных групп с целью изучения ЛОС, аэрозолей и других составляющих атмосферы.

# Chapter 1: Introduction

## 1.1 Composition of the atmosphere

### 1.1.1 Trace gases in the atmosphere

The Earth's atmosphere consists of nitrogen (78%), oxygen (21%), argon (<1%) and multiple gases found in very low quantities. The latter gases are normally referred to as trace gases. Examples of trace gases are important greenhouse gases like carbon dioxide and methane, or isoprene, which is emitted primarily by land plants. Additionally, the atmosphere contains aerosols. Aerosols (or particulate matter) are suspended solid or liquid particles in the atmosphere.

Trace gases can be inorganic or organic. Organic gases that stay in the gas phase and do not immediately form particles are referred to as volatile organic compounds (VOCs). Most inorganic trace gases present in the atmosphere are of little complexity, whereas organic trace gases vary greatly in structure and composition. The number of compounds with a given number of carbon atoms grows quickly with the number of carbon atoms. Methane is the only hydrocarbon containing only one C atom (Fig. 1). For two C atoms, there are already three hydrocarbons, ethane, ethene and acetylene. When we get to 10 C atoms, there are a large number of hydrocarbons, which can vary in the number and position of single, double and triple bonds and additionally in the geometrical structure. One example is β-pinene, a molecule that contains 10 carbon and 16 hydrogen atoms (Fig. 1) and is emitted by many plant species. In the air above a particular ecosystem, there can be more than 10 different compounds with molecular formula $C_{10}H_{16}$. Structure and molecular weight of compounds determine some of its key properties, including its volatility and reactivity in the atmosphere.

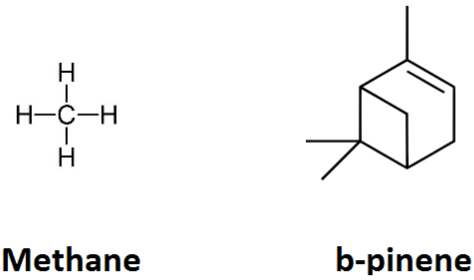


Fig. 1. The chemical structure of two example organic trace gases: methane and β-pinene.

The abundance of atmospheric compounds is given either as a concentration (e.g. number concentration in molecules $cm^{-3}$ or mass concentration in g $cm^{-3}$) or as mixing ratio. The mixing ratio of a gas A (MR(A)) in the atmosphere is defined as the number of moles of a certain gas, n(A), in a sample, divided by the number of moles of all air molecules, n(air), in the same sample. Eq. 1.1 shows that this molar mixing ratio is equivalent to the molecular (or number) mixing ratio, where N is the number of molecules, and $N_A$ is Avogadro's constant.

$$MR(A) = \frac{n(A)}{n(air)} = \frac{n(A)*N_A}{n(air)*N_A} = \frac{N(A)}{N(air)} \qquad (1.1)$$

For ideal gases, this is also equivalent to the often used volume mixing ratio.

The mixing ratios of trace gases in the atmosphere are low and vary greatly: from below ppq (parts per quadrillion or fmole $mole^{-1}$) to several ppm (parts per million or µmole $mole^{-1}$). Many gases presented in this thesis are in the ppb (part per billion, nmole $mole^{-1}$) or ppt (parts per trillion, pmole $mole^{-1}$) range.

The advantage of using number mixing ratio instead of concentration is that it does not depend on pressure, whereas the concentration decreases with decreasing pressure. This is important for atmospheric research where studies are performed at different altitudes, because pressure decreases strongly with altitude.

Despite very low mixing ratios, the trace gases are very important as they play important roles in climate change and influence air quality. Among the trace gases, greenhouse gases (GHG) such as carbon dioxide and methane, whose mixing ratios are relatively high in comparison to other trace gases (~390 ppm and ~1.8 ppm,

respectively), have the largest effect on climate change. Greenhouse gases are gases which absorb infrared radiation released from the Earth's surface and partly radiate the absorbed energy back to the surface. Consequently, they lead to a temperature increase of the Earth's surface. Essentially, they serve as a blanket for the Earth.

### 1.1.2 Aerosol in the atmosphere

Aerosol particles can be inorganic and organic. Inorganic particles are mainly comprised of nitrate, sulfate, chloride and ammonium. The main sources of inorganic aerosol are sea salt, mineral dust, livestock, biomass burning, volcanic eruptions and road traffic.

Organic aerosol constitutes 20 to 90% of the total aerosol mass (Kanakidou et al., 2005) and can be emitted in the atmosphere directly (primary organic aerosol, POA), but can also be produced via photochemical oxidation of volatile organic compounds (secondary organic aerosol, SOA). An important source of POA is fossil fuel combustion. The total secondary organic aerosol budget in the atmosphere is not fully understood yet. Bottom up estimations resulted in 70 TgC/year (Kanakidou et al., 2005), while top-down approaches resulted in 150-900 TgC/year (Hallquist et al., 2009; Goldstein and Galbally, 2007).

Aerosol particles can be of very different size ranging from nanometers to tens of micrometers. The smallest particles (0.01-0.1 µm) are referred to as nucleation mode particles, middle size particles (0.1-1 µm) as accumulation mode and the largest ones (1-10 µm) as coarse mode particles. Based on commonly used filter sampling techniques aerosol mass concentration is reported in two groups: PM2.5 and PM10, which contain particles smaller than 2.5 µm and 10 µm, respectively. Smaller particles have stronger effect on health, as they have relatively larger surface area and higher relative content of potentially toxic hydrocarbons (Nel, 2005). Moreover, they can penetrate deeper in lung tissue than bigger particles.

The residence time of particles in the atmosphere is on the order of a few days and therefore the absolute concentrations of aerosols can vary much depending on location. Mass concentration (in units of µg $m^{-3}$) is normally used to quantify the amount of aerosol in the atmosphere. Typical aerosol mass concentrations in the boundary layer are between 5 and 30 µg $m^{-3}$. Historically aerosol concentrations in the atmosphere were measured in the following way: first, aerosols were sampled on filters; second, filters were weighted in laboratory; third, the mass of aerosol found on the filter (obtained as a difference of a filter mass after and before the

sampling) was divided by the sampled air volume. This resulted in aerosol concentration in µg $m^{-3}$.

In general, it is important to study the composition of VOCs and aerosols and their transformation for four main reasons:

a) In presence of pollution the poisonous greenhouse gas ozone ($O_3$) is a byproduct of the chemical degradation of VOCs. High ozone mixing ratios in the troposphere are harmful for human beings, plants etc.
b) Ozone is a GHG, and higher $O_3$ mixing ratios contribute to anthropogenic global warming
c) Aerosols in the atmosphere scatter and absorb solar radiation leading to a cooling of the earth's surface. The cooling due to aerosols may have counteracted the warming due to greenhouse gases in the past.
d) Aerosols in the atmosphere are harmful for human beings, as they lead to cardiac and respiratory morbidity and mortality. Aerosols are estimated to be responsible for more than 500,000 deaths every year (Nel, 2005).

## 1.2 Composition of VOCs and aerosol in the atmosphere

VOCs are comprised of anthropogenic and biogenic volatile organic compounds (BVOC). There are tens of thousands of different VOCs in the air. Important anthropogenic VOCs sources are production, storage and use of fossil fuels as well as production and use of solvents. Examples of such VOCs are toluene, benzene and pentane. Moreover, biomass burning is an important VOC source.

BVOC emissions constitute approximately 90% of global annual VOC emissions which are estimated to be ~1150 Tg C $yr^{-1}$ (Guenther et al., 1995). The main source of BVOCs is vegetation, in particular emissions from tropical and extra-tropical forests. Important BVOCs are isoprene, monoterpenes and methanol.

Despite the fact that total annual VOC emissions are even higher than the methane emissions which are ~410 Tg C $yr^{-1}$ (Kirschke et al., 2013), the relative abundance of VOCs in the atmosphere is much lower (from few ppt to few ppb for isoprene against ~1700 ppb for methane), which is caused by the shorter atmospheric lifetime of VOCs. The methane lifetime is about 9 years (Dentener et al., 2003), whereas the isoprene lifetime (which is one of the most abundantly emitted BVOCs) is few hours only. The short lifetimes of VOCs make them important drivers of atmospheric chemistry processes (Fehsenfeld et al., 1992; Riipinen et al., 2011; Sahu, 2012). The lifetime of a compound A in the atmosphere with respect

to reaction with hydroxyl (OH, see below) radicals (equivalent for any other 'cleansing agent' in the atmosphere, e.g. ozone and $NO_3$) is defined in Eq. 1.2.

$$\tau_{OH} = \frac{1}{k_{OH*}[OH]} \quad (1.2)$$

where $\tau_{OH}$ is the lifetime of compound A with respect to reaction with OH radicals, $k_{OH}$ is the reaction rate coefficient of the compound A with the OH radical, [OH] is the concentration of the OH radical in the atmosphere, ~$8.1*10^5$ molecules $cm^{-3}$ on average (Prinn et al., 1992). The OH radical concentration varies during the day with lower night time concentrations and also depends on a season with higher concentrations in summer.

The total lifetime of a compound A ($\tau$) that is lost through several different reactions can be calculated according to Eq. 1.3.

$$\frac{1}{\tau} = \frac{1}{\tau_{OH}} + \frac{1}{\tau_{O_3}} + \frac{1}{\tau_{NO_3}} \quad (1.3)$$

where $\tau_{O_3}$ and $\tau_{NO_3}$ are the lifetimes of the compound A with respect to reactions with ozone and $NO_3$ radicals, respectively and $\tau$ is the total lifetime of a compound A.

As the OH radical is one of the main oxidants in the atmosphere, here we describe the oxidation mechanism of VOCs with OH radicals leading to the formation of ozone and oxidized organics (Fig. 2). Presence of NOx and sunlight is needed for these reactions to occur.

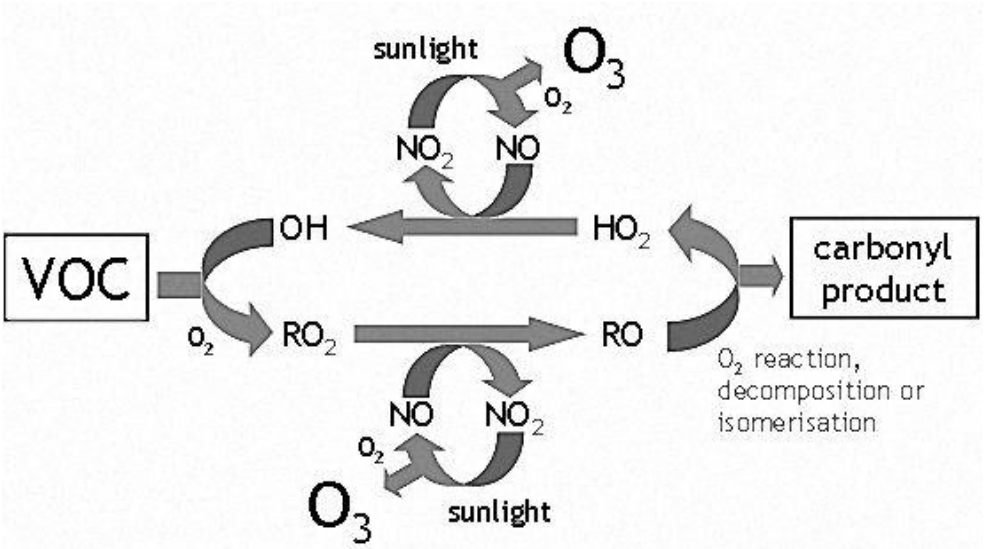


Fig. 2. Scheme of the VOC oxidation in the atmosphere. Presence of NOx in the atmosphere and sunlight is needed. The carbonyl product has a lower vapor pressure compared to the original VOC and can therefore more easily form aerosol particles (adopted from mcm.leeds.ac.uk).

The oxidation sequence of VOC, resulting in a carbonyl compound (a compound containing C=O functional group) and ozone molecule, is usually described in five main steps: 1) The reaction of the VOC with the OH radical resulting in production of a $RO_2$ radical; 2) reaction of the $RO_2$ radical with NO resulting in production of a RO radical and $NO_2$; 3) reaction of the RO radical with $O_2$ resulting in the production of a carbonyl compound and $HO_2$ radical; 4) reaction of the $HO_2$ radical with NO resulting in the production of an OH radical and $NO_2$. Finally (5), the two $NO_2$ molecules are photolyzed which results in the recycling of NO and production of two $O_3$ molecules.

The produced carbonyl compound has a vapor pressure lower than the original VOC. The further fate of the carbonyl compound depends on its volatility, so that the carbonyl compound might either react further with OH radical in the atmosphere (resulting in multiple functional group-compounds, which further decreases the vapor pressure) or contribute to organic aerosol formation in two possible ways: (a) condensation on pre-existing particles and/or (b) nucleation with other organic molecules to form a new particle (Fig. 3).

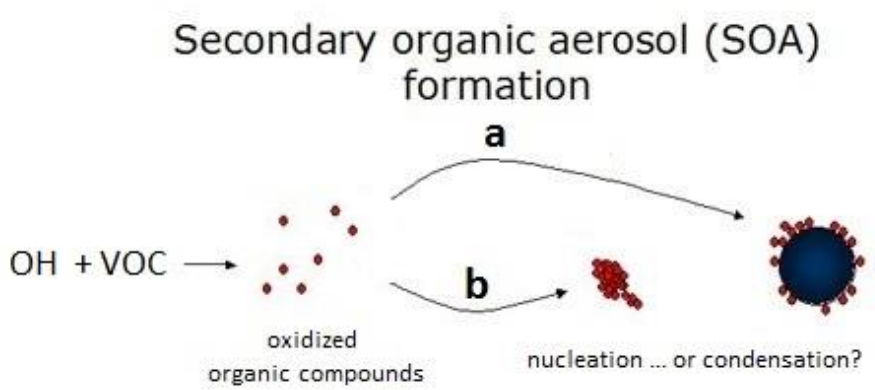


Fig. 3. VOC oxidation leading to the formation/growth of aerosol particles. First, the VOC reacts with OH radical and forms lower vapor pressure compounds. Next, two pathways are possible: a) the condensation of newly formed molecules on pre-existing particles; b) nucleation of newly formed molecules.

In order to characterize the volatility of organic compounds, we can use the saturation vapor pressure. At a given temperature, the compound with a higher saturation vapor pressure can build up a higher partial pressure (proportional to a number concentration) in the gas phase than the compound with a lower saturation vapor pressure. That is, the air can hold more molecules of this compound before condensation on pre-existing surfaces occurs. Volatility characterizes the ability of a substance to vaporize. The higher the saturation vapor pressure of a compound is, the higher its volatility is. The stronger hydrogen bonds connecting oxygen-containing molecules in the condensed state lead to lower saturation vapor pressures of oxygen-containing compounds than hydrocarbons. Therefore, carbonyl compounds have lower saturation vapor pressure than the VOCs they are formed from (see Fig. 2). Consequently, such carbonyl compounds form particles more easily than the precursor VOCs.

In general, organic compounds in the atmosphere have been categorized in 5 groups based on their volatility (approximated here as saturation concentration in $\mu g\ m^{-3}$, which is a direct equivalent to saturation vapor pressure but expressed in units of concentration): ELVOC, extremely low volatility organic compounds; LVOC, low volatility organic compounds; SVOC, semivolatile organic compounds; IVOC, intermediate volatility organic compounds; VOC, volatile organic compounds (Fig. 4, Donahue et al. (2012)).

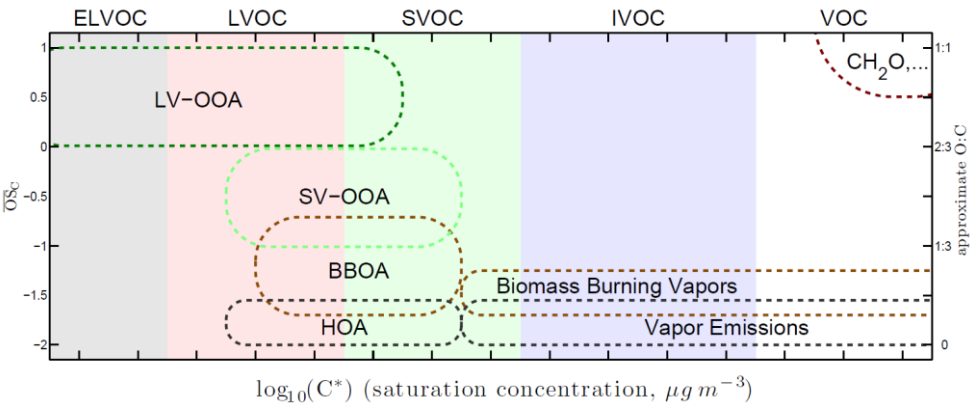


Fig. 4. Volatility (C* in µg m−3) and mean carbon oxidation state ($\overline{OS_C}$) for important atmospheric organics. The more positive OSC for a compound is, the higher O/C ratio for the compound is. The volatility ranges described in the text are indicated by colored bands: aerosols are located in the ELVOC (gray), LVOC (red) and SVOC (green) range (adopted from Donahue et al., 2012). Hydrocarbon-like OA (HOA) is freshly emitted organic aerosol with relatively high volatility and low oxidation state, biomass burning OA (BBOA) is biomass burning emitted aerosol with relatively high volatility and rather low oxidation state, semi-volatile oxygenated OA (SV-OOA) is relatively aged organic aerosol with relatively high volatility and relatively high oxidation state, and low volatility oxygenated OA (LV-OOA) is aged organic aerosol with low volatility and high oxidation state.

### 1.2.1 Chemical composition of organic aerosol

Organic particles are normally of very complex composition, which cannot be fully characterized, i.e. it is not possible to identify and quantify all constituting compounds. The following metrics are used to characterize the chemical composition of organic aerosol: O/C, H/C, and N/C. They quantify the ratio of the total number of oxygen, hydrogen, and nitrogen atoms to the total number of carbon atoms in aerosol, respectively. $\overline{OS_C}$ indicates the mean carbon oxidation state. As freshly emitted/produced aerosol normally has relatively few oxygen atoms and relatively many hydrogen atoms with respect to the number of carbon atoms, it would correspond to relatively low O/C and high H/C ratios. An aged aerosol formed by oxidation of the freshly emitted/produced aerosol will have higher O/C and lower H/C ratios, as during oxidation oxygen atoms are added and hydrogen atoms are removed. Thus, O/C and H/C ratios can be used to characterize aerosol age. Additionally, the O/C ratio is reversely related to aerosol volatility, which is an important aerosol characteristic. The O/C ratio is calculated via Eq. 1.4 (H/C and N/C ratios are calculated equivalently).

$$O/C = \frac{\sum_i N(O) * \frac{m(compound)_i}{MW(compound)_i}}{\sum_i N(C) * \frac{m(compound)_i}{MW(compound)_i}} \quad (1.4)$$

where N(O) and N(C) are the number of oxygen and carbon atoms in the compound 'i', respectively, $m(compound)_i$ is mass concentration of a compound 'i' and $MW(compound)_i$ is the molecular weight of a compound 'i'.

The mean carbon oxidation state ($\overline{OS_C}$) is also used to characterize the chemical composition of organic aerosol and is calculated via Eq. 1.5 (Holzinger et al., 2013):

$$\overline{OS_C} = \frac{1}{[TOT_C]} \sum_i \left( \frac{[species]_i (2nO_i + nN_i - nH_i)}{MW_i} \right),$$

with $$[TOT_C] = \sum_i \frac{[species]_i \, nC_i}{MW_i} \quad (1.5)$$

where $[TOT_C]$ represents the vector of the total measured concentration of carbon atoms (µmol $m^{-3}$), and $nN_i$ and $nH_i$ represent the number of nitrogen and hydrogen atoms in compound *i*, respectively.

Several types of organic aerosol based on the chemical composition are depicted in Fig. 5 (Jimenez et al., 2009): hydrocarbon-like OA (HOA), semi-volatile OOA (SV-OOA) and low volatility OOA (LV-OOA). HOA is freshly emitted organic aerosol with relatively high volatility and low oxidation state, SV-OOA is relatively aged organic aerosol with relatively high volatility and relatively high oxidation state and LV-OOA is aged organic aerosol with low volatility and high oxidation state (Fig. 4). The composition and absolute concentrations of organic aerosol and its types vary greatly by location. E.g., the total aerosol concentrations measured in Mainz, Germany and in Riverside, United States are 4.2 and 19.1 µg $m^{-3}$, respectively (Jimenez et al., 2009). Additionally, the relative contribution of HOA in Mainz is much bigger than in Riverside. This indicates that aerosols present in the Riverside air are more aged than in Mainz (Fig. 5) potentially caused by faster photochemistry in Riverside (34°N) than in Mainz (50°N), which lies ~1800 km further north.

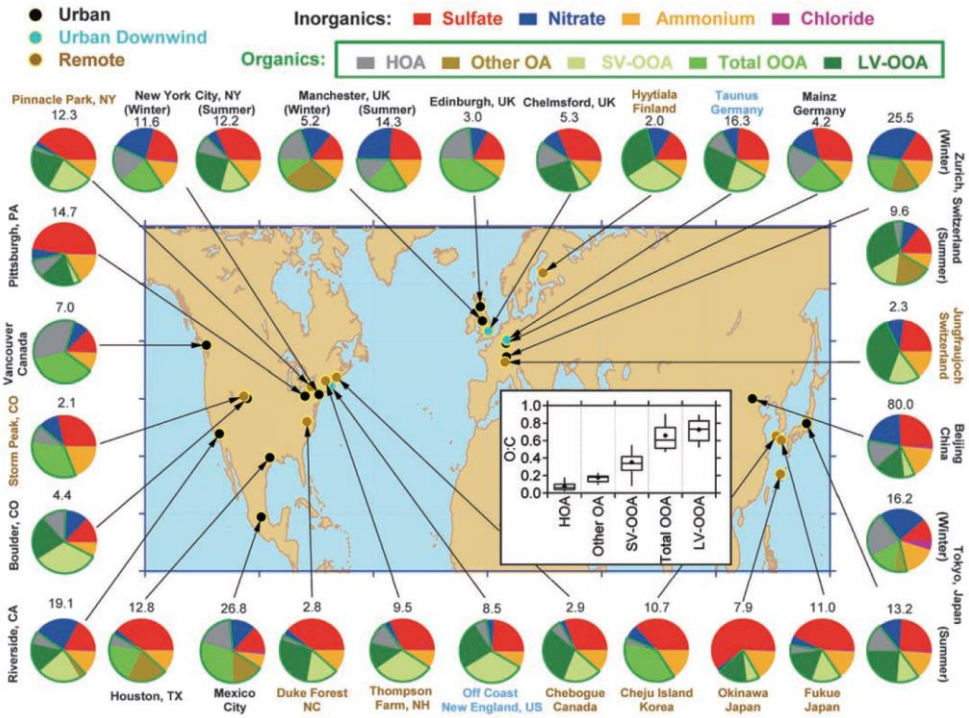


Fig. 5. Total mass concentration (in μg $m^{-3}$) and mass fractions of nonrefractory inorganic species and organic components in sub-micrometer aerosols measured with the aerosol mass spectrometer (AMS) at multiple surface locations in the Northern Hemisphere (adopted from Jimenez et al., 2009).

## 1.3 Climate effects of organic aerosol and VOCs

There are multiple indicators of climate change, such as changes in surface temperature, precipitation, severe events and sea level rise (Cubasch et al., 2013). The key drivers of climate change are GHG, the effect of which (and other climate change drivers) is quantified by radiative forcing (RF). RF is used in order to quantify the effect of GHG, aerosols and other drivers of climate change. RF is the change in average net radiation at the top of the atmosphere which occurs because of a change in mixing ratios of a GHG, or other climate change driver, in the climate system. The anthropogenic RF due to changes of emissions of various atmospheric constituents is shown in Fig. 6. The anthropogenic RF is mainly accounted for by emissions of carbon dioxide, methane, nitrogen oxides, carbon monoxide, non-methane VOC and aerosols (Fig. 6). Carbon dioxide and methane have the highest absolute RFs by emission precursor: 1.68 ± 0.35 W $m^{-2}$ and 0.97 ± 0.23 W $m^{-2}$, respectively.

The net indirect RF of VOCs is small (0.10 ± 0.05 W $m^{-2}$, depicted as NMVOC in Fig. 6), and it is accounted for by the following processes. The chemical degradation of VOCs in the atmosphere consumes the OH radical, decreasing the availability of the OH radical (e.g., Montzka et al., 2011). As the OH radical is the main removing agent of methane from the atmosphere, methane is slower removed from the atmosphere and thus an increase in VOCs causes a positive RF (Fig. 6). The oxidation of VOCs in the troposphere also leads to $O_3$ formation and the ultimate VOC oxidation product is $CO_2$. As $CO_2$ and tropospheric $O_3$ are GHGs, this adds to the positive RF of VOCs.

A second and more important effect of VOCs on climate change is associated with the formation of organic aerosol. Aerosol, and organic aerosol in particular, plays a very important role in the total RF (Fig. 6). The organic aerosol effects on climate can cause positive and negative RFs. The positive RF is caused by the black carbon which adsorbs the incoming solar radiation thus increasing the absolute amount of heat trapped near the surface leading to an increased temperature. The negative RF of aerosol is caused by two processes. First, aerosol itself reflects and scatters solar radiation back to space and, as a consequence, less solar radiation reaches the ground. This is called the direct aerosol effect. Second, aerosol particles can act as cloud condensation nuclei. More aerosols lead to smaller cloud droplets, which, reflect more radiation (for the same liquid water content) and slow the conversion of cloud drops into rain drops, thus increasing lifetime of clouds. The effects on clouds are called indirect effects. The net direct radiative forcing of aerosol is -0.77 – 0.23 W $m^{-2}$ (Fig. 6). Additionally, the total indirect RF associated with cloud adjustments due to aerosols is -1.33 – -0.06 W $m^{-2}$ (Fig. 6).

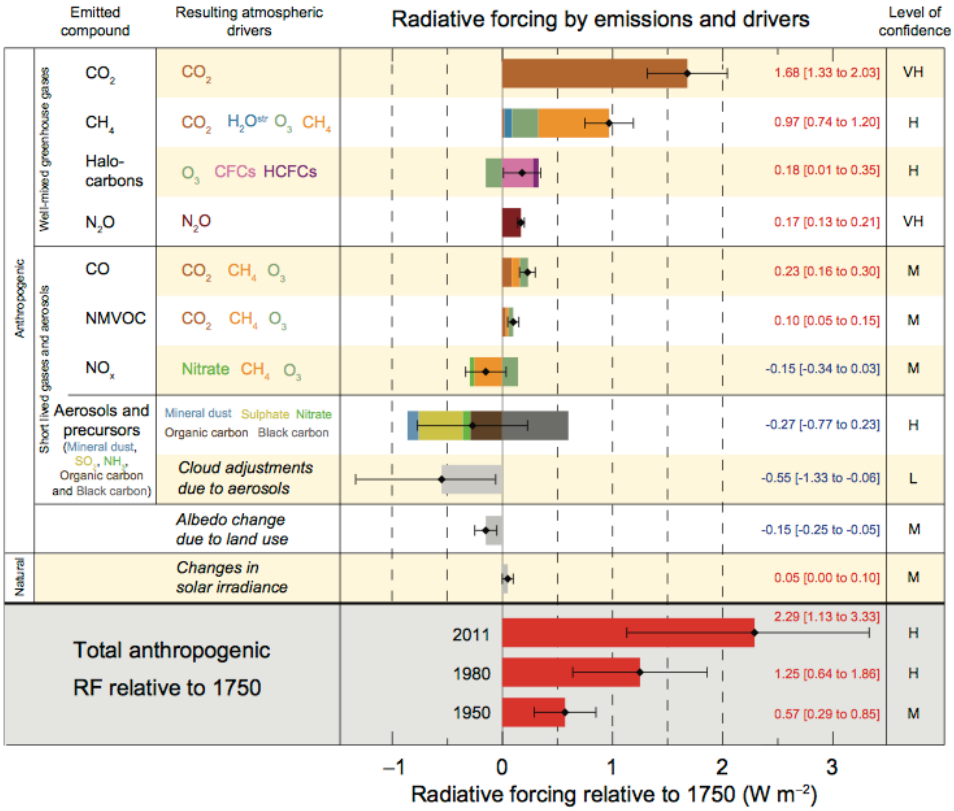


Fig. 6 .Radiative forcing in W $m^{-2}$ of components of the atmosphere. NMVOC refers to non-methane VOC (adopted from Myhre et al., 2013).

## 1.4 Instrumentation and measurement techniques

Multiple techniques are used to measure VOCs in the atmosphere. Proton-transfer-reaction mass spectrometry is a widely used technique, which was also utilized in the current work. Among other methods to study VOCs in the atmosphere, gas chromatography has been used intensively. This is a powerful technique allowing for precise VOC measurements with low limit of detection. However, this is a labor and time consuming technique which does not allow for an immediate monitoring of air composition, as analysis of air sample might take several minutes. This is often too slow for fast changes in atmospheric composition. Another technique to measure VOCs in the atmosphere is a laser-based gas detection technique (Harren and Cristescu, 2013), which allows high sensitivity measurements. However, it is problematic to apply this technique to

composition studies of air containing multiple VOCs, as VOCs 'fingerprints', based on which compound attribution is performed, might interfere.

Multiple techniques are also available to measure organic aerosol composition in the atmosphere. In situ thermal-desorption proton-transfer-reaction mass spectrometry (TD-PTR-MS) allows for a detailed chemical composition analysis of organic aerosol and was used in the current work. Among the other techniques to study chemical composition of aerosol, aerosol mass spectrometry (AMS) has been widely used (e.g., Jayne et al., 2000). This technique allows for in situ aerosol composition measurements. As an output, it provides concentrations of ammonium, sulfate, nitrate, chloride and organic aerosol. However, the information on the organic aerosol composition is with less detail compared to TD-PTR-MS, as the collected aerosols get evaporated at 600 ˚C and then ionized with a hard ionization method (electron ionization). Ulbrich et al. (2009) proposed a method to partly overcome these disadvantages by using a positive matrix factorization technique (PMF). Another method to study organic aerosol composition is thermal desorption aerosol gas chromatograph/mass spectrometer (TAG), which utilizes the same collection-thermal-desorption (CTD) cell described below while the analysis of the collected aerosol is performed with the 2-D gas chromatography mass spectrometry technique (e.g., Worton et al., 2012). This method allows for analysis of individual aerosol compounds, but only a limited set of compounds can be quantified. Among other techniques to study chemical composition of OA are micro-orifice volatilization impactor coupled to a chemical ionization mass spectrometer (MOVI-CIMS) (e.g., Yatavelli et al., 2010), particle-into-liquid sampler (PILS) (e.g., Weber et al., 2001), and filter inlet for gases and aerosols (FIGAERO) (Lopez-Hilfiker et al., 2014).

### 1.4.1 PTR-TOF-MS for VOCs analysis

Proton-transfer-reaction time-of-flight mass spectrometry (PTR-TOF-MS) allows precise in situ measurements of multiple VOCs in the air with high mass resolution (Jordan et al., 2009; Graus et al., 2010). PTR-TOF-MS (and/or its older modification PTR-MS where quadrupole mass spectrometer is used) has been used successfully in various research fields: atmospheric sciences (e.g., Park et al., 2013; Holzinger et al., 2013), indoor air quality studies (e.g., Schripp et al., 2010; Schripp et al., 2014), food sciences (e.g., Biasioli et al., 2011; Romano et al., 2014), human breath analysis (e.g., Riess et al., 2010; Aprea et al., 2014), etc. The core operating principle of the instrument is the chemical ionization with hydronium ions, which is a soft ionization technique with limited fragmentation

(Lindinger et al., 1998). The instrument is schematically shown in Fig. 7. First, water molecules enter the ion source where in a hollow cathode discharge the formation of $H_3O^+$ ions occurs. Second, $H_3O^+$ ions are transferred to the drift tube where they react with VOC molecules from the air sample and transfer of a proton occurs (Eq. 1.6).

$$VOC + H_3O^+ \rightarrow VOCH^+ + H_2O \quad (1.6)$$

Third, the obtained $VOCH^+$ ions pass the transfer lens system. Fourth, $VOCH^+$ ions get detected with a time-of-flight mass spectrometer, which has a high mass resolution of 4000, defined as a measure of the ability to distinguish two peaks of slightly different mass-to-charge ratios in a mass spectrum. Such high mass resolution allows for distinguishing ions with very similar molecular masses. E.g., ions $C_5H_9^+$ and $C_4H_5O^+$ having molecular masses of 69.070 Da and 69.034 Da, respectively, can be distinguished. This is an important advantage for air composition measurements, as the air contains multiple compounds often with same integer masses.

To calculate the mixing ratios of a VOC in the measured air sample [VOC] in nmol $mol^{-1}$, Eq. 1.7 is used:

$$[VOCH^+] = [H_3O^+]_0\{1 - \exp(-k[VOC]\Delta t)\} \approx [H_3O^+]k[VOC]\Delta t,$$

$$[VOC] = \frac{[VOCH^+]}{[H_3O^+]_0 k\Delta t} \quad (1.7)$$

where $[VOCH^+]$, $[H_3O^+]_0$ and $[H_3O^+]$ are the concentrations of the protonated VOC, $H_3O^+$ ions injected from the drift tube and $H_3O^+$ ions after traversing the drift tube in molecule $cm^{-3}$; k is the rate coefficient of the proton transfer reaction in $cm^3\ s^{-1}$ $molecule^{-1}$ (Eq. 1.6), $\Delta t$ is the reaction time in s. Normally, the instrument is operated under conditions when the concentration of the $H_3O^+$ ion is much higher than the concentration needed for the reactions with VOCs in the air sample. Therefore, $[H_3O^+]$ is only slightly smaller than $[H_3O^+]_0$ and we can assume $[H_3O^+]=[H_3O^+]_0$. Concentrations $[VOCH^+]$ and $[H_3O^+]_0$ are derived from the intensities of the corresponding ions which are measured by PTR-MS. For most compounds reaction rate constants are $1.7 – 2.5*10^{-9}$ $cm^3\ s^{-1}$ $molecule^{-1}$ (Zhao and Zhang, 2004).

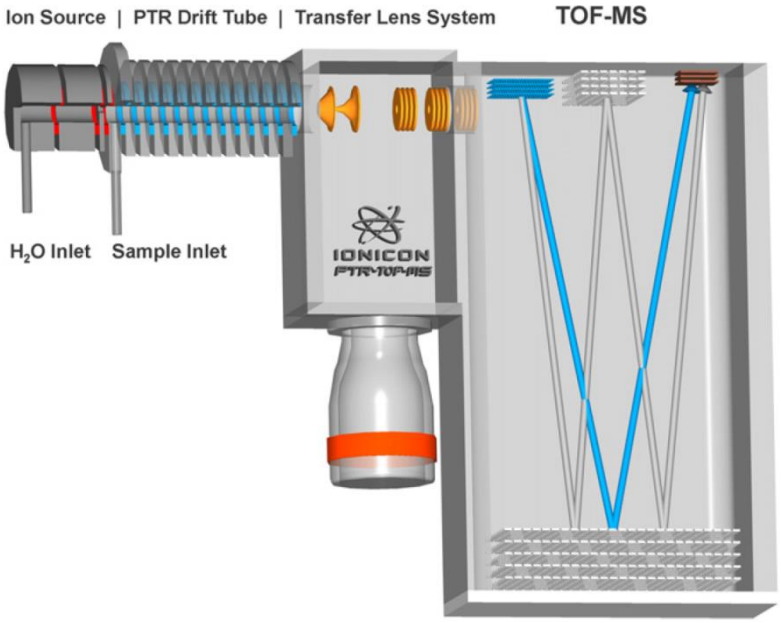


Fig. 7. Proton-transfer-reaction time-of-flight mass spectrometer. The following parts of the instrument are shown: water and air sample inlets, ion source, drift tube, transfer lens system, time-of-flight mass spectrometer (TOF-MS) (adopted from www.ionicon.com).

Despite its strong characteristics, the conventional PTR-MS technique cannot be used for the organic aerosol composition measurements because it requires gas phase compounds for proton transfer. Therefore, we developed external units attached to the PTR-MS, which are described in the next section, allowing for such measurements while utilizing strong capabilities of PTR-MS.

### 1.4.2 In situ TD-PTR-MS techniques for organic aerosol composition measurements

TD-PTR-MS (thermal desorption PTR-MS) is a relatively new technique to study the composition of organic aerosol in detail (Holzinger et al., 2010a) (Fig. 8). The organic aerosol composition is determined as follows. First, the air is sampled through an aerosol inlet with a PM2.5 pre-cutoff. Then, the air stream passes a humidifier where aerosols get humidified and then sampled in the collection thermal desorption (CTD) cell by colliding and sticking to the wall of the cell. The CTD-cell is a cell designed for organic aerosol sampling with consecutive thermal desorption (Williams et al., 2006). It allows for sampling of aerosol particles of size 0.07 µm –2 µm. The sampling surface of the CTD cell is sulfinert coated to

minimize surface effects during thermal desorption. After collection, the CTD cell's temperature is ramped from 50 to 350 ˚C in steps of 50 ˚C. The sampled organic compounds get desorbed and/or decomposed and are carried with a nitrogen flow into PTR-TOF-MS. As a result of a single aerosol sample measurement, a thermogram is obtained (Fig. 9). Peaks correspond to compound emissions at particular temperature steps. The PTR-TOF-MS is used as detector, as it allows for fast measurements with a high mass resolution. In our setup, two aerosol sampling inlets are used to allow for a higher time resolution of the measurements: while aerosol is sampled through one inlet, composition of aerosol collected in the second channel is analyzed.

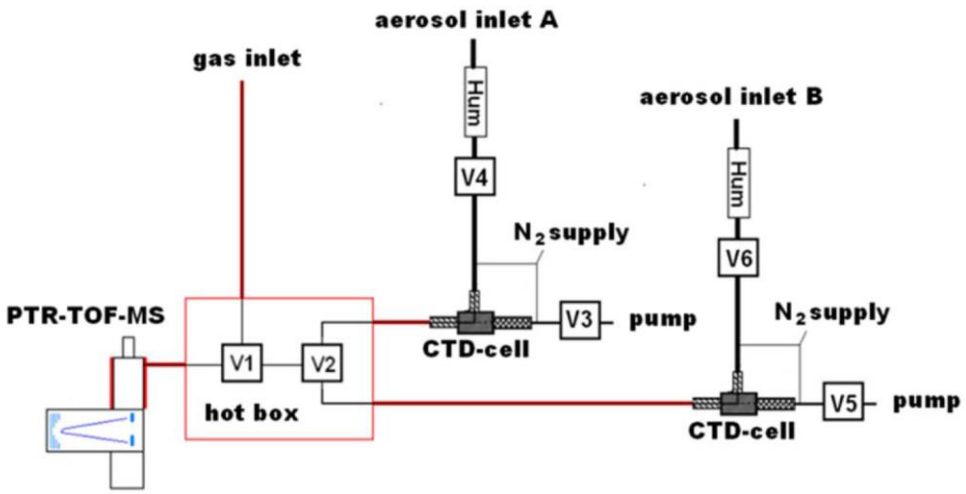


Fig. 8. The in situ TD-PTR-MS setup. The following valves are present: V1 – allows switching between two aerosol inlets, V2-V5 – allow switching between sampling and measuring modes for inlet A and B.

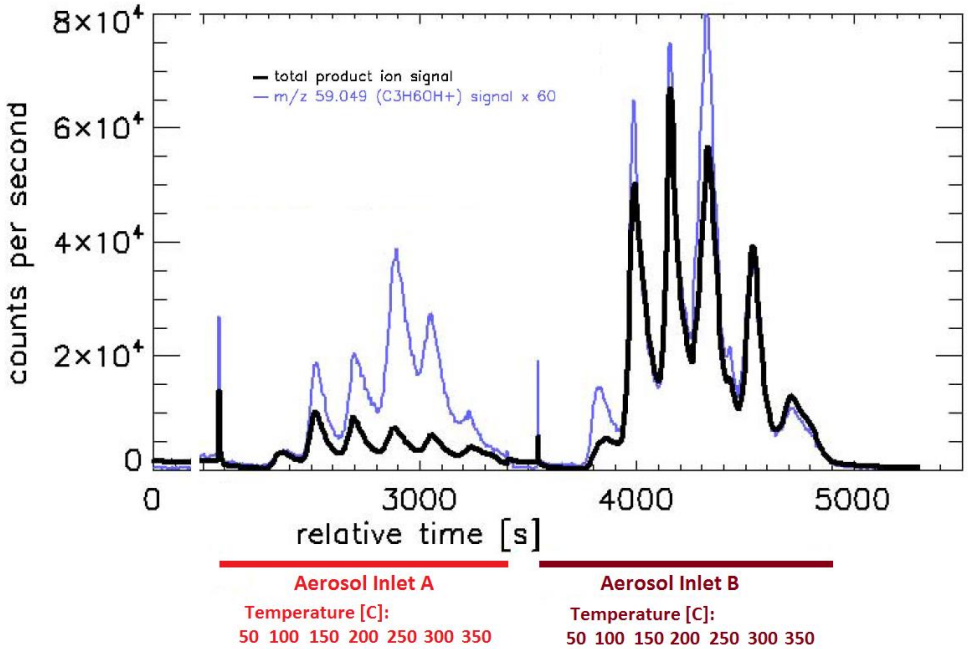


Fig. 9. Aerosol composition thermograms with example timelines of the total product ion signal and m/z 59.049 (adopted with changes from Holzinger et al., 2013).

The measurements of organic aerosol with in situ TD-PTR-MS technique on the mountain Sonnblick (Austria, 3108 m.a.s.l.) resulted in detection and quantification of 638 individual ion peaks. The results showed that oxygenated hydrocarbons constitute the bulk of the aerosol mass (75%) at this remote location (Holzinger et al., 2010b). The in situ TD-PTR-MS technique has been also used to show that the ambient organic aerosol desorption pattern is very different from the reaction chamber produced organic aerosol pattern (Holzinger et al., 2010a). That might indicate some limitation on the extrapolation of the results on organic aerosol obtained in the reaction chamber to the ambient conditions. Holzinger et al. (2013) grouped ions observed with the in situ TD-PTR-MS technique based on the correlation with organic aerosol types obtained by applying PMF method to the AMS data (HOA, LOA, SV-OOA and LV-OOA). It was shown that the mass spectra representing HOA and LOA contained the ions with highest masses, which is in agreement with higher thermal resistance of HOA and LOA. Holzinger et al. (2013) found that fragmentation of organic aerosol becomes more important that functionalization as organic aerosol ages.

## 1.5 Goals and outline

In the current thesis I focus on three projects dedicated to address issues in the atmospheric science fields described above.

Chapter 2 describes how I developed a setup to study the impact of pollution on plant emissions. This could allow for predictions of future vegetation emissions which influence the tropospheric ozone and particulate matter concentrations. The centerpiece of the setup is the combination of plant chambers with a reaction chamber that allows for photochemical processing of the plant emissions. Modern analytical tools such as proton-transfer-reaction time-of-flight mass spectrometer and gas chromatography allow for fast, precise, and detailed chemical analysis. Results from a pilot study demonstrated how capable the system is to investigate important environmental issues such as impact of UV-B radiation on plant emissions.

In Chapter 3 I report on the development of an offline aerosol measurement technique allowing for cheap and detailed analysis of chemical composition of OA from various locations. The new offline aerosol measurement technique (offline TD-PTR-MS) consists of filter sampling in the field followed by consecutive laboratory analysis. This technique allows for detection of a large amount of individual species constituting organic aerosol separately instead of measuring them as a bulk, as most other filter analysis techniques do. Filters used in this study were sampled at Cabauw, the Netherlands with simultaneous in situ TD-PTR-MS measurements. This allowed us to inter-compare the results on the organic aerosol composition obtained with the offline and in situ TD-PTR-MS techniques. Consequently, insights on organic aerosol filter sampling artifacts (positive and negative) were obtained.

Chapter 4 describes a research to study the applicability of the in situ TD-PTR-MS technique to measure total and speciated organics. The former is done based on the comparison with aerosol mass spectrometry (AMS). The latter is done based on the comparison with two-dimensional gas chromatography with a time-of-flight mass spectrometer detection unit (GC×GC) using the analysis of filter samples. In this study we use data obtained simultaneously with three instruments during the CalNex campaign in Pasadena, the United States.

# Chapter 2: A plant chamber system with downstream reaction chamber to study the effects of pollution on biogenic emissions

**J. Timkovsky, P. Gankema, R. Pierik and R. Holzinger**

Published in Environmental Science: Processes and Impacts, 16, 2301-2312, doi: 10.1039/c4em00214h, 2014.

## Abstract

A system of two plant chambers and a downstream reaction chamber has been set up to investigate the emission of biogenic volatile organic compounds (BVOCs) and possible effects of pollutants such as ozone. The system can be used to compare BVOC emissions from two sets of differently treated plants, or to study the photochemistry of real plant emissions under polluted conditions without exposing the plants to pollutants. The main analytical tool is a proton-transfer-reaction time-of-flight mass spectrometer (PTR-TOF-MS) which allows online monitoring of biogenic emissions and chemical degradation products. The identification of BVOCs and their oxidation products is aided by cryogenic trapping and subsequent in situ gas chromatographic analysis.

## 2.1 Introduction

Volatile organic compounds (VOCs) are reactive substances in the atmosphere which have a strong impact on atmospheric chemistry (Fehsenfeld et al., 1992; Riipinen et al., 2011; Sahu, 2012). Biogenic volatile organic compound (BVOC) emissions constitute approximately 90% of global VOC emissions which are estimated to be ~1150 Tg C/year (Guenther et al., 2006). Oxidation of BVOCs in the atmosphere in the presence of NOx leads to the formation of ozone. Tropospheric ozone is a greenhouse gas and a strong oxidant which makes it harmful for living organisms (Summerfelt and Hochheimer, 1997; Denman et al., 2007). Moreover, oxidation products of BVOCs contribute to secondary organic aerosol (SOA) formation through condensation on existing particles or the formation of new particles (Kulmala, 2003; Goldstein and Galbally, 2007). Aerosols and ozone can penetrate into the lungs of humans thus causing long- and short-term health effects (Harrison and Yin, 2000). Furthermore, aerosols and ozone have an impact on Earth's climate: ozone is a strong greenhouse gas and aerosols scatter and/or absorb solar radiation. Aerosols also influence the climate indirectly by serving as cloud-condensation nuclei (Andreae and Crutzen, 1997).

While BVOCs are known to affect the atmosphere, much remains unknown about how atmospheric pollutants affect plant VOC emissions. Increased ozone levels may increase or decrease BVOC emissions, depending on plant species and environmental conditions. For example, Beauchamp et al. (2005) showed that C6-volatile emissions increased after acute ozone exposure in tobacco plants, while Hartikainen et al. (2012) showed decreased VOC emissions upon elevated ozone levels in birch trees. In addition, Karl et al. (2010) showed that pollutants like oxygenated VOCs can be removed by plants through dry deposition. At the same time it is not understood how such deposition influences the ability of plants to emit BVOCs (Karl et al., 2010). Plant VOC emissions are affected by many environmental factors, including abiotic factors like temperature and light as well as biotic factors like herbivores, pathogens and neighboring plants (Guenther et al., 2000; Niinements, 2009; Kegge and Pierik, 2010; Kegge et al., 2013). Here we present a setup of plant chambers and a reaction chamber, which can be used to study interactions between BVOC emissions and pollution. A similar setup has been described by Mentel et al. (2009). Their facility is much larger (it uses trees rather than small potted plants) and optimized to simulate natural conditions. The smaller laboratory based setup that we describe here is flexible and adaptable to study specific processes at the plant level and represents an intermediate between the large facility described by Mentel et al.18 and a much simpler setup such as

used by Karl et al. (2005). The main features include automated operation to study real plant emissions under different environmental conditions. BVOC analysis is based on proton-transfer-reaction time-of-flight mass spectrometry (PTR-TOF-MS) which allows precise online measurements of different VOCs in the air with high mass resolution (Jordan et al., 2009; Graus et al., 2010). In addition, the PTR-TOF-MS is coupled to a gas chromatograph (GC) system in order to improve the identification of isomers (e.g. different monoterpenes). Results from an ozonolysis experiment with β-pinene and three experiments with birch (Betula pendula) seedlings (referred to as experiment A, B, and C) are shown here as an example to demonstrate the performance of the system.

## 2.2 Description of the setup

The schematic setup of the system is shown in Fig. 10. Two optional chamber setups are shown in panels A and B. Fig. 10C shows how the PTR-TOF-MS is connected to the different sampling ports of the chamber system, and Fig. 10D shows the functioning of the GC system.

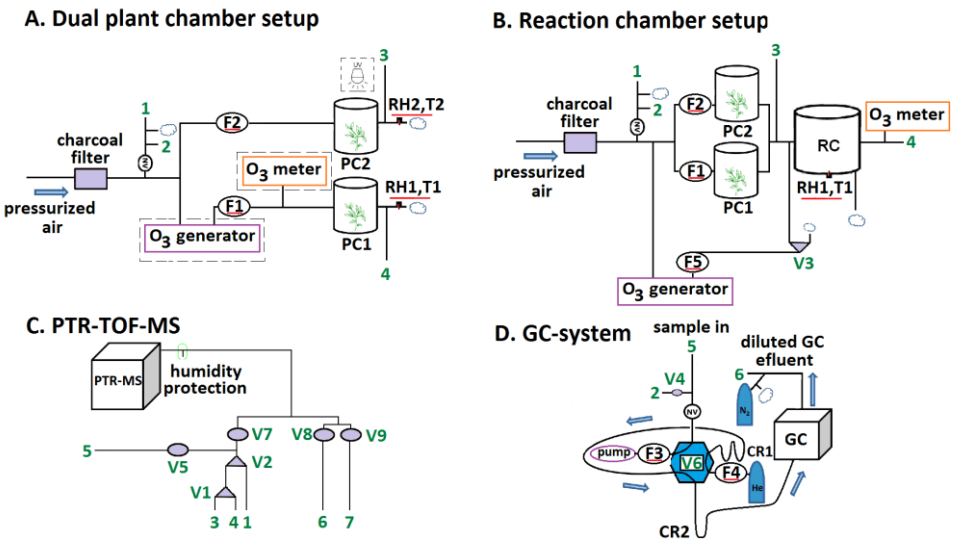


Fig. 10. Schematic overview of the setup with two optional chamber configurations (A and B), PTR-TOF-MS connections (C) and GC sampling system (D). The parts of the system inside dashed line boxes are optional (A). Port numbers 1, 3 and 4 indicate the sampling positions for the PTR-TOF-MS. The GC samples through port 5 and the GC-effluent is analyzed with the PTR-TOF-MS through port 6. Lab air is analyzed through port 7 and port 2 connects the GC system to purified air for cleaning. The following abbreviations were used: NV – needle valve, PC1, PC2 - large plant chambers; RC – reaction chamber, GC – gas chromatograph; V1-V5 and V7-V9 – 2-way (circles) and 3-way (triangles) valves, V6 is a 6-port Valco valve; F1,F2,F3,F4 - flow controllers; RH1, RH2, T1, T2 – temperature and relative humidity sensors; CR1, CR2 – sampling and focusing cryotraps; $N_2$, He – nitrogen and helium cylinders; small clouds depict overflow outlets. The parameters which are underlined in red are recorded during measurements. The little 'clouds' indicate overflow.

### 2.2.1 The plant and reaction chambers

Two types of plant chambers are available for experiments. Their internal volumes are 25 L and 785 mL, and we refer to them as large plant chamber and small plant chamber, respectively.

As large plant chambers we use two glass desiccators, each consisting of three parts: the cap, the desiccator body and the hose, which is located in the cap. The hose has a long outlet (l = 25 cm, ID = 9 mm), which is directed towards the bottom of the desiccator and allows sampling from the center of the plant chamber. The gas inlet to the chamber is located at the top of the hose.

The small plant chambers are custom built and consist of a glass cylinder (inner diameter 100 mm, height 100 mm), a glass lid and a dividable Teflon (PFTE) bottom plate sealed with spring clamps and Teflon coated O-rings. For UV-B treatment, we use a lid with 2 mm thick quartz glass and a broad spectrum UV-B lamp (UV21, 9 W, Waldmann, The Netherlands) at adjustable height above the plant chamber. The bottom plate has a 2 mm hole in the middle that fits around the stem of an individual plant, allowing measuring shoot emissions only. Inlet and outlet (inner diameter 18 mm) are positioned opposite each other 40 mm above the bottom of the chamber.

The custom-made reaction chamber is made from perfluoroalkoxy film (PFA, thickness 0.05 mm, HP Products, the Netherlands) and has a cylindrical shape. The walls were sealed by welding the PFA film with a heat gun (Steinel, Germany). The physical characteristics of the reaction chamber are the following: diameter = 45 cm, height = 50 cm, volume = 80 L. The bottom of the chamber is fixed to a ground plate covered with a PFA film. The axle of a polytetrafluoroethylene ventilator (PTFE, OD = 10 mm, Bola, Germany) is lead through the center of the ground plate, the ventilator is positioned in the center of the chamber. Operating the ventilator at 2 Hz keeps the chamber well mixed during experiments. All mounting parts in contact with the air inside the reaction chamber were made from Teflon (PTFE). The tightness of the reaction chamber was tested by filling the chamber with acetone at levels of ~350 nmol/mol and monitoring the mixing ratio without gas flow through the chamber. No significant leaks were detected.

The flow through the large plant chambers can be controlled by thermal mass-flow controllers (MKS Instruments, Germany) in the range 0-20 and 0-5 standard L/min (standard is referring to standard conditions: 1013.25 hPa, 273.15 K) for chamber 1 and 2, respectively. The flow through the small plant chambers can be also controlled by thermal mass-flow controllers (MKS Instruments, Germany) in the range 0-2 standard L/min. Although we operated the chambers without active mixing, tests showed that there was sufficient convection to completely mix the air inside the large plant chambers in less than 30 minutes (see section 2.2.5a), even at flow rates as low as 2.5 L/min (10 min residence time). We used pressurized (5 bars) ambient air which was purified through a custom made charcoal filter. The charcoal was cleaned once a week by removing the charcoal from the tube and placing it overnight in an oven at 160 $^{o}$C.

In the ‘dual plant chamber’ setup (Fig. 10A) the sampling ports are located directly at the outlets of the plant chambers and a third sampling port is located after the charcoal filter to monitor the incoming air. The elements of the system drawn in dashed line boxes are optional elements. The ozone generator can be used for studies with large plant chambers, whereas UV-B lamp can be used for studies with small plant chambers. In the ‘reaction chamber’ setup (Fig. 10B) the sampling ports are located directly after the reaction chamber, after the plant chambers, and after the charcoal filter. Relative humidity and temperature sensors (HMP 60, Vaisala, Finland) are located at the outlets to monitor humidity and temperature in all chambers.

We use Teflon (PFA) tubing to connect the large plant chambers, the reaction chamber, and instruments (length between plant and reaction chamber = 145 cm, ID = 9 mm). Defined amounts of ozone can be added before large plant chamber 1 (Fig. 10A) or the reaction chamber (Fig. 10B) with an ozone generator (Model 49i-PS, Thermo Scientific, US). This is done by turning on the generator (set to 1500 nmol/mol) and switching valve 3. The ozone addition to the large plant chamber 1 and the reaction chamber is controlled with a thermal mass-flow controller (MKS, Germany) in the range 0-2 L/min. Ozone is monitored (O3 analyzer model 49 W003, Thermo Environmental Instruments Inc., USA) at the outlet of either the large plant chamber 1 or the reaction chamber.

An array of nine 36W/840 TL-D lamps (Philips, the Netherlands) above the plant chambers is used to produce light levels of 130-150 µmol/$m^2$/s photosynthetically active radiation (PAR: λ = 400-700 nm) at leaf level inside the large plant chambers when the lid was closed. These light levels are within the range used by previous plant emission studies (van Poecke et al., 2001; Ibrahim et al., 2010; Falara et al., 2011; Kegge et al., 2013) and are common to plant growth chambers. A practical advantage of using light at these intensities is that we do not encounter significant heating in the large plant chambers and therefore active cooling is not required.

### 2.2.2 Analytical tools

#### 2.2.2a PTR-TOF-MS

Fig. 10C shows how the PTR-TOF-MS is switched between the three sampling ports of the chamber system, the effluent of the GC column (the PTR-TOF-MS is also used as detector for the GC system), and laboratory air, which can be routinely monitored as well. This valve system is implemented with 1/8”PFA tubing, four 2-way and two 3-way Teflon (PFA) solenoid valves (TEQCOM, port size 1/8’’,

orifice 0.125). We use a commercial PTR-TOF 8000 instrument (Ionicon Analytik GmbH, Austria), which has been described by Jordan et al.,20 with the following parameters: temperature of the drift tube, 60 ºC; temperature of the inlet tube, 60 ºC; drift tube pressure, 2.15 hPa; ion source voltages, Us = 140 V, Uso = 92 V; ratio of the applied to the drift tube voltage and the number of molecules in the drift tube, E/N, 134 Td; extraction voltage at the end of the drift tube, Udx=35 V. The ion source current is kept between 5 and 7 mA and we provide a water flow of 4 mL/min to the ion source. At normal operational conditions the intensity of the primary signal $H_3O^+$ (detected at m/z 21.023 as $H_3{}^{18}O^+$) is around $2.5*10^5$-$1*10^6$ cps. However, during experiments B and C the primary signal was low (~$5*10^4$ -$1*10^5$ cps), whereas during experiment A the primary signal was at its normal level (~$2.5*10^5$ cps). During the ozonolysis of β-pinene experiment the primary signal was ~$1*10^5$ cps. The ratios of the intensities $I(O_2^+)/I(H_3O^+)$, $I(NO^+)/I(H_3O^+)$ and $I(H_3O(H_2O)^+)/I(H_3O^+)$ were less than 0.02, less than 0.003 and less than 0.25.

The settings of the TOF are such that every 60 microseconds a pulse of ions is injected into the mass spectrometer, which corresponds to a mass range of 0-1157 Th. 16667 of these initial mass spectra are averaged and saved to one mass scan which corresponds to a time resolution of one second. The mass resolution ($m/\Delta m$, where $\Delta m$ is the full width at half maximum) is typically in the range of 3500-5000. Data processing is done with Interactive Data Language (IDL, version 7.0.0, ITT Visual Information Solutions), using custom made routines described by Holzinger et al. (2010b).

Mixing ratios of most compounds were calculated according to the method described in Holzinger et al. (2010a), which involves the use of default reaction rate constants ($3\times10^{-9}$ $cm^3$ $s^{-1}$ $molecule^{-1}$), default transmission efficiencies, and calculated reaction times. The accuracy of the calculated mixing ratios should be better than 50% for most compounds limited by the uncertainty in the used default reaction rate constant (Holzinger et al., 2010a). In addition, a commercially available calibration mixture (Apel–Riemer Environmental, Inc.) was used to calibrate the mixing ratios of monoterpenes, acetaldehyde and acetone with an accuracy of 17%, calculated as the sum of the precision of PTR-TOF-MS and the accuracy of the gravimetrically mixed calibration standard.

The mixing ratios of monoterpenes were calculated as the sum of the signals detected at m/z 81.069 and m/z 137.133 for experiments with pure compounds (here β-pinene). However, we found that in experiments with biogenic emissions

other compounds were also detected at m/z 81.069 (C6 alcohols or aldehydes). Calibration experiments with a gas standard containing α-pinene showed that 32% of the total amount of the monoterpene was found at m/z 137.133. Thus, for the experiments with biogenic emissions, mixing ratios of monoterpenes were calculated by multiplying the signal detected at m/z 137.133 by a calibration factor of 3.13.

### 2.2.2b GC system with VOCs cryogenic trapping

The GC system features two cryogenic traps that can be electrically heated with resistance wire and submerged into liquid nitrogen by pneumatic lifters. The sampling line (1/8'' PFA) is connected (port 5 in Fig. 10C and D) downstream of the two 3-way valves that connect the PTR-TOF-MS to the sampling ports of the chamber system. This ensures that GC-sampling and online monitoring with the PTR-TOF-MS occurs at the same time. The primary sampling trap is a W-shaped 1/8" stainless steel tube (ID = 1.5 mm) with sulfinert coating (Restek Inc.) which is connected with 1/16'' PEEK tubing to a 6-port stainless steel Valco valve (sulfinert coating). A needle valve before the trap is used to regulate the sampling flow and ensures that sampling is at low pressure (~200 hPa) to prevent condensation of oxygen. The collection efficiency has been tested for α-pinene, methanol and toluene to be close to 100% for sampling flows up to 35 mL/min. During operation the trap is pre-cooled for 5 minutes before sampling. We use a sampling flow of 30 mL/min which is measured with a thermal mass-flow meter (MKS Instruments, Germany) and maintained with a membrane pump (Vacuubrand GmbH, Germany) downstream of the sampling trap.

Switching the 6-port valve allows transferring the sample to the focusing trap, which consists of a U-shape 1/8''stainless steel tube with a glass capillary through it (ID = 320 µm, SGE Analytical Science, Australia). The sample is released by heating the sampling trap to 100 $^{o}$C within 2 minutes. A helium flow (ultrapure He, Air products) of 2 mL/min is used to transfer the sample to the focusing trap. Typically a period of 10 minutes is allowed to complete the transfer, which corresponds to a gas volume 5 times the internal volume of the sampling trap, the focusing trap and the transfer lines. Immediately thereafter the 6-port valve is switched back and the sample is injected into the GC column while the effluent is monitored with the PTR-TOF-MS. Injection is achieved by heating the focusing trap to 200 $^{o}$C within 75 seconds. In general, a two cryotraps system is advantageous because better peak shape can be achieved and the reduced amount of water in the sample prolongs the lifetime of the GC column. The first cryotrap

allowed for the initial sampling of VOCs. The second cryotrap was used to focus the presampled VOCs in a much smaller volume, allowing for a much quicker transfer of the VOCs from the cryotrap to the GC column. The amount of water in the sample transferred to the second cryotrap was reduced by ~90% via condensing on the line/Swagelok union located downstream of the sampling cryotrap. This water was removed from the system during the consecutive sampling step.

For the chromatography we use a 30 m DB-5MS column (ID = 0.25 mm, film thickness = 0.25 µm) with He as a carrier gas (2 mL/min, controlled with 20 mL/min thermal mass-flow controller, MKS Instruments, Germany). After injection the column is kept at 40 °C for one minute, heated to 150 °C at 5 °C/min and then to 250 °C at 20 °C/min.

For analysis the effluent of the GC column is diluted with 38 mL/min of nitrogen (ultrapure nitrogen, 5.7 purity, Air products), which is achieved by providing excess nitrogen and setting the flow into the PTR-TOF-MS to 40 mL/min (Fig. 10D). The mixture of effluent and nitrogen is transferred through 1/8'' PFA line to port 6 (Fig. 10C and D).

### 2.2.3 Automation and control system

Valve positions, flows, cryotrap positions, temperatures and other elements are automatically operated with a controlling set (National Instruments NI cDAQ-9178) that can be programmed in Labview's (LabVIEW 2011, National Instruments) user-friendly interface. Control sequences are created as simple text documents containing the commands for valve positions, set temperatures, etc.

The values of the elements underlined red in Fig. 10 are saved to an engineering log together with other parameters such as time, ozone mixing ratios in the reaction chamber, set value of ozone generator, sampling and focusing cryotrap temperatures, and temperature in the GC oven. These data are recorded every second to fit the time resolution of the PTR-TOF-MS.

### 2.2.4 Operation of the system

To demonstrate the operation of the system, Fig. 11 shows the course of the mixing ratios detected at m/z 81.069 ($C_6H_9^+$ fragment) for one cycle of experiment A. The PTR-TOF-MS was switched between the different ports to measure as follows (see Fig. 11): for 10 minutes reaction chamber air, for 5 minutes purified air, for 10 minutes large plant chambers air, for 25.5 minutes GC effluent, for 10 minutes large plant chambers air, for 36 minutes reaction chamber air (ozone addition to the reaction chamber happens during this period), for 25.5 minutes GC

effluent, for 5 minutes lab air. Thereafter, new two-hour cycles were started automatically.

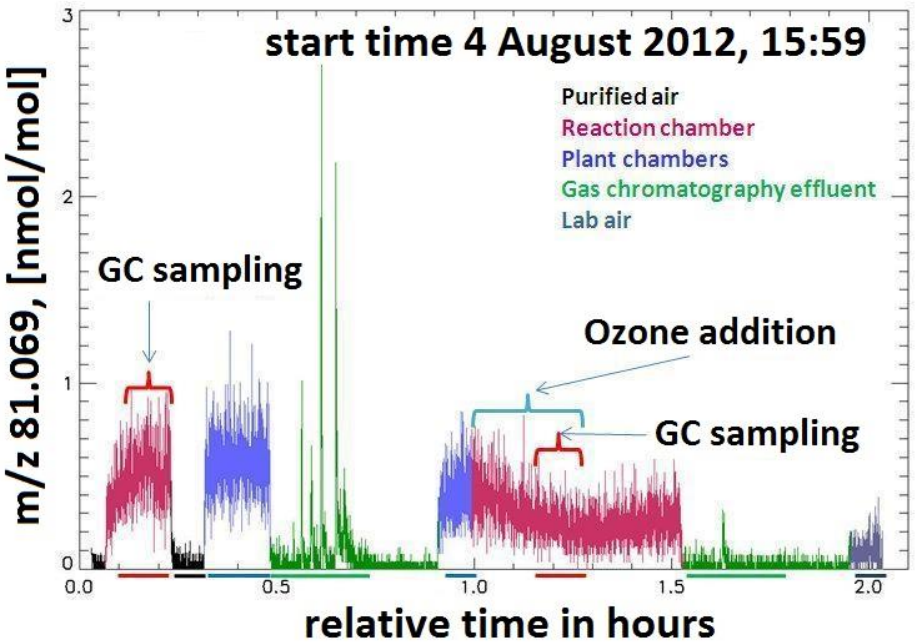


Fig. 11. The standard two-hour cycle of measurements. The signal observed at m/z 81.069 is shown as an example, and the color indicates what is measured at a given moment (see legend). The brackets in the plot area indicate GC sampling and ozone addition periods. Colored lines under the x-axis depict the averaging/integration period for averaged/integrated data as used in Fig. 12 and 16: last 7 minutes of first reaction chamber air, last 4 minutes of purified air, last 9 minutes of large plant chamber air, last 9 minutes of second large plant chamber air, last 7 minutes of second reaction chamber air (ozone treatment).

The periods of GC sampling (7 minutes each) are also indicated in Fig. 11. Ozone addition lasted for 17 minutes (see blue bracket in Fig. 11) and GC sampling was performed during the last 7 minutes of the ozone treatment.

The following periods (indicated in Fig. 11 by the respective lines below the x-axis) were used for averaging/integration: last 7 minutes of non-ozonated reaction chamber air measurements, last 4 minutes of purified air measurements, last 9 minutes of first large plant chamber air measurements, first 15 minutes of first GC chromatogram, last 4 minutes of second large plant chamber air

measurements, last 7 minutes of ozonated reaction chamber air measurements, first 15 minutes of second GC chromatogram.

During the experiment with small plant chambers, the PTR-TOF-MS was switched between the different ports to measure as follows: for 6 minutes small plant chamber 1 air, for 6 minutes small plant chamber 2 air, for 5 minutes purified air, for 5 minutes lab air. Thereafter, a new cycle was started automatically.

### 2.2.5 System performance

#### 2.2.5a Mixing in the plant chambers

An experiment to test mixing of air in the large plant chambers was conducted: flow through the empty plant chamber was maintained at 2.5 L/min and contained ~45 nmol/mol of limonene. The flow was produced by diluting a small flow (standard 1 mL/min) of headspace air from a flask with liquid limonene (Sigma Aldrich, 98%) into the larger flow of purified air. The mixing ratios were measured in the middle and at the bottom corner of the plant chamber with the PTR-TOF-MS and were equal to the incoming limonene mixing ratio after ~30 min. This indicated that the mixing in the plant chambers was as expected and sufficient for the experiments presented here.

#### 2.2.5b VOCs transfer between the large plant chambers and the reaction chamber

Fig. 12 presents online data (experiment B) of the large plant chambers and the reaction chamber without ozone addition. In general, there is good agreement between the mixing ratios in the reaction chamber and the large plant chambers for most compounds. However, for monoterpene and m/z 85.064 (corresponding to the molecular formula $C_5H_9O^+$) the mixing ratios were somewhat lower in the reaction chamber compared to the large plant chamber. This was likely caused by the fact that equilibrium was not yet completely reached by the time when reaction chamber measurements were performed after the preceding ozone addition to the reaction chamber (time difference was less than 3 residence times equal to 34.5 minutes). For m/z 69.070 and 71.049 in some cases lower mixing ratios were observed in the large plant chambers. This might be caused by contamination from the reaction chamber walls.

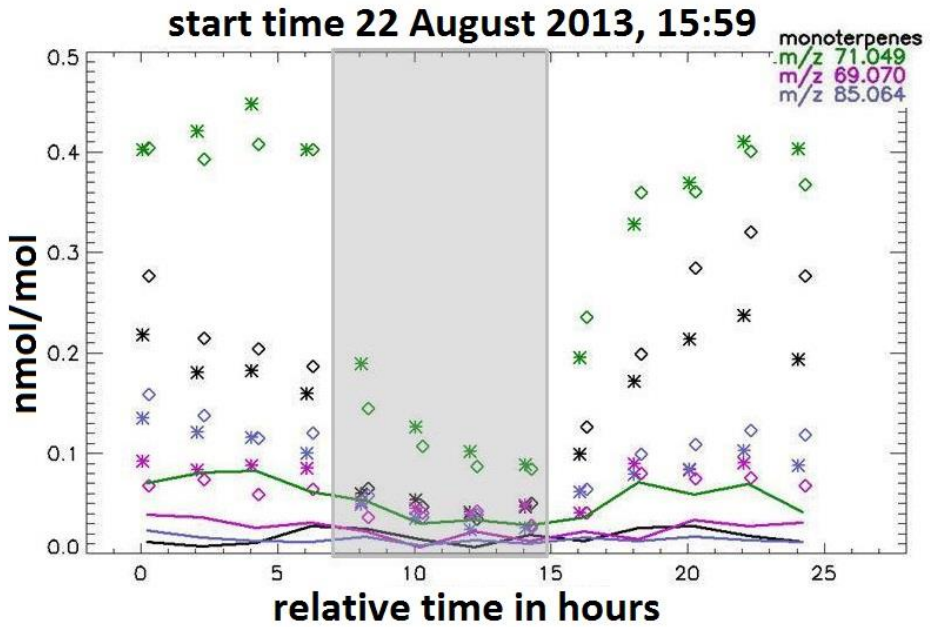


Fig. 12. Online measured mixing ratios in the large plant chambers (diamonds) and in the reaction chamber without ozone addition (asterisks), experiment B. The respective background levels (purified air) are shown as continuous lines. The shaded area indicates the dark period.

### 2.2.5c GC system

Example chromatograms obtained during experiment A are shown in Fig. 13. The five labeled peaks in panel C (Fig. 13) are attributed to a C6-leaf alcohol or aldehyde, 2-hexenal, α-pinene, d-limonene and β-phellandrene. The attribution is done based on the presence of other ions with the same retention times in combination with retention times database (Goodner et al., 2008), performed calibration measurements and previous studies (König et al., 1995). Two little peaks observed after α-pinene and d-limonene are not identified.

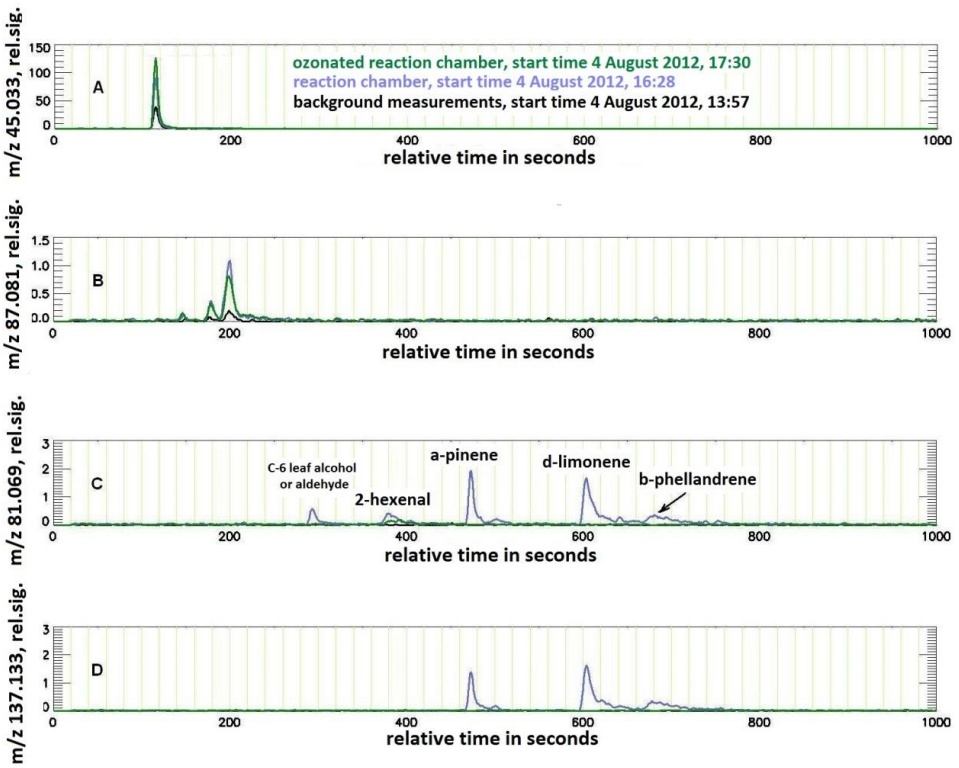


Fig. 13. Example gas chromatograms of experiment A. For every profile running mean over 5 points is used. The green line and the blue line correspond to sampling the ozonated and non-ozonated reaction chamber, respectively. The black line is a background chromatogram. M/z 45.033 corresponds to acetaldehyde, m/z 87.081 to methyl buthenol (MBO), m/z 81.069 to monoterpenes and additional compounds, m/z 137.133 to monoterpenes only.

A crucial point of the GC/PTR-TOF-MS system is the quantitative correspondence between GC and online measurements. Eq. 2.1 defines the recovery factor (RF) as the ratio between the amount of substance of a VOC measured with the GC setup ($n(VOC)_{GC}$) versus the amount of substance sampled ($n(VOC)_{sampled}$). The former was calculated by integrating the GC peak(s) at a particular m/z value, the latter was calculated from the online measured mixing ratio at the same m/z during the time of sampling and the sampled volume:

$$RF = \frac{n(VOC)_{GC}}{n(VOC)_{sampled}} \qquad (2.1)$$

In Table 1 we present recovery factors of several compounds based on experiments A, B and C. To calculate the recovery factors no background was subtracted from the measured signal. The obtained recovery factors are in the range 0.71 - 1.38 indicating a reasonable agreement between online and GC measurements. Deviations from unity are most likely due to different levels of instrumental background during the online and GC effluent measurements. Also, there might be an overestimation of compound mixing ratios in nitrogen-based GC effluent versus air-based online measurements.

Table 1. Recovery factors (RF) for several compounds, calculated from experiment A, B and C using Eq. 2.1. All chromatograms that sampled from the ozone free reaction chamber have been included into this analysis (n=40). Numbers shown are averages ± SD.

| Compound or m/z | Formula•$H^+$ | RF±SD |
|---|---|---|
| 33.033 | $CH_4OH^+$ | 0.75 ±0.10 |
| 43.018 | $C_2H_3O^+$ | 0.82 ±0.07 |
| 59.049 | $C_3H_7O^+$ | 0.71 ±0.08 |
| 61.029 | $C_2H_5O_2^+$ | 1.38 ±0.26 |
| 69.07 | $C_5H_9^+$ | 1.09 ±0.28 |
| 87.045 | $C_4H_7O_2^+$ | 1.10 ±0.16 |
| 87.081 | $C_5H_{11}O^+$ | 1.20 ±0.25 |
| monoterpenes | $C_{10}H_{17}^+$ | 1.23 ±0.31 |

### 2.2.6 First measurements

We performed a series of test measurements to demonstrate the functionality and performance of the system. For all performed analyses we considered ions above m/z 40, and ions detected at m/z 31.018 ($CH_3O^+$) and m/z 33.033 ($CH_5O^+$). In order to identify plant emissions and ozonolysis products we applied a Student's t-test (Leblanc, 2004; Weiner and Craighead, 2010) on the sets of data to be compared (e.g. mixing ratios in air entering the large plant chamber vs. mixing ratios in the large plant chamber; or mixing ratios in the reaction chamber with and without ozone, respectively). The Student's t-test returns a significance parameter,

p, indicating the probability that the two datasets are not different. As threshold we used p=0.05 indicating a 95% probability that the datasets are significantly different. The T-statistic parameter indicates the difference between the means of the two datasets (normalized by the variance) and was assigned separately for every type of experiment.

### 2.2.7 Ozonolysis of β-pinene

In order to test the functionality of the reaction chamber we performed an ozonolysis experiment with β-pinene, a reaction that has been widely studied (Arey et al., 1990; Hatakeyama et al., 1991; Orlando et al., 2000; Larsen et al., 2001; Wisthaler et al., 2001; Jaoui and Kamens, 2003; Lee et al., 2006). During this experiment the flow through the reaction chamber was maintained at 7 L/min by two flow controllers which were set to 5 L/min and 2 L/min, respectively. This resulted in an air residence time of 11.5 minutes in the reaction chamber. The larger flow contained ~350 nmol/mol of β-pinene, which was produced by diluting a small flow (20 mL/min) of headspace air from a flask with liquid β-pinene (Sigma Aldrich, 99%) into the larger flow of purified air. Ozone levels of 1.3 µmol/mol were produced in the 2 L/min flow by the ozone generator corresponding to ~370 nmol/mol ozone mixing ratio in the reaction chamber. Fig. 14 shows the course of β-pinene, some oxidation products, and the ozone mixing ratios. After ~one hour of adding ozone to the reaction chamber, β-pinene and ozone mixing ratios in the reaction chamber reached equilibrium: [β-pinene]~220 nmol/mol and [O3]~340 nmol/mol.

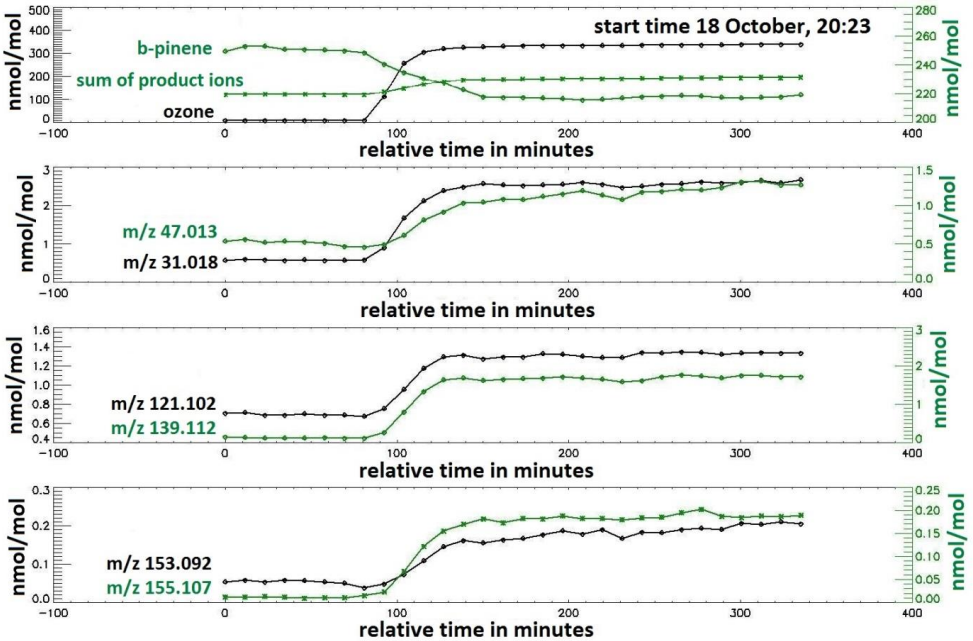


Fig. 14. Ozonolysis of β-pinene. The top panel shows the course of ozone, β-pinene (sum of m/z 81.069 and 137.133) and the sum of all product ions (note that an offset of 210 nmol/mol has been added). The lower panels show oxidation products detected at m/z 31.018 (formaldehyde), 47.013 (formic acid), 121.102 and 139.112 (attributed to nopinone), 153.092 ($C_9H_{13}O_2^+$), and 155.107 ($C_9H_{15}O_2^+$). Ozone was added to the reaction chamber 85 minutes after the start of the measurements. Presented points are averaged mixing ratios of 11.5 minutes time periods, which corresponds to the residence time of the air in the reaction chamber.

During β-pinene ozonolysis experiment analysis, we used 10 as threshold for the T-statistic parameter. Since reactions of ozone with contamination on the chamber walls were not constrained by a separate experiment, we applied additional filter by rejecting all species with a yield that was below 0.25%. As a result, among the oxidation products of β-pinene, we observed formaldehyde (detected as $CH_3O^+$, m/z 31.018), acetone (detected as $C_3H_7O^+$, m/z 59.049) and nopinone (detected as $C_9H_{15}O^+$, m/z 139.112 and fragmented as $C_9H_{13}^+$, m/z 121.102). The yields of all observed oxidation products are presented and compared to the yields from literature in Table 2. The comparison indicated that the yields obtained in this study are somewhat lower (except for acetone) than the yields described in literature. The lower yields were potentially caused by (i) the shorter residence time of air in the reaction chamber (11.5 minutes) in comparison with other studies (Arey et al., 1990; Hatakeyama et al., 1991; Orlando et al., 2000; Larsen et al.,

2001; Wisthaler et al., 2001; Jaoui and Kamens, 2003; Lee et al., 2006), (ii) lower β-pinene and ozone mixing ratios, and/or (iii) the absence of an OH scavenger (Aschmann et al., 2002) which would lead to a longer time for the system to reach equilibrium.

Table 2. Molar yields of ozonolysis products of β-pinene obtained in this study and in the literature (Lee et al., 2006[a]; Arey et al., 1990[b]; Hatakeyama et al., 1991[c]; Jaoui and Kamens, 2003[d]; Larsen et al., 2001[e]; Orlando et al., 2000[f]; Wisthaler et al., 2001[g]).

| **Product** | **m/z** | **Formula•$H^+$** | **Yield, % [literature]** | **Yield, % [this work]** |
|---|---|---|---|---|
| formaldehyde | 31.018 | $CH_3O^+$ | 23[e]-54[c] | 5.9 |
| | 33.033 | $CH_4OH^+$ | | 0.35 |
| | 41.038 | $C_3H_5^+$ | | 0.53 |
| | 43.018 | $C_2H_3O^+$ | | 4.17 |
| acetaldehyde | 45.033 | $C_2H_4O$ | 0.6[a] | 1.07 |
| formic acid | 47.013 | $HCOOH_2^+$ | 2.0[f]-38.0[e] | 1.76 |
| | 47.022 | no match | | 0.42 |
| acetone | 59.049 | $C_3H_7O^+$ | 2.0[f]-16.0[g] | 16.9 |
| acetic acid | 61.029 | $C_2H_5O_2^+$ | 1.4[a] | 0.98 |
| | 73.029 | $C_3H_5O_2^+$ | | 0.28 |
| | 83.05 | $C_5H_7O^+$ | | 1.81 |
| | 95.05 | $C_6H_7O^+$ | | 0.67 |
| | 107.085 | $C_8H_{11}^+$ | | 0.26 |
| | 109.065 | $C_7H_9O^+$ | | 0.36 |
| | 109.101 | $C_8H_{13}^+$ | | 0.43 |
| nopinone | 121.102; 139.112 | $C_9H_{15}O^+$ | 15[d]-79[c] | 6.5 |
| | 139.137 | $C_{10}H_{19}^+$ | | 1.23 |
| | 140.114 | no match | | 0.54 |
| m153 | 153.092 | $C_9H_{13}O_2^+$ | 1.9[d]-2.8[a] | 0.35 |
| m155 | 155.105 | $C_9H_{15}O_2^+$ | 0.8[a]-5.3[d] | 0.51 |
| m185 | 185.115 | $C_{10}H_{17}O_3^+$ | 0.1[a]-0.5[d] | 0.26 |

In addition to known compounds, several other compounds were observed, which had not been described previously. These newly observed compounds show the potential of the setup to identify more products of the oxidation of β-pinene, when improved cleaning protocols are followed and background measurements are performed. Finally, we observed that mixing ratios of sticky compounds like formic acid (m/z 47.013) increased slower in the reaction chamber than other compounds (Fig. 14), indicating that a fraction of these products are lost to the walls of the reaction chamber. However, the loss is limited and towards the end of the experiment (~200 min, Fig. 14) the gas phase levels of m/z 47.013 were in equilibrium.

### 2.2.8 Birch seedling experiments

The first experiment (A) was performed on 4-5 August 2012, the second (B) – on 22-23 August 2012 and the third (C) – on 24-25 August 2012. Birch (*Betula pendula*) seedlings were collected with their surrounding sandy soil from a forest close to the Utrecht University campus 1-2 days before the experiments, and placed in 250 mL pots. The seedlings were 1-2 years old. In each experiment, the plant leaves in the large plant chambers had a total dry weight of 4.1-5.3 g, and a total leaf area of 1296-1413 $cm^2$. Due to weather conditions, the soil of seedlings used in experiment C was very dry. After transfer to the lab, the seedlings were placed next to the large plant chambers, where the TL-D lamps produced light levels of 130-150 $\mu mol/m^2/s$ PAR with a light period from 7 am till 11 pm LT (16 h light, 8 h dark). Day and night temperatures in the large plant chambers were stable and equal to 25.7±0.1 and 22.0±0.1 ºC, respectively. Relative humidity was 40-60%. Three plants were put into each large plant chamber. After the lids were closed the air flow of 2.5 L/min was maintained for 30 minutes before the start of the experiment to allow plant emissions to stabilize. Some water condensation was observed in the plant chambers several hours after the start of the experiments.

After the experiment, leaves were harvested, fresh weight was measured and leaf area was determined with a Li-3100 Area Meter (Lincoln, Nebraska, USA). Dry weight was measured after placing the leaves in an oven at 70 $^oC$ for at least 48 hours.

Before experiments B and C, the reaction chamber was pre-cleaned overnight by flushing with purified air containing ozone mixing ratios of ~430 nmol/mol. To check if chambers were clean, background measurements (with purified air) of empty plant and reaction chambers were made. The experiments were performed according to the measurement cycle described in section 2.2.4.

### 2.3.1 Emission rates of birch seedlings

Emission rates (ER) of the birch seedlings were calculated according to eq. 2.2:

$$ER = \frac{[VOC]*F_{cham}}{DW} \quad (2.2)$$

Where [VOC] is the mixing ratio (in nmol/mol, with subtracted background), $F_{cham}$ is the air flow through the large plant chambers in mol/h, and DW is the leaf dry weight of the measured plants in g. The resulting emission rate has the unit of nmol/g(DW)/h. As a background we used the mixing ratios of species in the purified air supplied into the large plant chambers. All three experiments were used to calculate emission rates during the day (from the start of the experiment till 10 pm and from 9 am till the end of the experiment) and night (from 12 pm till 6 am).

During emission rates analysis as threshold for the T-statistic parameter we used 2.8. Consequently, a broad spectrum of the emitted compounds was observed indicating the good sensitivity of the system even towards the compounds emitted in low quantities during the day as well as during the night (Table 3). The observed monoterpene emission rates (0.69 nmol/g/h or 93.9 ng/g/h) were similar to rates reported by König et al. (1995) (101.1 ng/g/h). However, they were significantly lower than some of the rates reported by Hakola et al. (1998) (51-12469 ng/g/h) which could be explained by two factors. First, growth stage of plants strongly influences plant emission potentials and depends on a period of the year. Second, the lower light levels used in the current study would cause lower emissions.

Table 3. Average night and day emission rates of birch seedlings. All reported compounds have statistically significant emissions. Daytime light levels were 130-150 µmol/m$^2$/s PAR. Day and night temperatures in the large plant chambers were 25.7±0.1 and 22.0±0.1 ºC, respectively; '-' corresponds to no emission at night.

| Compound or m/z | Formula•H+ | Night emissions, nmol/h/g ± SD | Day emissions, nmol/h/g ± SD |
|---|---|---|---|
| 41.038 | $C_3H_5^+$ | 0.37 ± 0.13 | 0.68 ± 0.16 |
| 43.018 | $C_2H_3O^+$ | 0.64 ± 0.24 | 1.42 ± 0.36 |
| 43.054 | $C_3H_7^+$ | 0.14 ± 0.06 | 0.29 ± 0.07 |
| 45.033 | $C_2H_5O^+$ | 1.46 ± 0.64 | 3.35 ± 1.03 |
| 59.049 | $C_3H_7O^+$ | 1.55 ± 0.33 | 3.26 ± 0.89 |
| 61.029 | $C_2H_5O_2^+$ | 0.20 ± 0.18 | 0.39 ± 0.21 |
| 63.044 | $C_2H_7O_2^+$ | 0.06 ± 0.05 | 0.12 ± 0.06 |
| 69.07 | $C_5H_9^+$ | - | 0.15 ± 0.08 |
| 71.049 | $C_4H_7O^+$ | 0.17 ± 0.08 | 0.56 ± 0.29 |
| 71.085 | $C_5H_{11}^+$ | - | 0.08 ± 0.03 |
| 85.064 | $C_5H_9O^+$ | - | 0.23 ± 0.10 |
| 87.045 | $C_4H_7O_2^+$ | - | 0.10 ± 0.03 |
| 87.081 | $C_5H_{11}O^+$ | - | 0.10 ± 0.04 |
| monoterpenes | $C_{10}H_{17}^+$ | 0.22 ± 0.29 | 0.69 ± 0.53 |

The observed night time emissions for several species likely originate from the soil or pot, as *Betula pendula* leaf emissions have been shown to originate only from de novo production in response to light (Ghirardo et al., 2010). Covering pots with plants around the plant stem with Teflon film might exclude observed nocturnal emissions. The use of the small plant chambers (where no pots and roots are enclosed in the plant chamber) would exclude confounding emissions from the pot and/or soil in future experiments.

### 2.3.2 Ozonolysis of birch emissions

Ozonolysis of the birch seedling emissions was performed by ozone additions into the reaction chamber (see section 2.2.4). Yields of the ozonolysis products were calculated according to Eq. 2.3:

$$yield = \frac{[product]_{after} - [product]_0}{[monoterpenes]_0 - [monoterpenes]_{after}} \quad (2.3)$$

Where $[product]_{after}$ and $[product]_0$ are the mixing ratios (in nmol/mol) of the product after and before the ozone addition, and $[monoterpenes]_{after}$ and $[monoterpenes]_0$ - the mixing ratios (in nmol/mol) of monoterpenes after and before ozone addition, respectively.

During further analysis we used 3 as threshold for the T-statistic parameter. As contamination of the chamber walls was an issue for these experiments, the following two additional criteria had to be satisfied (further called 'filters'): a) the night time yield had to be smaller than the yield during the following day; b) the change in the mixing ratio upon ozonolysis had to be above 27 pmol/mol (which corresponds to the detection limit of PTR-TOF-MS).

Fig. 15 shows the course of the measured ozone and monoterpene mixing ratios. Minimum monoterpene mixing ratios and maximum ozone mixing ratios were observed at the same time in the reaction chamber demonstrating that chemical reactions with ozone were the cause of monoterpenes depletion (Atkinson and Arey, 2003). We modeled the monoterpene mixing ratios in the reaction chamber during the period shown in Fig. 15 in order to check if the degradation rate of monoterpenes was in agreement with the measured ozonolysis rate constants of the observed monoterpenes emitted from the birch seedlings. The initial monoterpenes mixing ratio, the mixing ratio of ozone, and first order kinetics were used. The initial monoterpenes mixing ratio was attributed to individual monoterpenes by using the information from the chromatogram shown in Fig. 13D. The relative fractions were 0.28, 0.47, and 0.25 for α-pinene, d-limonene, and β-phellandrene, respectively. The reaction rates for these compounds with ozone have been measured to be $8.7*10^{-17}$, $2.0*10^{-16}$ and $4.8*10^{-17}$ $cm^3$ $molec^{-1}$ $s^{-1}$, respectively (Shorees et al., 1991; Atkinson, 1997). Using this information the degradation of the monoterpenes was calculated separately and the total monoterpene mixing ratio at every time step was calculated as the sum of the individual contributions. The measured and modeled monoterpene mixing ratios (see Fig. 15) agree reasonably well, showing that the general description of the observed chemistry in the reaction chamber is adequate. Somewhat lower measured monoterpene mixing ratios in comparison to the calculated values were associated with the absence of an OH scavenger (Aschmann et al., 2002) in the system which could lead to a faster monoterpene degradation due to reactions with the OH radical.

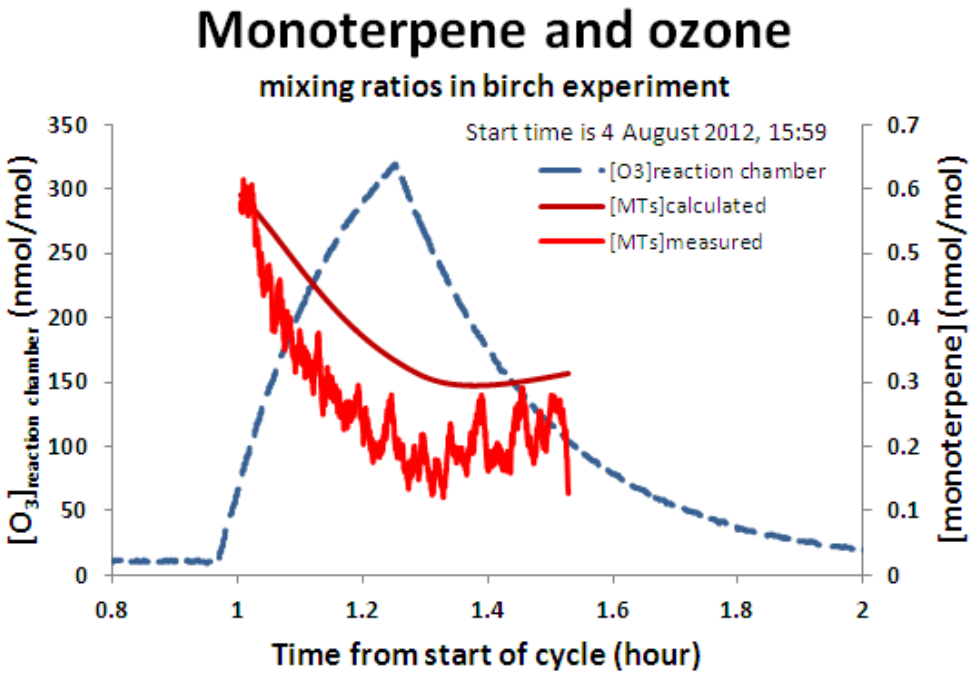


Fig. 15. Measured and modeled monoterpene and ozone profiles. $[O_3]_{reaction\ chamber}$ is the ozone mixing ratios in the reaction chamber. $[MTs]_{measured}$ corresponds to the monoterpene mixing ratios in the reaction chamber; $[MTs]_{calculated}$ corresponds to the monoterpene mixing ratios in the reaction chamber calculated as described in section 2.3.2. Presented measured monoterpene data are averaged over 2 minutes.

Fig. 16 shows averaged monoterpene mixing ratios measured online in the reaction chamber before and after ozone addition in experiment B. The decrease of monoterpene signal during/after ozonolysis as shown in Fig. 15 and described above was well reproducible. Due to the low primary signal the sensitivity of the instrument during experiment B was rather low which caused the detection of only few ions produced during the ozonolysis. Despite the reasonable understanding of the chemistry happening in the reaction chamber it was difficult to identify ozonolysis products from experiments A-C. The reaction chamber was not well cleaned before the start of experiment A and ozonolysis products were also from contamination, i.e. reactive organic species sticking to the walls of the reaction chamber system. For example, during experiment A the production of m/z 61.029 (calculated as a difference in mixing ratios for an ion in the reaction chamber with and without ozone added) during the night was higher than during the following day, despite much lower monoterpene levels during the night. This indicated a

significant contribution from contamination to the signal of the ion, and in experiment A a similar behavior was observed for many other ions. In the experiments B and C the proper cleaning procedure was applied, therefore the above mentioned problems were not encountered. The change in monoterpenes mixing ratio upon the ozone addition was below the detection limit of PTR-TOF-MS due to very low plant emissions in experiment C. Therefore, it was not possible to calculate the yields for experiment C and apply the filter (a).

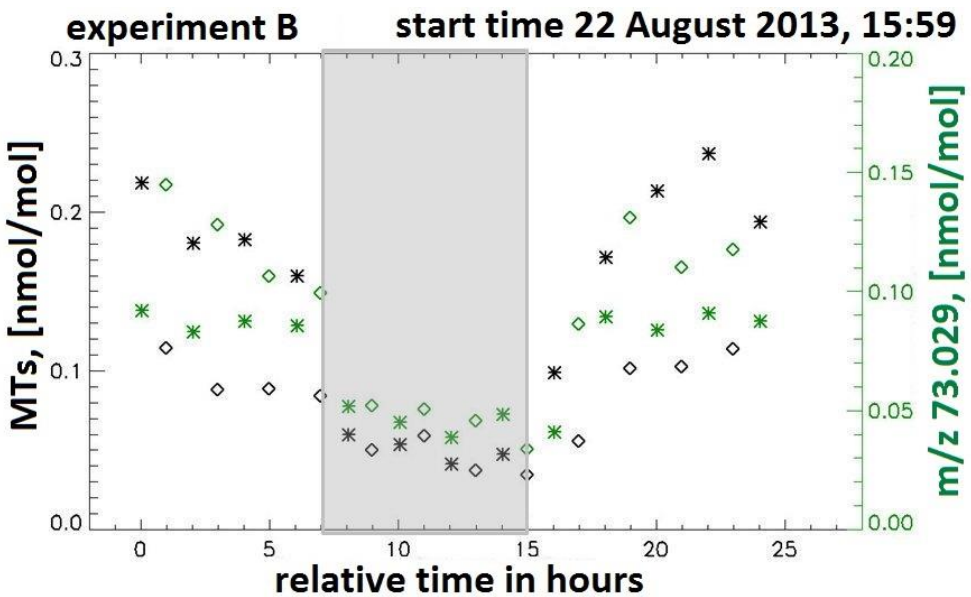


Fig. 16. Online measured mixing ratios of monoterpenes (MTs) and m/z 73.029 in the reaction chamber without ozone addition (asterisks) and during/after ozone addition (diamonds), experiment B. The shaded area indicates the dark period.

In order to overcome these issues the above mentioned filters were developed. Initially we detected 193 ions during experiments A, B and C. Of these, 43 and 60 ions passed the Student's t-test in experiment A and B, respectively. None of the 43 ions from experiment A and only 2 ions from the 60 ions from experiment B passed the additional filters (a) and (b): m/z 47.048 (corresponding to the molecular formula $C_2H_7O^+$) with a molar yield 25.9±9.8% and m/z 73.029 (corresponding to the molecular formula $C_3H_5O_2^+$) with a molar yield 29.5±8.2%.

Despite the low number of detected ozonolysis products, the above mentioned experiments demonstrated the capability of the system to detect ozonolysis products even at low mixing ratios of the parent compounds which can be improved by better reaction chamber pre-cleaning protocols and better (standard) PTR-TOF-MS performance, in which case the number of ions removed by filters (a) and (b) would be much reduced.

### 2.3.3 *Arabidopsis* experiments

*Arabidopsis thaliana* Col-0 plants were stratified (dark, 4 ºC, 3 days) and subsequently grown in soil (8 h light, 16 h dark, 160 μmol $m^{-2}$ $s^{-1}$ PAR, 20±2 ºC, 70% RH). After 10 days, seedlings were transferred to individual 70 mL pots. Four-week old plants were transferred to the plant chamber setup (same light period) and allowed to acclimatize before they were placed into the small plant chambers. The UV-B lamp was turned on from 10 am till 2 pm LT at an intensity of 0.1 W $m^{-2}$, so that the plant in small plant chamber #2 (with quartz lid) was exposed to UV-B light for four hours, while the plant in #1 (with glass lid) was not. We observed higher emissions of *Arabidopsis* plants upon UV-B exposure for several compounds. Fig. 17 shows the average emission of m/z 61.029 during the 4-hour UV-B exposure period in three individual experiments, as an example. This shows that changes in BVOC emissions upon UV-B exposure can be induced for the genetic model plant species *Arabidopsis thaliana*.

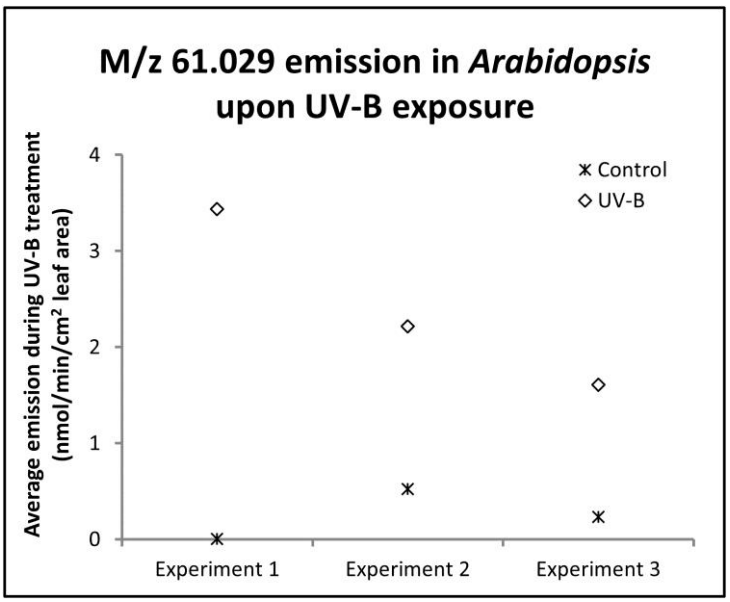


Fig. 17. Arabidopsis thaliana emissions of m/z 61.029 during a 4-hour UV-B exposure period in exposed and control plants. Four-week old plants of the ecotype Col-0 were used. Over the three individual experiment shown, average emissions of UV-treated plants were significantly higher than emissions of control plants (Student's t-test, p=0.047).

## 2.4 Conclusions

The setup to measure impact of pollution on plant emissions was tested and first results are shown to demonstrate the performance. In the β-pinene ozonolysis experiment the expected products were observed, although with somewhat lower yields than described in the literature. In the experiments with real plant emissions, mixing ratios in the large plant chambers and the reaction chamber were shown to generally coincide, showing good quantitative transfer of the VOCs between these components of the setup.

The sampling efficiency of the GC system has been tested. The recovery factors were within the range of 0.71 - 1.38, indicating that cryogenic sampling and the transfer through the GC system is adequate. The added value of the GC part of the system was clear from the analysis of birch seedling emissions, where it allowed us to distinguish three specific monoterpenes within the birch monoterpene emissions.

We performed experiments with birch seedlings and found emission of 14 species. The observed day time emission rates are in agreement with rates observed by König et al. (1995) and are lower than some rates observed by Hakola et al.(1998). The latter is likely caused by the difference in growth stage of the used plants and the fact that latter measurements were performed in the field, thus with higher light intensities. Addition of ozone to the birch seedling emissions resulted in decreased monoterpene mixing ratios. The modeled monoterpene mixing ratios in the reaction chamber agreed reasonably well with the measured levels. Our results show that our setup is capable of detecting ozonolysis products at low levels (<1 nmol/mol) of biogenic emissions, although few ozonolysis products were observed. The experiments performed with Arabidopsis thaliana plants using the small plant chambers and UV-B lamp show that our setup can also be used to study volatile emission responses upon UV-B, even in small plants like Arabidopsis. This opens up a range of possibilities to study the biological mechanisms underpinning plant volatile emissions, since there is a vast array of mutants and genetic information available on this important plant model species. The operation of the setup thus is flexible and the use of optional plant chambers allows for a broad spectrum of experiments. E.g., the discrepancy between the observed and predicted chemical loss of ozone via reactions with plant emissions, the impact of pollution on plant emissions can be studied. The full automatization of the system allows easy-to-perform long- and short-term measurements.

Further improvements and enhancements of the experimental setup include: a) attaching leaf thermocouples to plant leaves and including fans in the chambers; b) increasing light intensity in the plant chambers through for example LEDs, which cause lower heating than conventional lamps, to obtain plant VOC emissions that are more similar to those under natural conditions; c) installing a system to control OH and NOx mixing ratios in the reaction chamber, so that ozonolysis under NOx/VOC limiting conditions can be studied; and d) adding UV light to the reaction chamber, so that ozone yield from photochemical ozone production from plant emissions can be measured.

# Chapter 3: Offline thermal-desorption proton-transfer-reaction mass spectrometry to study composition of organic aerosol

**J. Timkovsky, U. Dusek, J.S. Henzing, T.L. Kuipers, T. Röckmann, and R. Holzinger**

Published in Journal of Aerosol Science, 79, 1-14 doi: 10.1016/j.jaerosci.2014.08.010, 2015.

## Abstract

We present a novel approach to study the organic composition of aerosol filter samples using thermal-desorption proton-transfer-reaction mass spectrometry (TD-PTR-MS) in the laboratory. The method is tested and validated based on the comparison with in situ TD-PTR-MS measurements. In general, we observe correspondence within the levels of uncertainty between in situ and offline TD-PTR-MS measurements for compounds desorbing at temperatures above 100°C and for quartz fiber filters that were sampled for more than one day. Positive sampling artifacts (50–80%, with respect to the in situ measurements) from adsorption of semivolatile organic gas phase compounds are apparent on filters sampled for one day. Detailed chemical analysis shows that these positive sampling artifacts are likely caused by primary emissions that have not been strongly oxidized. Negative sampling artifacts (7–35%, with respect to the in situ measurements) are observed for most filters sampled for two and three days, and potentially caused by incomplete desorption of aerosols (in particular, nitrogen-containing organics) from the filters during the offline measurements and chemical reactions on the filters.

## 3.1 Introduction

Atmospheric aerosols have been studied intensively because of their impact on climate and their health effects. Organic aerosol (OA) typically accounts for 20 to 90% of the total aerosol mass (Kanakidou et al., 2005). The chemical composition of organic aerosol is very complex and has not been resolved completely at a molecular level. It has been characterized using a suite of online and in situ instruments in field studies: for example, aerosol mass spectrometer (AMS) (e.g., Jayne et al., 2000), micro-orifice volatilization impactor coupled to a chemical ionization mass spectrometer (MOVI-CIMS) (e.g., Yatavelli et al., 2010), particle-into-liquid sampler (PILS) (e.g., Weber et al., 2001), filter inlet for gases and aerosols (FIGAERO) (Lopez-Hilfiker et al., 2014), in situ thermal-desorption proton-transfer-reaction mass spectrometer (TD-PTR-MS) (e.g., Holzinger et al., 2010a) and thermal desorption aerosol gas chromatograph/mass spectrometer (TAG) (Williams et al., 2006). These in situ methods are powerful tools to get information on aerosol composition, but field studies using these instruments are expensive and often can cover only limited time periods.

In order to be able to perform long-term aerosol measurements at low cost, sampling of aerosol on filters with offline analysis in the laboratory is often used (e.g., ten Brink et al., 2004; Subramanian et al., 2004; Viana et al., 2006; Viana et al.,2007). Among the advantages of offline methods are easy implementation of sampling and the possibility to sample a large volume of air, which allows for a low detection limit. Furthermore, filter samples can be stored and measured with offline methods later, whereas online aerosol composition data cannot be obtained or re-measured after a field campaign is over. Among the disadvantages of organic aerosol sampling on filters are complicated sampling artifacts. Two principal types of artifacts have been observed: positive (i.e. the aerosol concentrations determined based on the offline technique are overestimated) and negative (the corresponding concentrations are underestimated).

Positive artifacts can be caused by the adsorption of organic vapors on the filters and are difficult to quantify (Turpin et al., 2000), because they depend on sampling time, location and face velocity (Mcdow & Huntzicker, 1990; Turpin et al., 1994; Subramanian et al., 2004). Moreover, it was shown that filters manufactured by the same company, but having different lot number, exhibit different organic vapor adsorption capacity (Kirchstetter et al., 2001). Negative artifacts are caused by volatilization of compounds that have been already collected on filters, e.g. relatively light polycyclic aromatic hydrocarbons (PAHs) (Coutant et al., 1988).

Additionally, Schauer et al. (2003) showed that chemical reactions on the filters can cause a negative artifact for measurements of particle-bound PAHs in the atmosphere (up to 100% underestimation).

Both negative and positive artifacts are particularly influenced by semivolatile organic compounds (SVOCs), which partition between the gas and the condensed phases. Lipsky et al. (2006) showed that the degree of dilution strongly influences the partitioning of SVOCs in diesel exhaust. They discovered that SVOCs tend to be in the gas phase when the exhaust is diluted (causing negative artifacts on filter samples), and the SVOCs tend to be in the condensed phase when exhaust is undiluted (causing positive artifacts). Some attempts have been made to quantify the partitioning of SVOCs, but it is problematic to apply this quantification to real-atmosphere conditions (e.g., Mader & Pankow, 2001).

Attempts to correct for the artifacts using field blanks, backup filters and denuders have been performed. Nevertheless, the filter material itself influences the magnitude of sampling artifacts (Turpin et al., 2000). In general, quartz fiber filters are used for aerosol sampling due to their high temperature resistance. The latter is needed for organic carbon measurements, which require high temperatures for complete desorption. However, high positive artifacts are observed for the quartz filters due to their high specific area and consequently high gas adsorption. As an alternative, the use of Teflon filters is possible with lower specific area. On the other hand, these filters cannot withstand high temperatures needed to desorb most of OA (Turpin et al., 2000). The use of a quartz backup filter along with a quartz front filter is common. However, e.g., Watson et al. (2009) discovered in an extensive study that the use of backup filters (and field blanks) does not fully represent filter sampling artifacts. Viana et al. (2006) showed that the use of a diffusion denuder might reduce organic carbon (OC) mass observed without a denuder by 34%, therefore correcting for positive artifacts. However, they also found that the use of such a denuder does not provide a good comparability between high- and low-volume filter samplers.

While multiple studies have been performed to examine total organic carbon artifacts, there is only a limited number of investigations where artifacts are studied along with the chemical composition of OA. For example, Lambe et al. (2010) performed more detailed studies on the chemical composition of organic aerosols sampled on filters. They compared GC-MS analysis of organic aerosol desorbed from filter samples to in situ TAG measurements for a limited set of compounds (n-alkanes, PAHs, and hopanes). Based on the ambient air

measurements they found reasonable agreement for hopanes ($r^2$=0.55-0.95, slope=1.0-1.7) and PAHs ($r^2$=0.58-0.97, slope=0.8-1.0). However, for n-alkanes (C27-C32) the agreement was poor: $r^2$=0.17-0.85, slope=0.4-1.7, and the exact reason for this was not established.

The objectives of this study were (i) to introduce and validate a new offline analytical technique based on quartz fiber filter sampling and subsequent analysis by thermal-desorption proton-transfer-reaction mass-spectrometry (TD-PTR-MS) and (ii) to use this method to investigate some filter sampling artifacts in more detail. We evaluate and characterize the new offline method by comparison with in situ TD-PTR-MS measurements (Holzinger et al., 2010a). The in situ TD-PTR-MS measurements and filter sampling were performed at the same time and location and in both analyses the same instrument (PTR-TOF-MS) was used, facilitating direct comparison of the two datasets.

## 3.2 Experimental methods

### 3.2.1 Measurement campaign

The measurement campaign for comparison of the in situ TD-PTR-MS, the filter-based TD-PTR-MS (referred to as 'offline' method hereafter) and the Scanning Mobility Particle Sizer (SPMS) methods took place from 8 February 2011 till 7 March 2011 at the Cabauw Experimental Site for Atmospheric Research (CESAR)[1] about 20 km south-west of the city of Utrecht in the Netherlands (51.971 °N, 4.927 °E). The inlet for the in situ measurements was located at the height of ~5 m above the ground and a high volume filter sampler was located directly on the ground and sampled 2 m above the ground at a distance of ~4 m from the TD-PTR-MS inlet. The inlet of the SMPS was located at 60 m height on the Cabauw tall tower.

During the campaign 7 filters (CA5, CA6, CA10-CA13, CA15) and two field blanks (CA3 and CA14) were collected. The sampling times for the filters are shown in Table 4. The air mass history of the various air samples was evaluated by calculating 72h back trajectories using the model HYSPLIT (Draxler & Rolph, 2013; Rolph, 2013). During the campaign different synoptic conditions were encountered, which are generally characterized by the wind directions, which are

[1] http://www.cesar-observatory.nl/

indicated in Table 4. The offline measurements were performed in the laboratory within one month after the field campaign (end of March, 2011).

Table 4. Time periods during which the filters were located in the field. All filters, except for field blanks, are in bold and the respective sampling time periods are shown. The number of replicas per filter measured in the laboratory is shown. In case the main wind direction changed during sampling, 'A' corresponds to the first half of the sampling and 'B' – to the second half.

| Filter# | Sampling period | Sampling duration, h | # of replicas | Wind direction | Ambient air conditions |
|---|---|---|---|---|---|
| CA3 | 11 February 2011 ~14:00 - 17 February 2011 ~14:00 | 0 | 3 | | |
| **CA5** | **15 February 2011 14:00 - 16 February 2011 14:00** | **24** | **3** | **South westerly** | **Normal** |
| **CA6** | **16 February 2011 14:00 - 17 February 2011 14:00** | **24** | **3** | **South easterly** | **Normal** |
| **CA10** | **23 February 2011 13:15 - 25 February 2011 13:15** | **48** | **3** | **A.Westerly;B.Southerly** | **Normal** |
| **CA11** | **25 February 2011 13:15 - 27 February 2011 13:15** | **48** | **3** | **A.North westerly;B.South westerly** | **Mixed** |
| **CA12** | **27 February 2011 14:15 - 1 March 2011 14:15** | **48** | **3** | **Easterly** | **Polluted** |
| **CA13** | **1 March 2011 13:15 - 4 March 2011 13:15** | **72** | **1** | **Easterly** | **Polluted** |
| CA14 | 1 March 2011 ~13:00 - 4 March 2011 ~13:00 | 0 | 2 | | |
| **CA15** | **4 March 2011 14:52 - 7 March 2011 14:52** | **72** | **3** | **Northerly** | **Mixed** |

### 3.2.2 Instrument description

The measurements were performed using a standard PTR-TOF8000 instrument (Ionicon Analytik GmbH, Austria, from here on referred to as 'PTR-MS'), which has been described previously (Jordan et al., 2009; Graus et al., 2010). In short, this instrument allows for precise measurements of volatile organic compounds (VOCs) in air or nitrogen. The soft chemical ionization using $H_3O^+$ ions to protonate the VOCs is a proven technique of ionization with limited fragmentation. The time-of-flight mass spectrometer allows for a high mass resolution ($m/\Delta m \sim 4000$). Therefore, ions with differences in m/z bigger than ~30 mDa (depending on the mass value) can be distinguished (e.g., m/z 69.034 and m/z 69.070) and corresponding empirical formulas ($C_4H_5O^+$ and $C_5H_9^+$, respectively) can be attributed. The recorded mass spectra covered a mass range 15 - 1157 Da. 83340 individual mass spectra were averaged over time to obtain a time resolution of 5 s.

The general settings of the PTR-MS instrument were equal for both setups: drift tube temperature, 120 ˚C, inlet tube temperature, 180 ˚C, drift tube pressure, 2.3-2.5 hPa; ion source voltages, Us = 120-140 V, Uso = 92 V; E/N, 125-127 Td; extraction voltage at the end of the drift tube, Udx=24 V. The ion source current was kept between 4 and 5 mA and a water flow of 3.5-4 mL/min (unless otherwise stated volume flow rates refer to standard conditions: 1013.25 hPa, 273.15 K) was provided to the ion source. The intensity of the primary $H_3O^+$ ion signal (detected

at m/z 21.023) during all PTR-MS measurements was higher than 2.5 x $10^5$counts per second (cps) which ensured sensitivities of order of 10 cps/ppb.

### 3.2.2a The in situ TD-PTR-MS method

The in situ TD-PTR-MS setup consists of an aerosol inlet system coupled to the PTR-MS (Fig. 18A). It has been described in detail previously (Holzinger et al., 2010a). Briefly, ambient air was sampled through the copper inlet with a PM2.5 pre-cutoff. The sampled air passed through a humidifier and the particles were collected on the Collection-Thermal-Desorption (CTD) cell. The CTD cell is specified to sample particles in the size range 0.07-2 μm at relative humidity levels above 70% (Holzinger et al., 2010a). With respect to filter sampling the collection efficiency of in situ TD-PTR-MS is lower and therefore we expect that concentrations measured with the in situ technique are also lower (depending on the actual size distribution this may be 10-20%, but rarely above 30%). After collection, the particles were desorbed by heating up the CTD cell in steps of 50 ˚C for a duration of 3 min, starting at 50 ˚C and going up to 350 ˚C. A flow of nitrogen (ultrapure nitrogen, 5.7 purity, Air Products) transferred the desorbed species to the PTR-MS. As a result a thermogram was obtained, defined as a measured ion signal intensity profile over a range of temperatures.

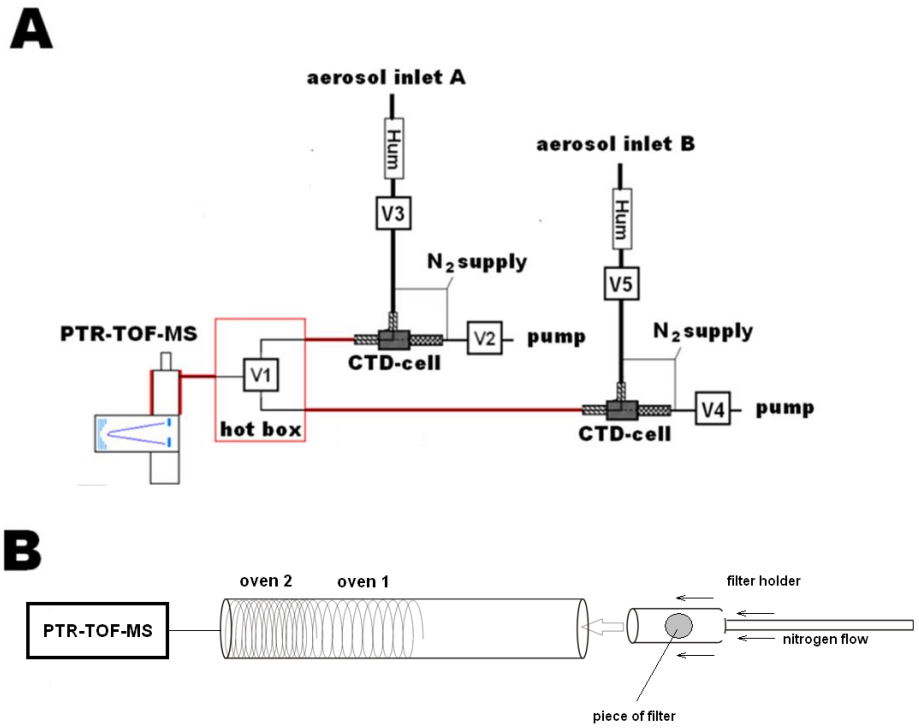


Fig. 18. The in situ (A) and offline (B) TD-PTR-MS setups. The following valves are present on scheme A: V1 – allows switching between two aerosol inlets, V2-V5 – allow switching between sampling and measuring modes for inlet A and B.

The system was equipped with two identical aerosol inlets (A and B). This setup allowed aerosol sampling with one inlet while analyzing the aerosols collected with the second inlet. The collection time for both inlets was 30 min. The whole in situ TD-PTR-MS measurement cycle is shown in Fig. 19, m/z 85.028 is used as an example. The instrument background was measured by passing ambient air through a Teflon membrane filter (Zefluor 2.0 μm, Pall Corp.) located in the system (one filter per inlet). The filters were changed once per week during the campaign. Background measurements were performed once per three measurements (Fig. 19). In a thermogram measurement we observed signals corresponding to the compounds that are volatilized at the various temperature steps between 100 and 350 ˚C. Normally, a signal slightly above or at background

level was observed at 50 ˚C, indicating that the collected aerosols did not significantly desorb at this temperature.

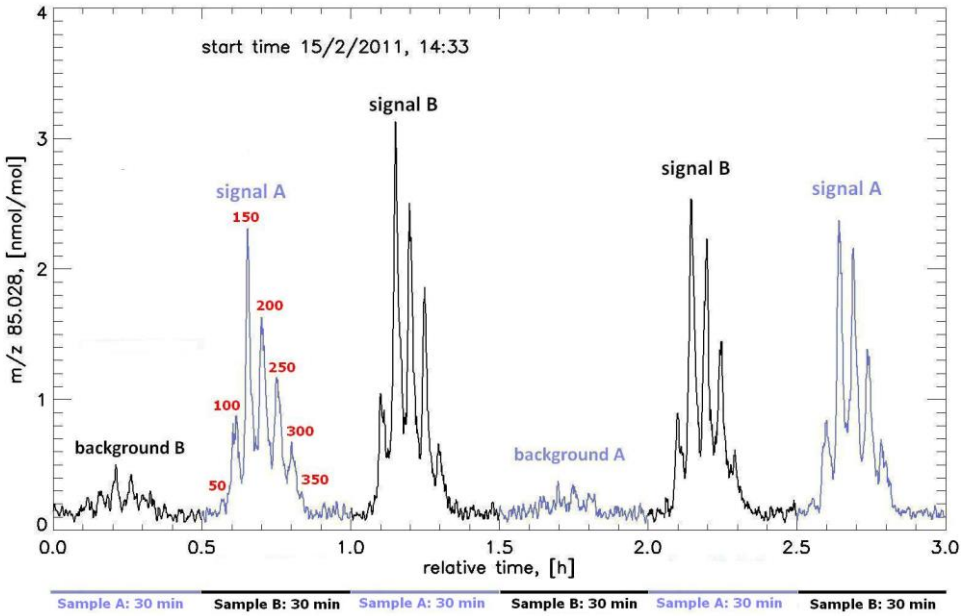


Fig. 19. The measurement cycle of the in situ TD-PTR-MS instrument; m/z 85.028 is used as an example. The time period during which sampling occurs for both inlets is indicated by the lines below the axis. The temperature steps (in degrees Celsius) are indicated in red for inlet A as an example. The aerosol signals from inlet A and B are indicated as 'signal A' and 'signal B', respectively. The background signals from inlet A and B are indicated as 'background A' and 'background B', respectively.

### 3.2.2b The offline method

*Filter sampling*

PM2.5 filter samples were collected on Whatman QMA quartz fiber filters using a high-volume (HiVol) filter sampler (model DHA 80) with a sampling flow of 500 L/min. The filter diameter was 15 cm, but only a part with a diameter of 14 cm was exposed to the air stream. The filters and handling equipment were carefully prepared in order to avoid contamination. The filters were preheated at 800 °C in an oven overnight, the filter holder was cleaned with ethanol, the handling tweezers were cleaned with acetone followed by ethanol; the aluminum foil used to store the filters before and after sampling was preheated in the oven at 500 ˚C for 3 hours. After the sampling was finished filters were brought to the laboratory and stored in the freezer at -20 ˚C.

During the field campaign, two one-day filters, three two-day filters and two three-day filters were collected. Also, two field blanks were obtained. The field blanks were treated as the regular filters but instead of being exposed to the air stream, they were kept in the filter stacks of the sampler for three and six days, respectively. The amount on the field blanks was small for most compounds compared to the amount on real samples (on average below 6%).

*Thermal desorption setup in the laboratory*

The oven setup for the analysis of filter aliquots consisted of a cylindrical quartz glass tube (ID = 8.8 mm) surrounded by two ovens (Fig. 18B): oven 1 was 10 cm in length and oven 2 was 15 cm in length. The nitrogen flow through the oven setup was 466 mL/min (ultrapure nitrogen, 5.7 purity, Airproducts) and controlled by a thermal mass-flow controller (MKS Instruments, Germany) with a range of 500 mL/min. A filter piece of 0.39 $cm^2$ was placed in oven 1 using a quartz glass filter holder and the temperature of oven 1 was increased from 100 ˚C to 350 ˚C in steps of 50 ˚C. Every step lasted for 3 min and consisted of a ramp and dwell period of ~10 sec and ~170 sec, respectively. Oven 2 was used as a PTR-MS inlet extension and kept at 180 ˚C (which is equal to the inlet temperature of the PTR-MS) to prevent the condensation of the volatilized gasses. The organic species that evaporated at each temperature step were carried by the flow of nitrogen through the oven setup and a fraction was sampled by the PTR-MS.

### 3.2.2c SMPS measurements

The SMPS instrument was operated with 5 min time resolution and the particle number size distributions covering the diameter range from about 10 nm to 516 nm were measured with a log-equidistant resolution of 70 size bins in this size range. A SMPS (e.g. ten Brink et al., 1983) generally consists of a sequential set-up of an impactor, neutralizer, differential mobility analyzer (DMA) and a condensation particle counter (CPC). The operated SMPS was a modified version of a commercially available instrument (TSI 3034). The hardware and set-up of impactor, neutralizer, DMA and CPC were unchanged including the connecting parts. The software which controls the high voltage in the DMA, the correction for multiple charge, and the inversion algorithm was modified to ensure reliable measurements that are comparable to other European measurements. Additionally, the technical standards for mobility size spectrometers as recommended within ACTRIS, were followed (Wiedensohler et al., 2012).

### 3.2.3 Data treatment

Data evaluation was done with Interactive Data Language (IDL, version 7.0.0, ITT Visual Information Solutions), using custom made routines described by Holzinger et al. (2010b). The in situ TD-PTR-MS and offline data files were analyzed together, and the produced unified mass list contained m/z values of 461 ions observed during the measurements. Based on analysis of the whole dataset, nine m/z values were excluded that were associated with high instrument contamination (217.016, 218.01, 219.047, 219.173, 220.048, 221.060, 221.152, 222.057, 292.921). In addition, m/z values below 40 Da (except for m/z 31.017 and 33.033) and m/z values associated with inorganic ions ($NO_2^+$ and $(H_2O)_2H_3O^+$) were excluded. After these corrections the mass list contained 359 organic ions, which were considered for the evaluation presented below. Note that we allowed negative values for the mixing ratios that were sometimes obtained after background subtraction (see below).

Random and systematic uncertainties associated with the collected data were considered. Random uncertainties were calculated according to the procedure described below. Main systematic uncertainties were caused by different gas phase compounds adsorption capacity in the CTD-cell and on the quartz filters, and are approached in the main analyses. Other systematic uncertainties, caused by, e.g., distance between the in situ and offline instruments inlets and different height of the inlets, were not quantified, but their impact is believed to be minor as generally a reasonable agreement between the two datasets was observed.

#### 3.2.3a The in situ TD-PTR-MS data

The mixing ratios of species obtained based on the in situ TD-PTR-MS data were grouped by the desorption temperature (50, 100, 150, 200, 250, 300, and 350 °C), sample type (filtered/unfiltered, i.e. background/aerosol), and inlet (A or B). The mixing ratios for each of these subsets were averaged. The dataset obtained in this way reduces the initial raw data with a 5s time resolution to 30 min time resolution per desorption temperature per sample type per inlet matching the sampling periods on the CTD cell. Due to a problem with the heating element for the CTD cell, there were no measurements through the inlet B during the first half of in situ TD-PTR-MS measurements while filter CA10 was sampled (23 February 2011, 13:15 – 24 February 2011, 16:43). This was taken into account by replacing missing data with the inlet A measurements of the corresponding time period. The further in situ TD-PTR-MS data treatment was done in two different ways (i and ii):

*i. for the comparison with offline data*

The in situ data were averaged over the time periods when filters were collected so that datasets could be directly compared. The median of the background mixing ratios over the filter sampling periods was subtracted from the average aerosol (unfiltered) signal. The mass concentration ($C_{insitu,i}$) of an observed ion 'i' signal at a particular temperature step for a given inlet (A or B) was calculated according to Eq. 3.1:

$$C_{insitu,i} = \left((avg(VMR_{i,samp}) - med(VMR_{i,bgd})\right) \times M_i \times F_{inlet} \times t / S \qquad (3.1)$$

where avg($VMR_{i,samp}$) is the average of the mixing ratios of the ion 'i' over a filter sampling period (in nmol $mol^{-1}$ as measured in the PTR-MS), med($VMR_{i,bgd}$) is the median of the instrument background mixing ratios of the ion 'i' over a filter sampling period (in nmol $mol^{-1}$ as measured in the PTR-MS), $M_i$ is the molecular weight (in g $mol^{-1}$) of ion 'i' (after subtraction of one a.m.u. to account for the molecular mass of the added hydrogen ion), $F_{inlet}$ is the flow through the CTD cell during desorption in mol $min^{-1}$, S is the size of the air sample from which the aerosols were collected (i.e. sampled volume) in $m^3$, and t is the duration of a single temperature step in min. The resulting mass concentration has the unit of ng $m^{-3}$. Finally, the data from inlet A and B were averaged for every ion. As will be shown below, the highest artifacts appeared at the temperature level of 100 ˚C. Therefore, the in situ data were split into two groups based on temperature: group T100 contains organics desorbing at 100 ˚C and group T150-350 contains organics desorbing at 150, 200, 250, 300 and 350 ˚C. For data presented in sections 3.3.2a and 3.3.2c we used m/z bins (bin size 20 Da) and averaged the m/z values of ions within the respective bins. The mass concentrations corresponding to a given m/z bin were the sum of the concentrations of all ions present in the respective mass range.

The uncertainties were up to 20% for the flow through the CTD cell, 4% for the size of a sample and typically less than 10% for the mixing ratios (mostly attributed to counting statistics and the uncertainty in the residence time in the drift tube). Note that the uncertainty in the mixing ratio does not include the uncertainty in the reaction rate constant for proton transfer, which is typically in the range 1-5 x $10^{-9}$ $cm^3$ $s^{-1}$ $molecule^{-1}$ (Zhao and Zhang, 2004) and can thus deviate significantly from the default value (3 x $10^{-9}$ $cm^3$ $s^{-1}$ $molecule^{-1}$) that we used here. However, assuming that the uncertainties in the reaction rate constants at a

particular m/z value are the same for both methods and cancel out, the total uncertainty ($\Delta C_i$) is calculated by means of standard error propagation to be ~22%.

*ii. for the in situ TD-PTR-MS and SMPS data comparison*

Total OA mass concentrations ($OA_{tot}$) for a given time period based on the inlet A and B data and all temperature steps was calculated according to Eq. 3.2. In short, in situ TD-PTR-MS mixing ratios of all considered ions were multiplied by the respective molecular masses and the obtained values were summed up for all considered ions (359 ions). From this the background was subtracted obtained as a sum of the median of the background mixing ratios over a filter sampling period multiplied by the respective molecular masses. The resulting value was multiplied by $F_{inlet}$*t/S, which resulted in total OA mass concentrations $OA_{tot}$ (in ng $m^{-3}$).

$$OA_{tot} = \left( \sum_{i=all\_ions} \sum_{j=all\_Ts} (VMR_{i,j,samp} \times M_i) - \sum_{i=all\_ions} \sum_{j=all\_Ts} (med(VMR_{i,j,bgd}) \times M_i) \right) \times F_{inlet} \times t / S \quad (3.2)$$

where $VMR_{i,j,samp}$ is the mixing ratio (in nmol $mol^{-1}$) of an ion 'i' at a given time and given temperature, med($VMR_{i,j,bgd}$) is the median of the background mixing ratios of an ion 'i' over a filter sampling period for a given temperature (in nmol $mol^{-1}$) and $M_i$ is the molecular weight (in g $mol^{-1}$) of the ion 'i' (minus one a.m.u.); the rest of the parameters are the same as in Eq. 3.1. The resulting total uncertainty of $OA_{tot}$ is calculated by means of standard error propagation to be ~20%.

### 3.2.3b The offline TD-PTR-MS data

Fig. 20 illustrates offline measurements and data treatment for a filter sample and a field blank (m/z 85.028 is used as an example). Similarly to the in situ TD-PTR-MS data treatment, mixing ratios obtained with a 5s time resolution in the offline measurements were averaged over time for every temperature step. Next, the first 1.25 min of the measurements in the oven (before the temperature ramp was started) was averaged for every considered ion and used as instrument background and directly subtracted from the ion signal intensities obtained at other temperature steps. This procedure was applied to both normal filter samples and field blanks. In total, 5 field blank measurements were used: 3 replicas for CA3 and 2 replicas for CA14, all replica measurements were treated equally. The mixing ratio of the ion 'i' for the field blank ($VMR_{i,fb}$) was calculated as a median of the mixing ratios of all field blank measurements at each temperature step.

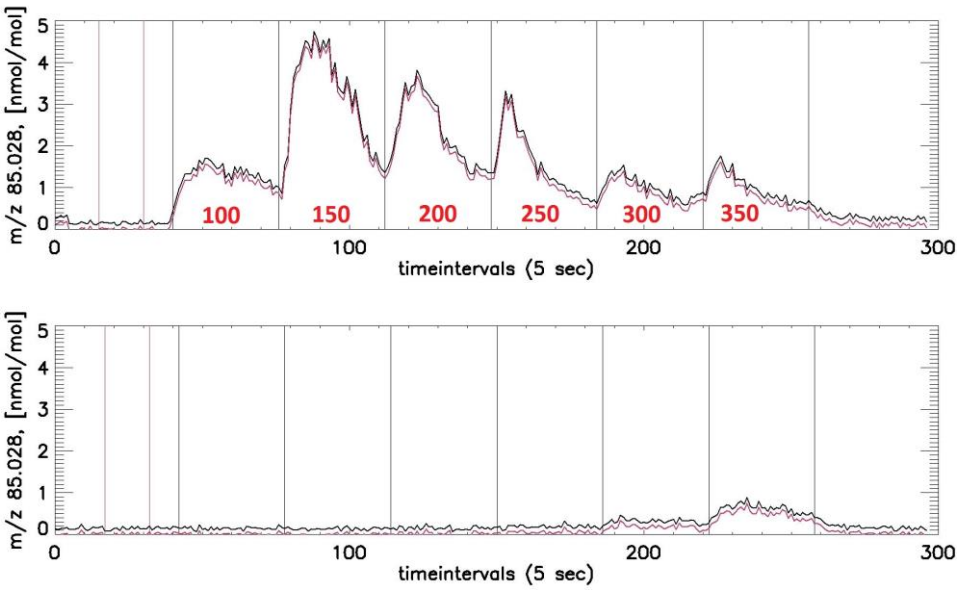


Fig. 20. Example of an offline measurement of m/z 85.028 of the filter CA12 (upper chart) and the field blank CA3 (lower chart). The black line is the original time series and red line is the time series obtained after subtraction of the instrument background (i.e. the mean signal between the first two vertical lines plotted in red). The vertical black lines indicate the integration borders of the temperature steps. The temperature steps (in degrees Celsius) are indicated in red for the upper chart as an example.

For the filter samples, we used Eq. 3.3 to obtain mixing ratio of the ion 'i' ($VMR_i$), corrected for the field blank and instrument background:

$$VMR_i = VMR_{i,0} - VMR_{i,instrbgd} - (VMR_{i,fb} - VMR_{i,instrbgd\_fb}), \qquad (3.3)$$

where $VMR_{i,0}$ is the uncorrected mixing ratio of the ion 'i', and $VMR_{i,fb}$ is the mixing ratio of the ion 'i' on the field blank, $VMR_{i,instrbgd}$ and $VMR_{i,instrbgd\_fb}$ - are the respective background mixing ratios during sample and field blank measurements, all in nmol $mol^{-1}$.

After the field blank and background subtraction, the resulting mixing ratio $VMR_i$ (nmol $mol^{-1}$) was converted to the mass concentration $C_{off,i}$ in ng $m^{-3}$ using Eq. 3.4.

$$C_{off,i} = \frac{VMR_i * M_i * V_{nitrogen}}{V_{samp} * f}, \qquad (3.4)$$

where $VMR_i$ is the mixing ratio obtained in Eq. 3.3 and $M_i$ is the molecular weight of the ion 'i' (minus one a.m.u.), $V_{nitrogen}$ is the volume of nitrogen used for

desorption at a single temperature step in mol, $V_{samp}$ is the sampled air volume in $m^3$, f is the area of the measured filter aliquot divided by the area of the whole filter (fraction of the filter). The resulting mass concentration has the unit of ng $m^{-3}$. All steps mentioned above were done separately for every temperature level and every organic ion, and then the resulted mass concentrations were grouped into group T100 (data obtained at 100 ˚C) and group T150-350 (data obtained at 150, 200, 250, 300 and 350 ˚C) to match the in situ TD-PTR-MS data.

The uncertainties in $VMR_{i,0}$ were calculated by propagating the uncertainties in measured mixing ratios on individual filter replicas (10%) to the average mixing ratio over all filter replicas, which resulted in 6% uncertainty. As above, the uncertainties in the mixing ratios due to the uncertainty in reaction rate constant were not considered (see section 3.2.3a). The uncertainties in the other mixing ratios ($VMR_{i,instrbgd}$, $VMR_{i,fb}$ and $VMR_{i,instrbgd\_fb}$) were neglected as for the most significant ions (comprising on average 80% of the total mass) the signal was higher than the background plus two standard deviations. Therefore, the uncertainties in $VMR_i$ were assumed to be equal to the uncertainties in $VMR_{i,0}$ (6%). The uncertainties were up to 0.7% for the volume of nitrogen, 2% for the sampled volume, 5% for aliquot fraction. This resulted in the maximum total uncertainty of ~8% for the mass concentration of individual ions ($\Delta C_{off,i}$) calculated by means of error propagation.

### 3.2.3c The SMPS data

The raw SMPS data had a time resolution of 5 min and were averaged to match the sampling time of the TD-PTR-MS. In order to transform initial particle size-binned SMPS data (in number of particles per a size bin) into mass concentration B (in ng $m^{-3}$) Eq. 3.5 was used.

$$B = \frac{4}{3}\pi * \left(\frac{D_p}{2}\right)^3 * n_N(D_p) * \rho \quad , \qquad (3.5)$$

where $D_p$ is the bin-central diameter (in μm) and $n_N(D_p)$ is the number of particles per $cm^{-3}$ that have diameter between $D_p$ and $D_p + dD_p$, ρ is the average particle density in g $cm^{-3}$, 1.5. The obtained SMPS aerosol mass concentrations in ng $m^{-3}$ were used to be compared with the in situ TD-PTR-MS mass concentrations.

### 3.2.3d Evaluation of ion weight and chemical composition

In order to perform the analysis based on different classes of chemical compounds, the masses from the mass list were associated with molecular formulas based on the mass library (Holzinger et al., 2010b; Holzinger et al., 2013). The library

contains species with up to 8 atoms of oxygen and up to 2 atoms of nitrogen. Hydrocarbons, species containing 1, 2 and 3 oxygen atoms and nitrogen-containing species were grouped in the following classes of ions: HCs, O-1, O-2, O-3 and N-compounds, respectively. All other species (mostly species that could not be matched) were grouped into the class 'other compounds'. Species belonging to O-1, O-2 or O-3 class contained no nitrogen atoms. Species belonging to N-compounds class could contain oxygen atoms. Total OA mass concentrations of a particular group of ions measured during a filter sampling period k with insitu technique ($OA_{insitu,k}$) and on filters ($OA_{off,k}$) were calculated by summing up OA mass concentrations $C_{insitu,i}$ and $C_{off,i}$ of the ions in the group, respectively.

For 288 of the 359 ion masses more than one chemical formula was possible. In these cases we applied the following rules: if the mass was odd, then the advantage was given to a formula containing only carbon, oxygen and hydrogen. If no such formula could represent a considered mass, then the formula containing nitrogen was chosen. If the mass was even, then in most cases it would attribute to nitrogen- or carbon-13-containing compounds. The preliminary advantage was given to carbon-13-containing compounds. But for this formula to be selected, the signal of the ion had to be lower than the signal of the ion with m/z-1 multiplied by the number of carbons contained in the compound and the factor 0.022. Otherwise, the formula containing nitrogen was chosen. If there were still several formulas after applying the criteria, the formula with the smallest deviation from the detected mass was chosen.

To compare the measurements of the ion classes mentioned above, the ratio of offline and in situ mass concentrations (R) was calculated as the average of $OA_{off,k}/OA_{insitu,k}$ ratio over all filter sampling periods for the chosen ion class using Eq. 3.6.

$$\mathrm{R} = \mathrm{average}\left(\sum_{k=filters} \frac{\mathrm{OA_{off,k}}}{\mathrm{OA_{insitu,k}}}\right) \tag{3.6}$$

The uncertainty of R (ΔR) was calculated in three steps. In the first step, the uncertainties in $OA_{insitu,k}$ and $OA_{off,k}$ were calculated. The uncertainty of $OA_{insitu,k}$ ($\Delta OA_{insitu,k}$) was calculated using Eq. 3.7.

$$\Delta OA_{insitu,k} = \frac{\sqrt{\sum_{i=ions} \Delta VMR_i'^{\,2} * VMR_i'^{\,2} + 0.042 * \left(\sum_{i=ions} VMR_i'\right)^2}}{\sum_{i=ions} VMR_i'} \tag{3.7}$$

where 'ions' refers to the ions in the chosen class of compounds, $VMR_i'$ is the OA mixing ratio of the ion 'i' averaged over a filter sampling period k with subtracted background (equal to avg($VMR_{i,samp}$)-med($VMR_{i,bgd}$) in Eq 3.1), 0.042 is a factor taking into account uncertainties in the size of a sample and the flow through the CTD cell during desorption (S and $F_{inlet}$ in Eq. 3.1). $\Delta VMR_i'$ is the uncertainty of the OA mixing ratio $VMR_i'$ (3.4%) calculated as follows. First, the uncertainties in the mixing ratios of an individual ion ($\Delta VMR_{i,samp}$, 10%) and ($\Delta VMR_{i,bgd}$, 10%) were propagated to the average mixing ratio over a filter sampling period. Then the squared root of the sum of the resulting relative uncertainties was taken to estimate the uncertainty of $VMR_i'$.

The uncertainty of $OA_{off,k}$ ($\Delta OA_{off,k}$) was calculated using Eq. 3.8.

$$\Delta OA_{off,k} = \frac{\sqrt{\sum_{i=ions} \Delta C_{off,i}{}^2 * C_{off,i}{}^2}}{\sum_{i=ions} C_{off,i}}, \quad (3.8)$$

where 'ions' refers to the ions in the considered class of compounds and $\Delta C_{off,i}$ is the uncertainty of $C_{off,i}$ (8%).

In the second step, the uncertainty of $r_k = \frac{OA_{off,k}}{OA_{insitu,k}}$ for a filter sampling period k ($\Delta r_k$) was calculated as a squared root of the sum of the squared relative uncertainties $\Delta OA_{off,k}$ and $\Delta OA_{insitu,k}$. In the third step, the uncertainty of the average ratio R was calculated using Eq. 3.9.

$$\Delta R = \frac{\sqrt{\sum_{k=N} \Delta r_k{}^2 * (r_k)^2}}{\sum_{k=N} r_k}, \quad (3.9)$$

where N is the number of filter sampling periods considered (7).

## 3.3 Results

### 3.3.1 Comparison of the in situ TD-PTR-MS and SMPS data

In Fig. 21 we compare OA measured by the in situ TD-PTR-MS with the total aerosol mass concentrations (in ng $m^{-3}$) obtained from the SMPS measurements in the time period from 15 February 2011 till 5 March 2011. Overall, the organic mass detected with the TD-PTR-MS constitutes 7% of the aerosol mass detected with the SMPS. The temporal variation of organic and total aerosol mass concentration is similar, and similar clean and polluted periods can be distinguished with both instruments. The correlation coefficient between in situ

TD-PTR-MS data (averaged over both inlets) and SMPS data is 0.54 ($r^2$), indicating that the fraction of the OA in the total aerosol is rather stable over the abovementioned time period. A higher correlation is not expected due to several reasons: (i) the significant contribution of inorganic aerosol to the SMPS signal, (ii) different sampling heights and locations and (iii) different cutoffs for two instruments (2.5 µm for the in situ TD-PTR-MS and 0.5 µm for the SMPS measurements). The correlation coefficient between mass concentrations obtained from inlet A and inlet B data is 0.89 ($r^2$), and the mass concentrations agree within the estimated accuracy of ±30% (Holzinger et al. 2013), indicating a reasonable qualitative and quantitative correspondence between the two inlets.

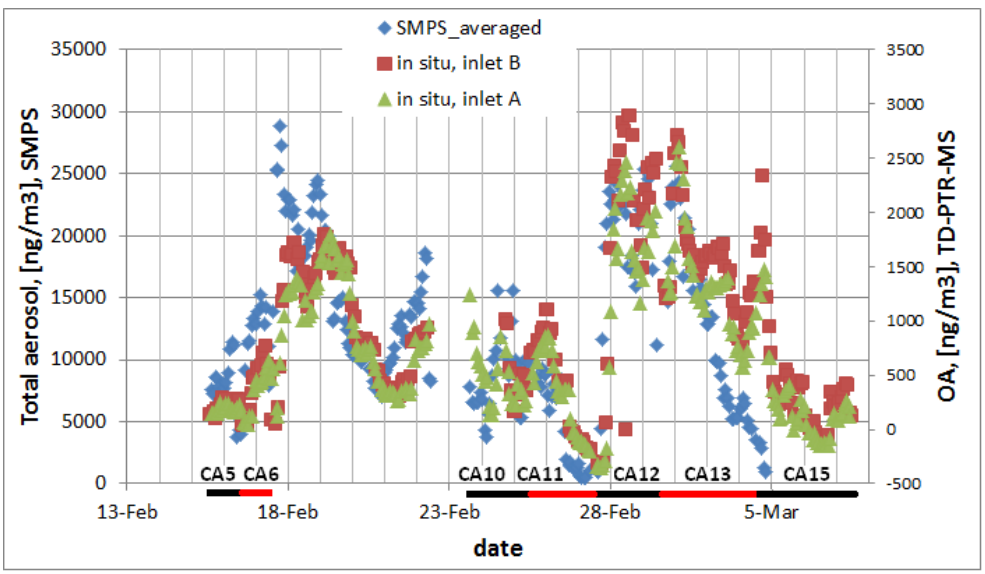


Fig. 21. Comparison of the organic aerosol mass concentrations measured with the in situ TD-PTR-MS technique (inlet A and inlet B) and total aerosol mass concentrations measured with the SMPS method (SMPS_averaged). The sampling periods for the filters are underlined below the x-axis with the respective filter names above. The cutoffs are 2.5 µm for the in situ TD-PTR-MS and 0.5 µm for the SMPS instrument.

### 3.3.2 Comparison of the offline and in situ TD-PTR-MS data

The periods of filter sampling are indicated in Fig. 21. The time periods corresponding to the sampling periods of CA5, CA6, CA10, CA11, CA12, CA13 and CA15 are referred to as t5, t6, t10, t11, t12, t13 and t15, respectively. These

time periods can be separated into three categories depending on the ambient air conditions: normal (t5, t6, t10), polluted (t12, t13) and mixed (t11, t15).

### 3.3.2a Comparison based on different m/z ranges

For the presented analysis, separation of the detected ions into the following three mass ranges has proven to be most indicative: 31 < m/z < 191, 191 < m/z < 291, m/z > 291 Da (Fig. 22). Fig. 22A and B show scatter plots of offline mass concentrations versus in situ TD-PTR-MS mass concentrations for the groups T100 and T150-350 with the 1:1 line shown for reference. For most compounds from group T100 (constituting 0.1-3% of the total OA mass measured with the in situ technique), much higher concentrations are measured by the offline method (see Fig. 22A). A poor correlation ($r^2$ = 0.21) between the offline and the in situ TD-PTR-MS method is observed. The ratio of the total measured OA mass on the filters to the total aerosol mass measured with the in situ TD-PTR-MS (further called 'ratio') is 10.12. Such a high ratio can be explained by the adsorption of organic gas phase compounds on the quartz fiber filters during sampling. This kind of adsorption is much reduced during the in situ TD-PTR-MS sampling, because a significantly smaller surface area is exposed to the air stream and the material onto which air is sampled is more inert. A large fraction of the adsorbed gases evaporates at the lowest desorption temperature of 100 °C. Relatively few compounds from the actual aerosol evaporate at this temperature (100 °C), as seen by the mostly low concentrations in the in situ TD-PTR-MS measurements. Only for a few m/z bins in the mass range m/z > 291 Da (green points, Fig. 22A) the in situ TD-PTR-MS method yields similar or even higher concentrations than the offline method, but these points are mostly in the low concentration range. For the mass range m/z > 291 Da the ratio is 2.47, which is considerably lower than the ratio for all ions (10.12). This suggests that compounds with high molecular weight are less affected by the positive sampling artifact.

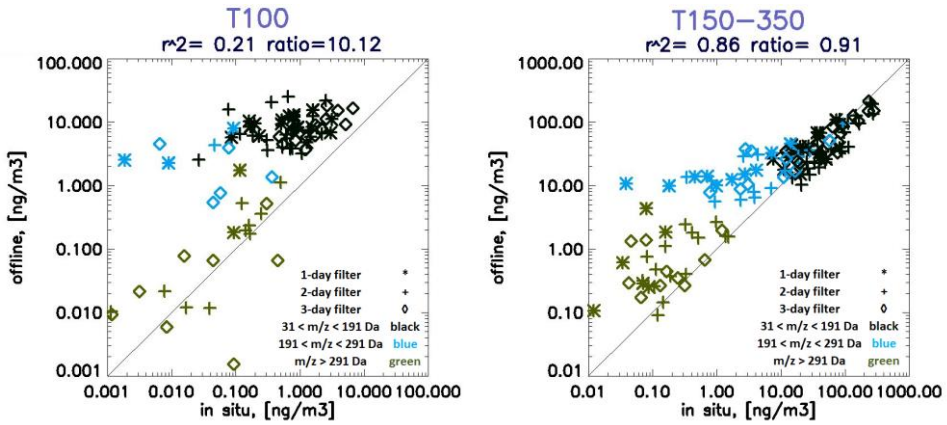


Fig. 22. Correlation plots for the offline and in situ TD-PTR-MS data (shown as 'offline' and 'in situ', respectively): A – group T100 (compounds desorbed at 100 ˚C), B – group T150-350 (compounds desorbed at 150-350 ˚C). Black data points correspond to m/z values in the range 31 < m/z < 191, blue – to m/z values in the range 191 < m/z < 291, green – to m/z values > 291 Da. Asterisks are used to indicate 1-day filters, pluses – 2-day filters, diamonds – 3-day filters.

For compounds in the T150-350 group the correlation between the offline and in situ TD-PTR-MS measurements is high with $r^2$ = 0.86 and the ratio is close to unity (0.91). The ions in the mass range 31 < m/z < 191 Da (black data points) carry the bulk of OA mass and follow closely the 1:1 line, with mass concentrations in the range of 10-300 ng $m^{-3}$. The concentrations of ions in the mass range 191 < m/z < 291 Da (blue data points in Fig. 22B) are typically measured higher with the offline method. In fact, the total concentration of ions in the considered m/z bins is in the range of ~5 to ~100 ng $m^{-3}$ for the offline measurements, while the in situ TD-PTR-MS data exhibit a wider range of ~0.03 to ~100 ng $m^{-3}$. The higher concentrations measured with the offline TD-PTR-MS are again likely caused by the contribution of adsorbed gas phase compounds to the OA signal. Ions detected in the mass range m/z > 291 Da (green data points in Fig. 22B) show mixed features. The concentrations of ions of several m/z bins closely follow the 1:1 line, while ions of other m/z bins exhibit higher concentrations when measured with the offline method. The data points for the ions in this mass range are poorly correlated ($r^2$ = 0.01), and the ratio of 5.23 is much larger than for all ions (0.91). The observed positive artifact for many ions in this group is attributed to adsorption of semivolatile gas phase compounds on the quartz filters, which do not fully desorb at 100 ˚C. Overall, the contribution of ions in the mass range m/z > 291 Da to the total signal is minor (less than 2% of the

measured OA mass) and therefore this group of ions is not considered in the following section.

### 3.3.2b Bulk comparison of total OA and OA in different m/z ranges

The total OA mass concentrations for in situ TD-PTR-MS and offline measurements are calculated for the following mass ranges: all ions, 31 < m/z < 191 Da and 191 < m/z < 291 Da for group T150-350 (Table 5). For the group T100 we calculated only the total concentration of all ions (Table 6).

Table 5. Total measured aerosol concentrations (in ng $m^{-3}$) with the offline and in situ TD-PTR-MS techniques for group T150-350 (compounds desorbed at 150-350 ˚C) for three mass ranges: a) all ions, b) m/z < 191, c) 191 < m/z < 291. Number of days during which air was sampled on filters is indicated. Ratio (offline / in situ) and difference (offline - in situ) are shown as well.

| FILTER ID | *CA5* | *CA6* | **CA10** | **CA11** | **CA12** | CA13 | CA15 |
|---|---|---|---|---|---|---|---|
| a) all ions | | | | | | | |
| offline, ng/m3 | 342.4 | 536.1 | 316.4 | 341.1 | 1237.5 | 1112.9 | 371.5 |
| in situ, ng/m3 | 191.9 | 353.2 | 486.4 | 366.9 | 1543.6 | 1386.6 | 324.9 |
| ratio | 1.8 | 1.5 | 0.7 | 0.9 | 0.8 | 0.8 | 1.1 |
| difference | 150.4 | 182.9 | -170.0 | -25.8 | -306.1 | -273.7 | 46.6 |
| b) 31 < m/z < 191 | | | | | | | |
| offline, ng/m3 | 256.8 | 421.5 | 260.6 | 279.2 | 1011.4 | 953.7 | 305.1 |
| in situ, ng/m3 | 181.7 | 331.8 | 451.9 | 346.9 | 1392.6 | 1292.7 | 307.0 |
| ratio | 1.4 | 1.3 | 0.6 | 0.8 | 0.7 | 0.7 | 1.0 |
| difference | 75.0 | 89.7 | -191.4 | -67.7 | -381.2 | -339.0 | -1.9 |
| c) 191 < m/z < 291 | | | | | | | |
| offline, ng/m3 | 76.0 | 106.5 | 50.6 | 55.0 | 219.5 | 154.9 | 61.7 |
| in situ, ng/m3 | 10.1 | 22.1 | 32.5 | 19.0 | 147.8 | 91.1 | 17.8 |
| ratio | 7.5 | 4.8 | 1.6 | 2.9 | 1.5 | 1.7 | 3.5 |
| difference | 65.9 | 84.4 | 18.2 | 36.0 | 71.8 | 63.8 | 43.9 |
| # of sampling days | 1 | 1 | 2 | 2 | 2 | 3 | 3 |

Table 6. Total measured aerosol concentrations (in ng $m^{-3}$) with the offline and in situ TD-PTR-MS techniques for the group T100 (compounds desorbed at 100 ˚C). Number of days during which air was sampled on filters is indicated. Ratio (offline / in situ) and difference (offline - in situ) are shown as well.

| all ions | | | | | | | |
|---|---|---|---|---|---|---|---|
| FILTER ID | CA5 | CA6 | CA10 | CA11 | CA12 | CA13 | CA15 |
| offline, ng/m3 | 77.2 | 104.8 | 54.9 | 49.1 | 175.0 | 100.2 | 55.9 |
| in situ, ng/m3 | 4.1 | 11.2 | 8.6 | 3.9 | 0.9 | 27.0 | 5.4 |
| ratio | 18.7 | 9.4 | 6.3 | 12.6 | 189.8 | 3.7 | 10.3 |
| difference | 73.1 | 93.6 | 46.2 | 45.2 | 174.0 | 73.2 | 50.5 |
| # of sampling days | 1 | 1 | 2 | 2 | 2 | 3 | 3 |

The bulk comparison also shows that the compounds detected on the filters at 100 ˚C are mostly due to gas phase SVOCs because for all time periods the ratios are much higher than unity (Table 6). For the CA12 filter sampled during the polluted period, the ratio (189.8) is more than 10 times higher than for the other 2- and 3-day filters. This is likely caused by the polluted conditions during the t12 period and presumably high levels of SVOCs in the gas phase. On the other hand, the in situ detected OA at 100 °C is only 0.9 ng $m^{-3}$, which is the lowest among all time periods, potentially reflects over-correction of the background and additionally explains the high ratio (189.8). In fact, both artifacts are likely to cause this exceptional discrepancy between the in-situ and the offline method at 100 ˚C. Overall, the total OA mass detected at 100 ˚C with both the in situ and the offline method represents only a rather small fraction of the OA mass detected at 150-350 ˚C (0.1-3% for in situ, 9-23% for offline measurements).

In Table 5 a clear difference between 1-day and 2-, 3- day filters can be seen for the group containing all ions corresponding to the compounds that desorb at 150-350 ˚C: the ratios are higher for 1-day filters (1.5-1.8) than for 2-, 3- day filters (0.7-1.1). It has been previously shown that positive artifacts are higher for the filters sampled during shorter time periods. Subramanian et al. (2004) found a positive offset in the measured aerosol mass concentrations of ~0.5 µg-C/$m^3$ for filters sampled for 24 h and an even larger offset of ~0.7 µg-C/$m^3$ for filters sampled for 4-6 h. The adsorption of gas phase SVOCs is likely the main process leading to such positive artifacts and in our dataset it is strongest for 1-day filters (50-80% of the total aerosol mass).The relative percentage of the positive artifacts observed here are higher than the artifacts described in the literature for 1-day quartz fiber filters (up to 30% of organic carbon mass, e.g. Subramanian et al., 2007). This might be caused by the lower absolute aerosol concentrations measured in the current study and is also reflected by absolute differences

(0.2-0.3 µg/$m^3$, see CA5 and CA6 in Table 5 and Table 6) that are at the lower end of reported ranges in the literature.

For 1-day filters the difference in the total OA mass concentrations measured with the offline and in situ techniques is similar for mass ranges 31 < m/z < 191 Da and 191 < m/z < 291 Da (see Table 5, 'difference'). That indicates a similar absolute contribution of gas phase SVOCs to the positive artifacts for these mass ranges for 1-day filters. However, for 2- and 3- day filters a positive artifact was observed for mass range 191 < m/z < 291 Da (18.2 - 71.8 ng $m^{-3}$), and for the mass range 31 < m/z < 191 Da a negative artifact prevails (- 1.9 to - 381.2 ng $m^{-3}$). With the exception of CA15, for 2- and 3- day filters the negative artifact was higher than the positive artifact. The total offline OA was therefore 7 - 35% lower than the in situ measurement, e.g., for the t13 time period we observe OA mass concentration 1112.9 ng $m^{-3}$ with the offline technique and 1386.6 ng $m^{-3}$ with the in situ technique (Table 5).

Negative artifacts may be caused by evaporation of condensed SVOCs from particles sampled on the filters as was shown for 3- and 4-ring PAHs by Coutant et al. (1988). However, Holzinger et al. (2013) showed that more volatile aerosol (semivolatile and primary OA) can be associated with ions with m/z > 200 Da, that is the mass range (191 < m/z < 291 Da) where a positive artifact prevails even for the 2- and 3-day filters. Therefore, a second process must contribute and cause the negative artifact in the mass range 31 < m/z < 191 Da, that is the incomplete desorption of OA components from the large surface of the quartz filters during heating and possibly catalytic chemical reactions that produce other (undetectable) species. This is consistent with the findings of Holzinger et al. (2013) who showed that low volatility OA is rather desorbed by thermal decomposition than by evaporation and that undetectable products such as $CO_2$ and CO are produced along with detectable species with molecular weights below 200 Da. These processes are the likely cause for the observed negative artifact since they are expected to be stronger for the offline method due to the stronger affinity of aerosol compounds to the quartz fiber filter surface.

Only a very minor negative artifact was observed for CA15 sampled during mixed (mostly clean) air mass conditions, possibly indicating a compensation of positive and negative artifacts in the mass range 31 < m/z < 191. This may be explained by the following. Presumably lower levels of condensed SVOCs are sampled and consequently there is less organic mass to evaporate. This hypothesis is supported by the fact that final sampling of CA15 filter was performed in the clean air

conditions (see Fig. 21) with likely lower concentrations of SVOCs, and the fact that SVOCs on the filters are in equilibrium with sampled air (e.g., Turpin et al., 2000).

The highest absolute negative artifacts were observed for the filters CA12 and CA13 sampled during the polluted conditions (-306.1 and -273.7 ng $m^{-3}$, respectively). This might be caused by the higher volatility of condensed compounds sampled in the polluted conditions, causing desorption of some of these compounds during sampling on the filters. Such compounds could be hydrocarbon-like OA, which possess higher volatility than other OA (Huffman et al., 2009) and can explain the highest negative artifacts during the pollution event in case contribution of these compounds to the total measured OA is substantial.

### 3.3.2c Comparison based on the chemical composition

Due to the high mass resolution of the PTR-MS it is possible to assign empirical formulas to the measured masses and therefore determine the chemical composition. This allows to investigate in more detail the behavior of different compound classes on filters. Fig. 23 shows the ratios of offline/in situ TD-PTR-MS measurements for the considered ion classes (‘other compounds’, O-1, O-2, O-3, N-compounds and HCs) with error bars indicating uncertainty calculated by means of standard error propagation. Note that the ion classes are no direct projection of compound classes in OA. For example, a hydrocarbon ion can be also produced from oxygenated compounds when the oxygen group is lost in the process of thermal desorption or proton transfer ionization. For group T100 (not shown), ratios of offline/in situ TD-PTR-MS measurements for all ion classes are significantly higher than unity ($5 < \text{ratio} < 48$). The highest artifacts were observed for the following classes of compounds at 100 ˚C (the ratios are given in the brackets): N-compounds (48), O-3 (30), other compounds (16) and O-2 (16). In group T150-350 most classes of compounds have ratios close to unity. Only hydrocarbons and ‘other compounds’ have ratios substantially higher than unity (3.70±0.54 and 1.56±0.15, respectively). To understand the absolute contribution of a chemical class to artifacts, the fractions of the total OA mass (based on the in situ measurements and averaged over all filter sampling periods) for group T150-350 were calculated to be 0.15, 0.23, 0.21, 0.21, 0.16 and 0.04 for ‘other compounds’, O-1, O-2, O-3, N-compounds and HCs, respectively. Our results suggest that the positive artifact results to the largest part from primary emissions and not from compounds that have been heavily processed in the atmosphere. Although hydrocarbon ions may also be produced from oxygenated compounds

(see above), hydrocarbon ions are nevertheless a tracer for primary emissions that have not been strongly processed in the atmosphere.

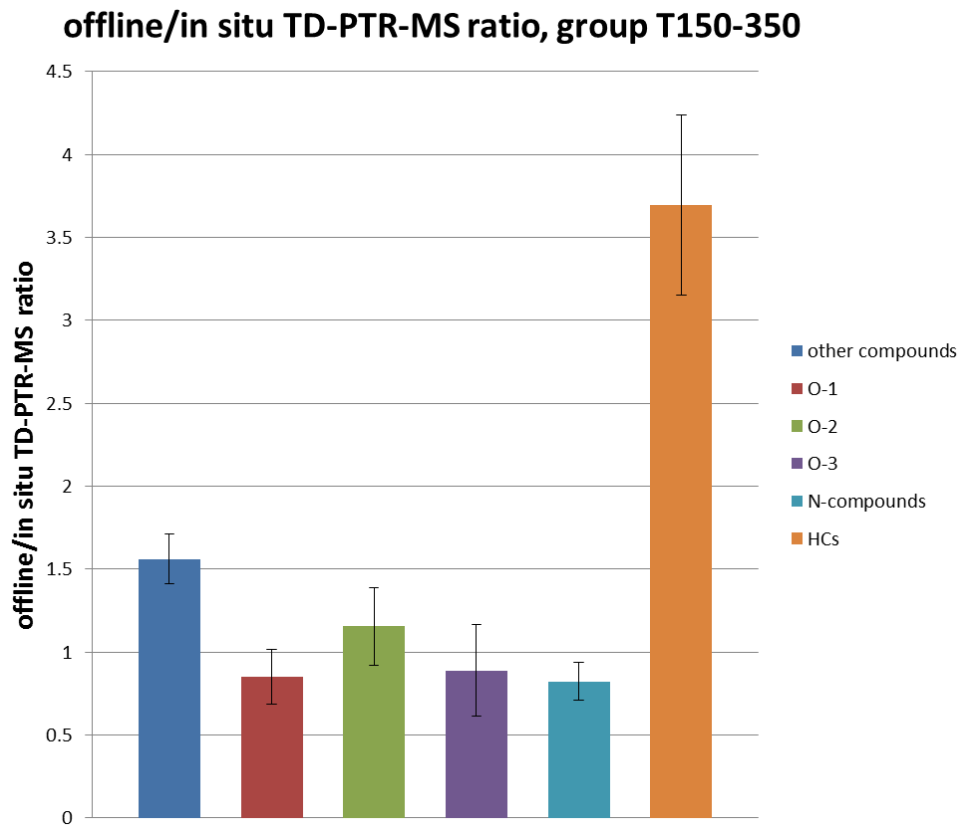


Fig. 23. Chemical speciation plot for the offline/in situ TD-PTR-MS ratios with the corresponding standard error bars for six classes of compounds in the T150-350 group: 'other compounds', O-1, O-2, O-3, N-compounds and HCs.

N-compounds are found to be slightly but significantly lower on filters compared to the in situ measurements (ratio=0.82±0.11). This might be caused by artifacts occurring during filter sampling and/or during the thermal desorption process in the laboratory. However, losses of N-containing species during filter sampling are unlikely, since Holzinger et al. (2013) showed that nitrogen-containing compounds in the OAs are typically less volatile than other compounds. Therefore we suggest

that the higher affinity of N-containing species to the surface of the quartz fiber filters causes incomplete desorption and thus the lower detected signals.

For O-1, O-2 and O-3 compounds the ratios (0.85±0.17, 1.15±0.23 and 0.89±0.28, respectively) are not significantly different from unity indicating a good quantitative correspondence between offline and in situ measurements. This suggests that oxygen-containing compounds may contribute only to a minor extend to observed positive and negative artifacts, and that no significant charring on the filters occurs to these compounds during thermal desorption.

## 3.4 Conclusions

An offline method to study the chemical composition of organic aerosol using filter sampling followed by analysis in the laboratory using PTR-TOF-MS has been presented and compared to in situ TD-PTR-MS measurements. The high mass resolution of the PTR-TOF-MS allows a more detailed investigation of nature of the artifacts occurring during filter sampling, including chemical speciation.

At the 100 ˚C desorption step the offline measurements yielded much higher mass concentrations of most compounds than the in situ measurements (offline/in situ ratio is ~10). The likely reason for higher offline yields is adsorption of gas phase SVOCs on the large surface of the quartz filters.

Generally good correlation between offline and in situ method was observed for the desorption steps 150-350 ˚C ($r^2$ is 0.86 and offline/in situ ratio is 0.91). However, for filters sampled for 1 day (CA5, CA6) a large positive artifact has been observed (50-80% of the total aerosol mass) and also attributed to the adsorption of SVOCs on the large quartz fiber filter surface. For the filters sampled for 2 and 3 days (CA10-CA15) the agreement between offline and in situ PTR-MS measurements for total organic mass was quantitatively better than for 1-day filters. However, for most 2- and 3-day filters negative artifacts occurred. The negative artifacts were attributed to incomplete desorption of aerosols from the filters during the offline measurements and chemical reactions on the filters.

A chemical composition analysis was performed for the compounds detected at 150–350 ˚C. For oxygen-containing compounds the correspondence between the offline and in situ TD-PTR-MS measurements was within the levels of uncertainty. For hydrocarbon ions and ions molecular formula of which could not be identified, significantly higher concentrations were measured by the offline method (3.70±0.54 and 1.56±0.15, respectively). For nitrogen-containing compounds

lower concentrations were measured by the offline technique, which potentially indicates a high affinity of these compounds to the quartz filter surface. However, the latter needs to be investigated further.

# Chapter 4: Organic aerosol composition measurements with advanced offline and in-situ techniques during the CalNex campaign

**J. Timkovsky, A.W.H. Chan, T. Dorst, A.H. Goldstein, B. Oyama and R. Holzinger**

Submitted to Atmospheric Measurement Techniques.

## Abstract

Our understanding of formation processes, physical properties and climate/health effects of organic aerosols is still limited in part due to limited knowledge of organic aerosol composition. We present speciated measurements of organic aerosol composition by two methods: in situ thermal-desorption proton-transfer-reaction mass spectrometry (TD-PTR-MS) and offline two-dimensional gas chromatography with a time-of-flight mass spectrometer (GC×GC/TOF-MS). 153 compounds were identified using the GC×GC/TOF-MS, 123 of which were matched with 64 ions observed by the TD-PTR-MS. A reasonable overall correlation of 0.67 ($r^2$) was found between the total matched TD-PTR-MS signal (sum of 64 ions) and the total matched GC×GC/TOF-MS signal (sum of 123 compounds). A reasonable quantitative agreement between the two methods was observed for most individual compounds with concentrations which were detected at levels above 2 ng/$m^3$ using the GC×GC/TOF-MS. The analysis of monocarboxylic acids standards with TD-PTR-MS showed that alkanoic acids with molecular masses below 290 amu are detected well (recovery fractions above 60%). However, the concentrations of these acids were consistently higher on quartz filters (quantified offline by GC×GC/TOF-MS) than those suggested by in situ TD-PTR-MS measurements, which is consistent with the semivolatile nature of the acids and corresponding positive filter sampling artifacts.

## 4.1 Introduction

Aerosol particles are ubiquitous in the atmosphere, and are important for two main reasons. Firstly, they scatter and absorb solar radiation, and change cloud properties affecting climate on Earth (Boucher et al., 2013). Secondly, they penetrate into human lungs, causing increased mortality (e.g., Pope and Dockery, 2006). Atmospheric aerosol has various sources, both natural and anthropogenic (e.g., de Gouw and Jimenez, 2009). Organic aerosol (OA) comprises 20 to 90 % of the total aerosol mass (Kanakidou et al., 2005). OA can be emitted directly (primary OA, POA), but can also be produced in the atmosphere via photochemical oxidation of volatile organic compounds (secondary OA, SOA).

Elucidating aerosol chemical composition is key to understanding sources and formation processes, and to effectively controlling aerosol amounts in the atmosphere (e.g., Ulbrich et al., 2009). For example, *n*-carboxylic acids are one of the three major classes of organic molecular markers used extensively for OA source apportionment (Sinabut et al., 2005). They are known to be primarily emitted (Legrand and De Angelis, 1996) and produced from secondary photochemical reactions (Kawamura and Sakaguchi, 1999).

During the Calnex campaign Veres et al. (2011) observed a strong correlation of gas phase organic acids concentrations with the oxidants ($O_3$ and $NO_2$) concentrations. Vogel et al. (2013) reported that the contribution of organic acids to the total submicron OA can be up to 60%.

Even though many in-situ techniques have been deployed to study OA composition (e.g., Jayne et al., 2000; Holzinger et al., 2010a; Weber et al., 2001), it is still commonly characterized on the bulk level using descriptors such as oxygen-to-carbon (O/C) ratio, volatility distribution, or total organic carbon mass. Only a limited number of in-situ studies have researched OA at a molecular level using high time resolution (two-hourly or better) measurements (e.g., Williams et al., 2014; Yatavelli et al., 2014; Zhao et al., 2013). Therefore, more detailed studies from various locations and time periods are needed to better understand chemical composition and sources of OA.

Here we deployed two different techniques allowing for detailed chemical composition measurements of OA: (1) in-situ thermal-desorption proton-transfer-reaction mass spectrometry (TD-PTR-MS), and (2) offline filter analysis by comprehensive two-dimensional gas chromatography coupled to time-of-flight mass spectrometry (GC×GC/TOF-MS). The in situ TD-PTR-MS technique was developed at Utrecht University, the Netherlands (Holzinger et al.,

2010a; Holzinger et al., 2013). This technique yields the concentration of many organic ions obtained after the thermal desorption and ionization of organics in aerosols. As a result, one can identify chemical composition of hundreds of compounds constituting the original aerosol and/or fragments of these compounds. 25-60% of the total OA can be directly measured with this technique (Holzinger et al., 2013). GC×GC/TOF-MS has been applied to organic aerosol analysis to provide additional separation using two-dimensional gas chromatography (e.g., Hamilton et al., 2004; Kallio et al., 2006). Analysis of the samples described in this work has previously been reported with regard to distinguishing the alkane isomers in unresolved complex mixtures (Chan et al., 2013). Here we focus on compounds with a broader range of functional groups that are clearly resolved using GC×GC/TOF-MS.

In this study we aim to use the GCxGC/TOF-MS measurements of individual compounds and aerosol mass spectrometer measurements of total organic aerosol to better understand the strengths and weaknesses of the TD-PTR-MS technique for measuring individual chemicals and total organic aerosol, respectively. The comparison is done based on two days of measurements during the CalNex (California Research at the Nexus of Air Quality and Climate Change) 2010 campaign in Pasadena, California.

## 4.2 Experimental methods

### 4.2.1 Measurement campaign

The data presented in this paper were obtained during the CalNex field campaign in Pasadena, California performed from 15$^{th}$ May till 16$^{th}$ June, 2010. The site is located approximately 18 km northeast of downtown of Los Angeles on the campus of California Institute of Technology (34.1408° N, 118.1223° W). More than 40 groups participated in this campaign collecting data characterizing chemical composition, transformation and quantity of gas and particle constituents of the atmosphere. The in situ TD-PTR-MS and aerosol mass spectrometer (AMS) instruments were located in neighboring air-conditioned containers, and the high volume $PM_{2.5}$ filter sampler was located on the roof of one of the building on the campus ~200 m southeast of the containers. The inlet for the TD-PTR-MS instrument was located at the top of a 10 m scaffolding tower and was equipped with $PM_{2.5}$ cyclones. The AMS inlet was located 2 m above the roof of the container housing the instrument and AMS instrument measured submicron aerosols ($PM_1$). Filter samples were collected on quartz fiber filters

(TissuquartzTM Filters, 2500 QAT-UP, Pall Life Sciences), which were 20 cm × 25 cm, allowing for high-volume $PM_{2.5}$ sampling at ~1 $m^3$ $min^{-1}$.

### 4.2.2 Instrument description

#### 4.2.2a The in situ TD-PTR-MS method

In situ aerosol measurements were carried out with an aerosol sampling unit with two identical inlet systems attached to a proton-transfer-reaction time-of-flight mass spectrometer (PTR-TOF-MS, further referred to as 'PTR-MS') (Fig. 24A). The setup has been described in detail elsewhere (Holzinger et al., 2010a; Holzinger et al., 2013). In short, the air flow passes through 12 m long copper inlet tubes (ID=6.5 mm), particles are humidified in a humidifier and then they are collected in a collection-thermal-desorption (CTD) cell. Afterwards, the cell is heated up in steps of 50°C up to 350°C and the emitted species are carried with a flow of nitrogen (ultrapure nitrogen, 5.7 purity, Air Products) into the PTR-MS. The PTR-MS was operated with the following settings: drift tube temperature, 120 ˚C, inlet tube temperature, 180 ˚C; ion source voltages, Us = 140 V, Uso = 92 V; E/N, 130 Td; extraction voltage at the end of the drift tube, Udx=24 V. The intensity of the primary $H_3O^+$ ion signal (detected at m/z 21.023) was typically higher than 5 x $10^5$counts per second (cps).

After the measurements from the first inlet are finished, the valve system is switched automatically to allow aerosol measurements from the second inlet to start. Subsequent to the measurements from the second inlet, gas phase measurements (not considered in the current paper) are carried out and then the measurement cycle starts over (see Fig. 1 in Holzinger et al., 2013).

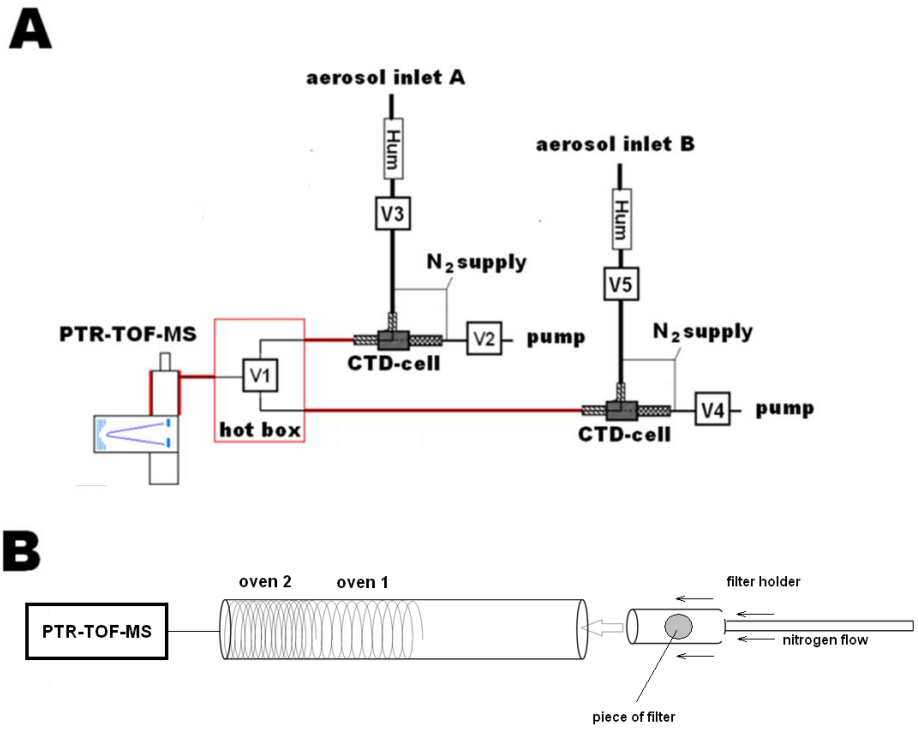


Fig. 24. The in situ (A) and offline (B) TD-PTR-MS setups. The following valves are present on scheme A: V1 – allows switching between two aerosol inlets, V2-V5 – allow switching between sampling and measuring modes for inlet A and B. (The figure and the caption are taken from Timkovsky et al., 2015)

### 4.2.2b Filter sampling with offline GC×GC/TOF-MS analysis

Filter samples were analyzed offline using comprehensive two-dimensional gas chromatography coupled to a time-of-flight mass spectrometer (GC×GC/TOF-MS, hereafter referred to as GC×GC). Details of the analysis method are described in Chan et al. (2013). In brief, filter punches (total area of 1.6 $cm^2$) were thermally desorbed at 320 °C under helium (TDS3, Gerstel) to a two-dimensional gas chromatograph (Agilent 7890 and Zoex modulator). Comprehensive GC×GC was performed using a 60 m × 0.25 mm × 0.25 µm non-polar capillary column (Rxi-5Sil MS, Restek) for the first-dimension separation (by volatility), and a medium-polarity second dimension column (1 m × 0.25 mm × 0.25 µm, Rtx-200MS, Restek). The second dimension column was maintained at 15 °C

above the main oven temperature using a secondary oven. Effluent from the second column was analyzed using a high-resolution ($m/\Delta m \sim 4000$) time-of-flight mass spectrometer (HR-TOF, Tofwerk, Thun, Switzerland) using 70 eV electron impact ionization. Peak detection and compound identification was performed using GC Image software (LLC). Around 1100 peaks were measured at above detection limits. Compounds were identified by confirmation with authentic standards or by mass spectral library search, or, in some cases, based on a unique ion (such as m/z 85 for gamma lactones, 217 for steranes) and its location in the 2-dimensional chromatogram. Identification of otherwise unresolved branched and cyclic alkanes has also been done on these samples using soft ionization with vacuum ultraviolet radiation (Chan et al., 2013) but these alkanes are not included among the compounds discussed here.

Among the 1100 resolved peaks, the 153 compounds reported here were positively identified with the GC×GC technique, classified by compound groups: aromatic esters, benzofuranones, oxygenated polycyclic aromatic hydrocarbons (oxyPAHs), phthalates, 2-alkanones, 3-alkanones, alkanoic acids, alkyl esters, delta-lactones, gamma-lactones, nitrogen-containing aromatic compounds (N-aromatic), polycyclic aromatic hydrocarbons (PAHs), sulfur-containing compounds (S-compounds), amides, hopanes, alkanes and several compounds were identified at a single m/z value (multiple). Another 31 compounds were classified into these compound groups without positive identification. Compound class nicknames are presented in the brackets and further used in the article to refer to them.

#### 4.2.2c Aerosol Mass Spectrometer (AMS)

The AMS measurements used in the current study has been described previously in detail (Hayes et al., 2013). In short, AMS allows for measurements of nonrefractory submicron aerosol (organic and inorganic) (DeCarlo et al., 2006). The operational principle of AMS can be presented briefly as follows. Air is sampled through a critical orifice with a consecutive focusing, acceleration and separation of particles by size. Next, particles are vaporized at 600°C, ionized by electron ionization (70 eV) and detected with a high resolution time-of-flight mass spectrometer. Details of AMS operation and data analysis can be found in Hayes et al. (2013).

#### 4.2.2d Preparation and measurement of standards

In this paper we present measurements of two types of standards: single compounds and a mixture of compounds. The following single compounds were measured: decanoic, pentadecanoic and octadecanoic acids. Known quantities of

each acid were first dissolved in ethanol, and then an aliquot of the solution containing 10 µg of a substance was placed on a quartz filter with a diameter of 5 mm. Next, two minutes were allowed to let most of the solvent evaporate before the filter was inserted in the oven, which is a part of the offline TD-PTR-MS system described in detail by Timkovsky et al. (2015) (Fig. 24B). Each measurement was repeated 3 times, and 2 blank filters were measured at the beginning and at the end of each measurement sequence.

A mixture containing 77 representative organic compounds and C8-C40 alkanes (this mixture is further called 'multicomponent mixture') was carefully prepared by dissolving respective compounds in deuterated acetone. An aliquot of the solution with 0.062 to 20 ng of the substances was placed on quartz filters. In this paper we focus only on acids contained in this standard (21 acids). Again, three filter replicas and two blank filters were measured with the offline TD-PTR-MS.

The filter measuring procedure is described in detail by Timkovsky et al. (2015). In short, the sample is placed in the oven and allowed to stabilize for two minutes. Next, the temperature of the oven is increased stepwise from 100 $^{o}$C to 350 $^{o}$C in increments of 50 $^{o}$C every 3 minutes. The desorbed compounds are carried by the 200 mL/min flow of nitrogen (ultrapure nitrogen, 5.7 purity, Air Products) into the PTR-MS. The operating conditions of the PTR-MS were the same as for the in situ TD-PTR-MS measurements (see section 4.2.2a).

### 4.2.3 Data treatment

#### 4.2.3a In situ and offline TD-PTR-MS data

Data evaluation was done with Interactive Data Language (IDL, version 8.1.0, ITT Visual Information Solutions) using custom made routines described by Holzinger et al. (2010b). The initial mass lists consisted of 717 and 748 masses for multicomponent mixture and CalNex measurements, respectively. Ions associated with primary ions and contaminations from the ion source were removed from the mass lists by filtering out m/z < 40 a.m.u (except for m/z 31.017 and 33.033). Inorganic ions (i.e. ions in the m/z range 40-50 Da, that were matched with an inorganic formula) were also removed from the mass lists. Finally, the mass lists contained 653 and 726 masses for standard and CalNex measurements, respectively. The mixing ratios of ions were calculated from the measured intensities by applying the same protonation reaction rate constant for all ions ($3\times10^{-9}$ cm$^3$ s$^{-1}$ molecule$^{-1}$) (Holzinger et al., 2010b).

For the in situ data analysis, the initial mass spectra were first averaged to obtain data with a time resolution of 5 s. Second, the data were averaged over the measured temperature step (3 min each) and the data for all temperature steps were summed. Third, the resulted mixing ratios were converted to mass concentrations for individual ions by multiplying by ion molecular mass, volume of nitrogen used for desorption for one measurement cycle and dividing by the volume of air sample from which aerosols were collected. Forth, the data from inlet A and B were merged and averaged to match the filter sampling times. Fifth, the resulted mass concentrations were averaged over the whole comparison period (30-31 May) for the data presented in section 4.3.2b. The maximum total uncertainty of ~54% (mostly due to the uncertainty of the reaction rate coefficient) was calculated for these mass concentration based on the method described by Timkovsky et al. (2015).

The same two initial steps were taken for the analysis of the offline TD-PTR-MS data. The obtained data with a 3 min resolution were processed according to the procedure described in Timkovsky et al. (2015). In short, the instrument background and blank corrected mass at a single temperature step ($A_T$) was calculated according to Eq. 4.1:

$$A_T = (VMR_{i,0} - VMR_{i,instrbgd} - (VMR_{i,fb} - VMR_{i,instrbgd_{fb}})) * M_i * V_{nitrogen} \quad (4.1)$$

where $VMR_{i,0}$ is the uncorrected mixing ratio of the ion *i*, and $VMR_{i,fb}$ is the mixing ratio of the ion *i* observed on the field blank, $VMR_{i,instrbgd}$ and $VMR_{i,instrbgd\_fb}$ are the instrument background mixing ratios of the ion *i* observed during the sample and field blank measurements, respectively (all in nmol $mol^{-1}$). $M_i$ is the molecular weight of the ion *i* (minus one amu) and $V_{nitrogen}$ is the volume of nitrogen used for desorption at a single temperature step in mol. As a next step, the six masses $A_T$ measured for the 50°C intervals between 100°C and 350°C were summed to obtain the total mass of the substance which then compared with the known amount of the substance initially placed on the filters.

### 4.2.3b GC×GC quantification

GC×GC data were analyzed using GC Image (LLC). Peak volumes of quantification ions were used to calculate compound signal, and then converted to the total ion signal based on the mass spectral distributions in the NIST08 library. The total ion signals were then converted to on-column mass based on mass calibrations conducted using a representative set of commercially available organic

compounds as external standards. For those compounds not commercially available, surrogate standards were assigned based on similarities in molecular structure. Deuterated internal standards were also used to correct for run-to-run variability in instrument response. Mass concentrations were then calculated based on the ratio of filter punch area to total filter area and sampling flow rate.

### 4.2.3c Mass matching process

In order to match ions measured by the TD-PTR-MS with compounds put on the filters and those measured with the GC×GC technique (further referred to as 'known compounds') the following procedure was applied. First, we assumed that all known compounds were detected at their protonated mass, or in the case of oxygenated compounds at the dehydrated fragment (i.e. protonated mass - 18.010, the molecular weight of the H2O fragment). Other fragmentation patterns are possible, but not considered here. We matched the protonated and fragment masses with the ion masses detected by the TD-PTR-MS. A match was assigned if the difference between the protonated or fragment mass of the known compound and an ion detected with the PTR-MS was smaller than 250 ppm (corresponding to the mass resolution of the PTR-MS). Compounds were considered as not detected when either the detected amount by the TD-PTR-MS was negative after background subtraction or the abovementioned difference was above 250 ppm.

In the case where only one of these ions (parent or fragment) was present in the PTR mass list, the signal of this single ion was attributed to the known compound. If a $M_r$ obtained after 18.010 amu subtraction was equal to the Mr already present in the mass list with matches, the intensities of these two masses were summed and the corresponding ions were further considered as isobars. The concentrations of the compounds measured with the GC×GC technique and corresponding to the two masses were also summed. The mass value of the ion with lowest m/z value in the group, i.e. fragmented ion, was chosen to represent this group of ions. For example, 6H-Indolo[3,2,1-de][1,5]naphthyridin-6-one was detected at m/z 221.089 amu and its fragment was detected at m/z 203.087 Da. However, fluoranthene and pyrene were also detected at 203.087 Da. Consequently, 6H-Indolo[3,2,1-de][1,5]naphthyridin-6-one, fluoranthene and pyrene were considered as a single compound with $M_r$ of 203.087 Da, and their measured concentrations were summed in both TD-PTR-MS and the GC×GC data. Whenever more than one compound was measured at the same mass, the most abundant compound (based on the GC×GC measurements) from the considered group was chosen to represent all of the compounds. For example,

phenaleno[1,9-bc]thiophene and anthraquinone were detected at the same m/z value (209.059 Da) with the TD-PTR-MS technique. The total averaged mass concentration of phenaleno[1,9-bc]thiophene and anthraquinone was 1.57 ng/m$^3$ and 27.70 ng/m$^3$, respectively (based on the GC×GC measurements). Thus, anthraquinone represents 95% of the signal at that mass, and all of the signal at 209.059 amu was attributed to anthraquinone. In the case where structural isomers were identified with the GC×GC technique, the corresponding GC×GC concentrations were summed. Mass concentrations of 22 alkanes measured by the GC×GC were summed and all alkanes were considered as one compound with $M_r$ of 113.133 Da as all alkanes are detected with the PTR-MS at the same set of masses (43.055 Da, 57.070 Da, 71.086 Da, and a few other masses). This resulted in the decrease of the GC×GC dataset, from 153 to 132 compounds.

Applying these rules we were able to match 123 of the 132 distinguishable compounds measured with the GC×GC technique, to corresponding 64 ions measured with the TD-PTR-MS technique (see Table A1). The contribution of the unidentified 9 compounds is minor (<2%) compared to the total mass concentration of the 123 compounds. While we applied rather relaxed rules when attributing detected m/z values to known compounds, we found that in practice the matches were much closer than 250 ppm: the median difference for 64 ions was 41 ppm.

## 4.3 Results

### 4.3.1 Monocarboxylic acid standards measured by the TD-PTR-MS

To calibrate the in situ TD-PTR-MS technique for measurements of monocarboxylic acids, a series of filters with known quantities of the acids were prepared and measured with the offline setup. Fig. 25 shows the ratio of the detected amount of substance and the amount of monocarboxylic acids that was applied on the filter, i.e. fraction of acid recovered. The measurements of single compounds (pink triangles in Fig. 25) and the multicomponent mixture (blue triangles and black crosses in Fig. 25) are shown together in this figure. Only the signal of the protonated ion has been used to calculate mass concentrations of alkanoic acids measured with the offline TD-PTR-MS technique. In total, 24 monocarboxylic acids are measured (Fig. 25). The lowest fractions (i.e. lower amounts detected by the TD-PTR-MS) are observed for the high molecular mass acids ($M_r$>300 Da). This could be caused by significantly lower than 100% desorption efficiency off the filters at temperatures up to 350 ˚C and thermal

decomposition of these high molecular weight substances (e.g., charring) (Yu et al., 2002).

Five out of the 21 monocarboxylic acids ($M_r$>305 Da) that were put on the filters in the multicomponent mixture were not detected with the offline TD-PTR-MS technique (red in Table 7). This might be caused by the fact that these acids (except for triacontanoic acid) have the highest background signal among the acids with $M_r$>305 Da. Triacontanoic acid is the heaviest acid injected onto the filters and likely indicates the lower volatility limit of the compounds which could be measured with the offline TD-PTR-MS technique. Other heavy monocarboxylic acids ($M_r$>300 Da) are strongly underestimated with the offline TD-PTR-MS technique (fraction of acid recovered≤0.02). Therefore, we can generally conclude that heavy acids ($M_r$>300 Da) are not detected well with this technique, which is likely caused by some of the aforementioned reasons.

Alkanoic acids with $M_r$<290 amu are detected reasonably well (fractions recovered above 60%, Fig. 25). Acids containing one or more double bonds with Mr<290 amu (further referred to as 'n-enoic acids') are not detected as well (less than 38%), which is possibly caused by their higher affinity to quartz filters and lower resistance to thermal decomposition. The higher affinity leads to a release at higher temperatures, so that thermal decomposition becomes a competitive desorption pathway and eventually dominates over evaporation.

Based on the presented measurements, a calibration factor for alkanoic acids with $M_r$<290 amu is developed. Using the averaging of the fractions recovered of 6 alkanoic acids with $M_r$<290 amu (3 single standards and 3 from the multicomponent mixture), a calibration factor of 1.45 is found, and applied to the alkanoic acid concentrations discussed in section 4.3.2b and 4.3.2c. There are three likely explanations for the higher than unity calibration factor. First, the same reaction rate coefficient is applied to mixing ratio calculations of all compounds measured by the PTR-MS, and the real reaction rate coefficient for alkanoic acids can be lower than applied (Zhao and Zhang, 2004). Second, a partial thermal decomposition of the acids may occur on filters. Third, lighter alkanoic acids could have (e.g., decanoic) evaporated off of the filter before the filter was placed in the oven for analysis. The first reason is, however, less likely because similar measurements of 3 alkanoic acids with $M_r$<290 amu on aluminum foil indicated that the total amount of the acids can be observed with the offline TD-PTR-MS technique for the heavier acids (penta- and octadecanoic acids), while a lower fraction (more loss through evaporation) is observed for the lighter decanoic acid.

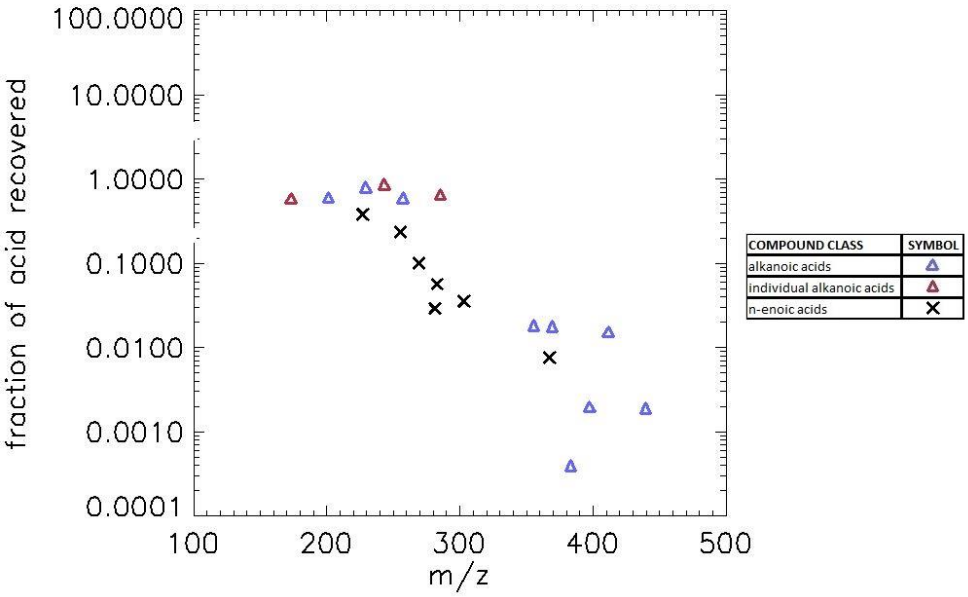


Fig. 25. The ratio of the amount of a substance on the filters measured with the offline TD-PTR-MS technique to the known amount of the substance put on the filters (fraction of acid recovered).

Table 7. Molecular formula, masses and fraction recovered of 24 protonated monocarboxylic acids measured as standards on quartz filters individually (in italic) and in the multicomponent mixture. Acids indicated in red are not detected with the offline TD-PTR-MS technique.

| Compound | Molecular formula•$H^+$ | Molecular weight | Fraction |
|---|---|---|---|
| *Decanoic acid* | $C_{10}H_{21}O_2^+$ | 173.154 | 0.59 |
| Lauric acid | $C_{12}H_{25}O_2^+$ | 201.185 | 0.60 |
| cis-9-Tetradecenoic acid (Myristoleic acid) | $C_{14}H_{27}O_2^+$ | 227.201 | 0.38 |
| Myristic acid | $C_{14}H_{29}O_2^+$ | 229.217 | 0.80 |
| *Pentadecanoic acid* | $C_{15}H_{31}O_2^+$ | 243.232 | 0.87 |
| cis-9-Hexadecenoic acid (Palmitoleic acid) | $C_{16}H_{31}O_2^+$ | 255.232 | 0.23 |
| Palmitic acid | $C_{16}H_{33}O_2^+$ | 257.248 | 0.60 |
| cis-10-Heptadecenoic acid | $C_{17}H_{33}O_2^+$ | 269.248 | 0.10 |
| cis,cis-9,12-Octadecadienoic acid (Linoleic acid) | $C_{18}H_{33}O_2^+$ | 281.248 | 0.03 |
| cis-9-Octadecenoic acid (Oleic acid; Elainic acid) | $C_{18}H_{35}O_2^+$ | 283.264 | 0.06 |
| *Stearic acid* | $C_{18}H_{37}O_2^+$ | 285.279 | 0.66 |
| cis-5,8,11,14,17-Eicosapentaenoic acid (Timnodonic acid) | $C_{20}H_{31}O_2^+$ | 303.232 | 0.04 |
| cis-11-Eicosenoic acid (Gondoic acid) | $C_{20}H_{39}O_2^+$ | 311.295 | - |
| cis-13-Docosenoic acid (Erucic acid) | $C_{22}H_{43}O_2^+$ | 339.326 | - |
| Docosanoic acid (Behinic acid) | $C_{22}H_{45}O_2^+$ | 341.342 | - |
| Tricosanoic acid | $C_{23}H_{47}O_2^+$ | 355.358 | 0.02 |
| cis-15-Tetracosenoic acid (Nervonic acid) | $C_{24}H_{47}O_2^+$ | 367.358 | 0.01 |
| Tetracosanoic acid (Lignoceric acid) | $C_{24}H_{49}O_2^+$ | 369.373 | 0.02 |
| Pentacosanoic acid | $C_{25}H_{51}O_2^+$ | 383.389 | 0.0004 |
| Hexacosanoic acid (Cerotic acid; Cerotinic acid) | $C_{26}H_{53}O_2^+$ | 397.405 | 0.0020 |
| Heptacosanoic acid | $C_{27}H_{55}O_2^+$ | 411.420 | 0.02 |
| Octacosanoic acid (Montanic acid) | $C_{28}H_{57}O_2^+$ | 425.436 | - |
| Nonacosanoic acid | $C_{29}H_{59}O_2^+$ | 439.452 | 0.0019 |
| Triacontanoic acid (Melissic acid) | $C_{30}H_{61}O_2^+$ | 453.467 | - |

### 4.3.2 Comparison of the in situ TD-PTR-MS and offline GC×GC data

#### 4.3.2a Total measured OA signal

In Fig. 26 we present the time series of total OA mass concentrations measured by the in situ TD-PTR-MS and the AMS instruments (further named 'total OA_PTR' and 'total OA_AMS', respectively), the total concentration of the 123 compounds measured by the GC×GC, and the total concentration of the corresponding 64 masses measured by the TD-PTR-MS (further named '123 compounds_GC×GC' and '64 masses_PTR', respectively) over 2 days. The 64 masses constitute 25% of the total OA mass measured by the TD-PTR-MS.

In general, the total OA_PTR and the total OA_AMS correlate well with a correlation coefficient ($r^2$) of 0.84. The average percentage of the total OA detected by the TD-PTR-MS is 33%. Potential reasons for undetected OA by the

TD-PTR-MS, that is fragmentation in the PTR-MS and thermal decomposition in the CTD cell, have been discussed in Holzinger et al. (2013).

A reasonable qualitative and quantitative correlation is observed between the 123 compounds_GC×GC and the 64 masses_PTR: a correlation coefficient ($r^2$) equals to 0.67. On average, the TD-PTR-MS detected 98% of the total mass of the '123 compounds_GC×GC'. However, one can notice that the correlation between the 123 compounds_GC×GC and the 64 masses_PTR is better during the first than the second day of the measurements. This might relate to a different wind direction during the second day and to the fact that the TD-PTR-MS and the HiVol filter sampler were located ~200 m apart during the campaign. Indeed, the prevailing wind directions were northeast on May 30 and northwest and west on May 31, based on 48h back trajectories using the model HYSPLIT (Draxler & Rolph, 2013; Rolph, 2013).

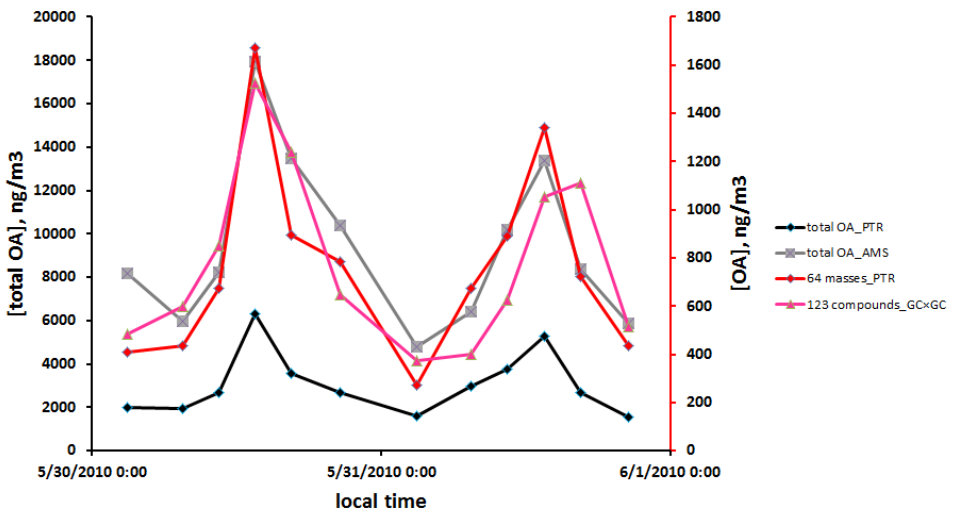


Fig. 26. The two-day cycle of total OA mass concentration (in black, total OA_PTR) and OA mass concentration of 64 masses (in red) measured with the in situ TD-PTR-MS technique, and total OA mass concentration (in grey, total OA_AMS) measured by the AMS and OA mass concentration of 123 compounds (in pink) measured with the GC×GC technique. Left y-axis (in black) corresponds to total OA_PTR and total OA_AMS, and right y-axis (in red) corresponds to 64 masses_PTR and 123 compounds_GC×GC.

### 4.3.2b Comparison by compound class

Fig. 27 presents mass concentrations of compounds measured with the in situ TD-PTR-MS technique versus corresponding mass concentrations measured with the GC×GC technique (referred to as 'PTR' and 'GC×GC', respectively) averaged over the whole comparison period with 1:1 line shown for reference. Compound classes are shown according to the scheme introduced in section 4.2.2b.

In general, the concentrations of organic species measured with the two techniques agree reasonably well for most compounds with mass concentrations above ~2 ng/m$^3$ as measured by GCxGC (see the thin black lines above and below the 1:1 line in Fig. 27 that mark the 0.25<PTR/(GC×GC)<2 boundaries). The PTR/(GC×GC) ratio indicates the ratio of the amount of a substance measured with the TD-PTR-MS technique to the amount of the substance measured on the filters with the GC×GC technique. The ratio is expected to be within the boundaries of 0.5 and 2 if the accuracy for both, TD-PTR-MS and GCxGC, is ±33%. An accuracy of 54% for TD-PTR-MS and 40% for GCxGC is consistent with wider boundaries of 0.4 and 3.2. The upper boundary (2) suggested by Fig. 27 is lower than the upper boundary suggested by the stated accuracy levels (3.2). This may indicate that the stated accuracy levels are an overestimate of the real accuracy. The lower boundary (0.25) suggested by Fig. 27 is somewhat lower than the value expected from the stated accuracies (0.4). This may be caused by condensation of semivolatile gas phase compounds on the large surface of the quartz filters, which is a well-known sampling artifact and constitutes a positive bias of the GCxGC data. For some compounds (such as hopanes and oxygenated PAHs), GCxGC detects less than the TD-PTR-MS. In general, for compounds with mass concentrations below 2 ng/m$^3$, the TD-PTR-MS method yielded substantially higher mass concentrations. It should be noted that the 132 compounds measured with the GC×GC technique represent about 10% of the total OA mass, with another 5-10% associated with the unresolved complex mixture (UCM) (Chan et al., 2013). There are likely additional species not quantified with the GCxGC, that are detected as a sum by PTR-MS at the corresponding m/z values.

On the other hand, for alkanes and one amide substantially lower concentrations were detected with the TD-PTR-MS technique (the corresponding points are located at a substantial distance from 1:1 line). For alkanes this can be explained by the fact that the main masses at which alkanes are detected (43.055 Da, 57.070 Da, 71.086 Da) were not considered because large contamination from the gas phase did not allow to quantify the condensed fraction. More complicated

fragmentation in the PTR-MS can likely explain the lower concentrations found for the amide (N,N-dibutyl-formamide). For all compounds of the class of alkanoic acids (except for decanoic acid), the concentrations were measured to be lower by the TD-PTR-MS, which is likely caused by a positive sampling artifact that is common to quartz filter collection. The latter will be discussed in the following section.

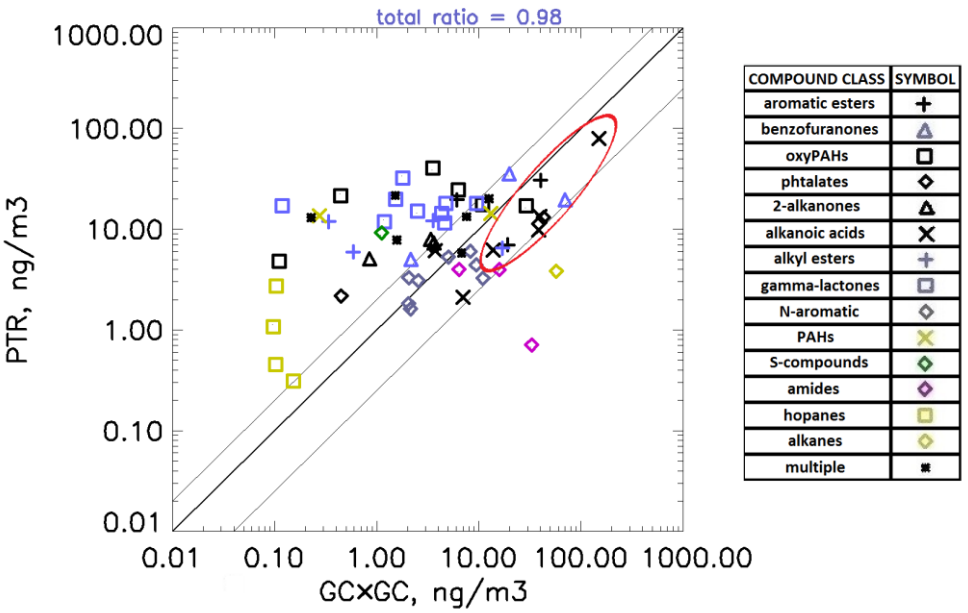


Fig. 27. Comparison of aerosol mass concentrations measured with the in situ TD-PTR-MS and GC×GC technique. The legend shows classes of compounds depicted, which are described in detail in the text. The total PTR/(GC×GC) ratio is 0.98. The red oval highlights (among other species) four alkanoic acids which are discussed in section 4.3.2c. The thin diagonal lines indicate the upper and lower boundaries of the reasonable PTR/(GC×GC) ratio (0.25 and 2).

### 4.3.2c Alkanoic acids

The four alkanoic acids shown in Fig. 27 as black crosses in a red oval are n-dodecanoic, n-tridecanoic, n-tetradecanoic and n-hexadecanoic acids. These 4 compounds are among the most abundant species measured by the GC×GC (3 among the 7 compounds with the highest concentrations, see Fig. 27). To calculate the mass concentrations of the alkanoic acids measured with the in situ TD-PTR-MS technique, only the intensity of the parent ion signal was considered

and multiplied by the calibration factor (1.45) developed for alkanoic acids (see section 4.3.1). Even after applying this correction factor, the PTR/(GC×GC) ratios for the acids are below unity (Table 8). The semivolatile nature of the acids is a likely reason for this disagreement, due to known positive filter sampling artifacts and, therefore, overestimation of the mass concentrations obtained with the GC×GC technique. This hypothesis is supported by the fact that positive artifacts have been shown to be more severe on filters with short air sampling duration. For example, Timkovsky et al. (2015) demonstrated substantial positive filter sampling artifacts on filters sampled for 24 hours, which were much reduced with sampling durations of 48 and 72 hours.

The fraction of the amount of a compound in the particle phase ($F_{p,i}$, amount in the particle phase divided by the total amount in the particle and the gas phase) can be calculated according to the procedure described by, e.g., Yatavelli et al. (2014). Compounds for which $F_{p,i}$ is significantly lower than unity are considered to be semivolatile. $F_{p,i}$ is calculated based on the activity coefficient, vapor pressure, ambient temperature and total OA mass concentration. We used the average activity coefficient calculated for alkanoic acids (1.6) based on Chandramouli et al. (2003). If a component has an activity coefficient above unity within a mixture, the component has a weaker interaction with other molecules in the condensed phase than with itself, and its effective vapor pressure is higher than the pure component vapor pressure. Vapor pressures for do-, tetra- and hexadecanoic acids (Table 8) have been measured by Cappa et al., 2008. Assuming that the logarithm of the vapor pressure of an alkanoic acid has a linear dependency on the number of carbon atoms in the molecule (Goldstein and Galbally, 2007), we calculate the vapor pressure for tridecanoic acid to be $3.2*10^{-6}$ hPa using known vapor pressures of do-, tetra- and hexadecanoic acids (Table 8). Using an ambient temperature of 25˚C and total OA of 9.4 $\mu g/m^3$ (measured by the AMS), $F_{p,i}$ was found to be substantially lower than unity for 3 out of the 4 acids (do-,tri- and tetradecanoic acids, Table 8). This confirms their semivolatile nature and their potential to cause positive filter sampling artifacts when gas phase molecules condense on the large surface of the quartz filters. This is also consistent with Sihabut et al. (2005) who observed a high contribution from gas phase to particle phase measurements on filters of alkanoic acids containing between 10 and 14 carbon atoms.

Since $F_{p,i}$ for hexadecanoic acid is unity, it is expected to be fully in the particle phase and is not prone to positive filter sampling artifacts (Table 8). This is again consistent with Sihabut et al. (2005), who showed that only a little contribution to particle phase measurements is observed from gas phase with filter sampling of

alkanoic acids containing between 15 and 18 carbon atoms. The PTR/(GC×GC) ratio (0.53) for hexadecanoic acid is within the expected range (0.4-3.2) given by the combined accuracies of TD-PTR-MS and GC×GC. However, further study is needed to exclude the possibility that this low ratio may have resulted from a negative sampling artifact for the in situ TD-PTR-MS.

We also compared our results to Williams et al. (2010) and found that they experimentally observed on average higher $F_{p,i}$ values for alkanoic acids: 0.92, 1.0 and 1.0 for do-, tri- and hexadecanoic acid, respectively. This might relate to the fact that for measuring gas phase fractions they applied Teflon filters to remove particle phase components, which could, however, also remove a part of the gas phase compounds, causing the obtained $F_{p,i}$ values to be overestimated.

The full two-day time series for the four alkanoic acids obtained with the TD-PTR-MS and the GC×GC method are presented in Fig. 28. The clear diurnal cycle detected by the TD-PTR-MS for all four acids indicates consistency of the measurements. The cycle is also consistent with the diurnal variation of semivolatile compounds observed by the TD-PTR-MS (Holzinger et al., 2013) and the AMS (Hayes et al., 2013) during the same field campaign. The highest correlation coefficient (r, 0.69) between the TD-PTR-MS and GC×GC measurements is observed for hexadecanoic acid among the four acids (Table 8), which is the most abundant and least volatile compound within this compound group. It is mainly present in the particle phase, and thus is subject to relatively low positive filter sampling artifacts (Fig. 28D). Poor correlation is observed for tri- and tetradecanoic acid (Fig. 28B and Fig. 28C, respectively) which is likely caused by the semivolatile nature of the acids and potential measurement artifacts by the GCxGC technique. The latter may be due to the fact that the acids were not derivatized prior to GCxGC analysis. For dodecanoic acid a reasonable qualitative correlation is observed. However, quantitative agreement is poorer than for the other measured acids, which is likely caused by the relatively high volatility of the acid. As shown in Timkovsky et al. (2015), the larger concentrations measured by GCxGC may be caused by condensation of the gas phase fraction of the acids during filter sampling. The poor correlation for tri- and tetradecanoic acid is currently not understood.

Table 8. Calculated partitioning coefficients $F_{p,i}$, observed PTR/(GC×GC) ratios averaged over the considered period, vapor pressures of dodecanoic, tridecanoic, tetradecanoic and hexadecanoic acids, and correlation coefficients (r) of the TD-PTR-MS and the GC×GC measurements of the acids.

| Compound | $F_{p,i}$ | PTR/(GC×GC) ratio | vapor pressure, hPa | r, 2GC vs PTR |
|---|---|---|---|---|
| Dodecanoic acid | 0.03 | 0.25 | 2.3E-05 | 0.65 |
| Tridecanoic acid | 0.17 | 0.45 | 3.2E-06 | -0.68 |
| Tetradecanoic acid | 0.48 | 0.31 | 7.0E-07 | 0.46 |
| Hexadecanoic acid | 1.00 | 0.53 | 1.3E-09 | 0.69 |

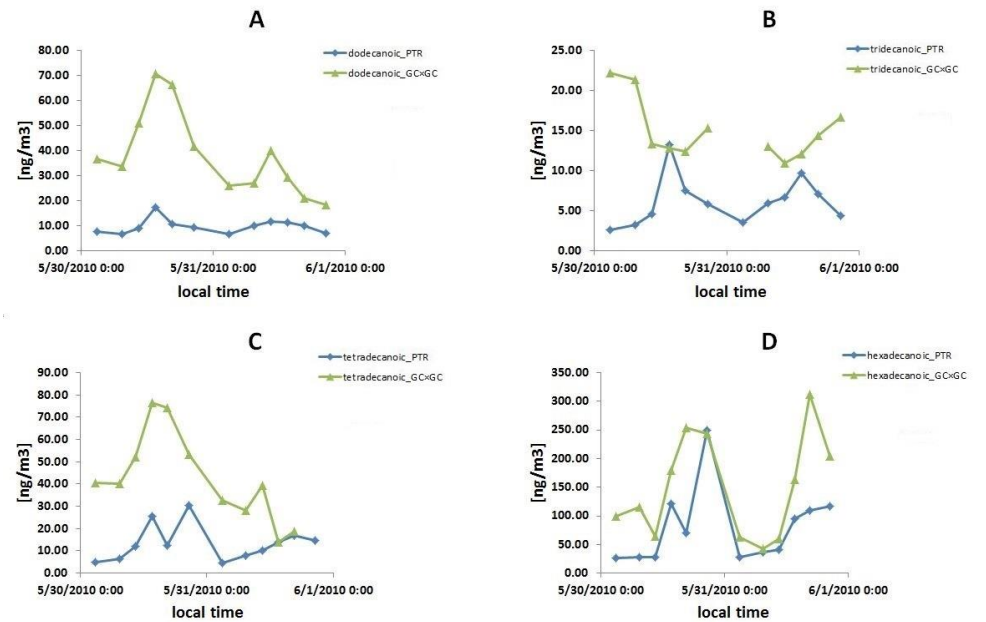


Fig. 28. Time profiles for mass concentrations measured with the TD-PTR-MS and the GC×GC techniques for four alkanoic acids: dodecanoic (panel A), tridecanoic (panel B), tetradecanoic (panel C) and hexadecanoic (panel D).

## 4.4 Conclusion

A comparison of the in situ TD-PTR-MS and offline quartz filter analysis by the GC×GC/TOF-MS technique, the calibration measurements with the offline TD-PTR-MS technique, and the general comparison of the in situ TD-PTR-MS and the aerosol mass spectrometer (AMS) technique have been presented. Overall, a reasonable agreement is observed for temporal changes in the bulk organic aerosol (OA) between the AMS and TD-PTR-MS with correlation coefficient of 0.84 ($r^2$). Reasonable agreement is also observed between temporal changes in the

123 compounds measured from quartz filters by the GC×GC/TOF-MS and the 64 corresponding masses detected by the TD-PTR-MS, with $r^2$ of 0.67.

The calibration measurements showed that n-alkanoic acids with molecular mass ($M_r$) below 290 amu are detected at recovery fractions above 60%. Monocarboxylic acids heavier than 300 amu, and monocarboxylic acids containing double bonds in the range 220 <$M_r$<290 amu exhibit recovery fractions below 4% and 38%, respectively. This is likely caused by the fact that higher temperatures are needed to desorb these compounds from the filters and that thermal decomposition starts taking place before the compounds are fully desorbed. Future measurements of other light unsaturated acids ($M_r$<226 amu) are needed to test whether their recovery fractions are close to unity, as it is the case for light alkanoic acids ($M_r$<290 amu). Based on the measured recovery fractions of n-alkanoic acid ($M_r$<290 amu) measurements, a calibration factor of 1.45 has been established and applied to the in situ TD-PTR-MS measurements of alkanoic acids ($M_r$<290 amu).

For the comparison of the in situ TD-PTR-MS and the offline GC×GC/TOF-MS technique, 123 of 132 compounds measured by the GC×GC/TOF-MS could be matched with ions measured by the PTR-MS. The applied mass matching algorithm took the loss of a water molecule into account, while other fragmentation patterns were not considered. The comparison indicated that the techniques agree reasonably well for single compounds: for most compounds with mass concentrations above 2 ng/m$^3$ the PTR/(GC×GC) ratio was between 0.25 and 2. Compounds detected at levels below 2 ng/m$^3$ with the GC×GC/TOF-MS exhibited higher concentrations at the corresponding ions detected by the TD-PTR-MS. This is likely caused by other organic compounds that were detected by the TD-PTR-MS at the corresponding m/z values, but were not specifically identified with the GC×GC/TOF-MS technique (only 132 compounds were identified out of the ~1100 resolved peaks).

All classes of compounds were detected well by the TD-PTR-MS, except for alkanes. The positive filter sampling artifacts, caused by the semivolatile nature of the do-, tri- and tetradecanoic acids, likely resulted in the higher concentrations observed by the GC×GC/TOF-MS and lower correlations between the GC×GC/TOF-MS and TD-PTR-MS measurements.

Table A1. The affiliation of ion masses observed by the PTR-MS with the GCxGC measured compounds. Mean concentrations as measured by the TD-PTR-MS and the GCxGC technique are presented, ng/m$^3$.

| m/z, amu | Molecular formula | Compound class | GCxGC compound | mean PTR concentration, ng/m3 | mean GCxGC concentration, ng/m3 |
|---|---|---|---|---|---|
| 100.041 | C4H5NO2 | N-aromatics | 2,5-Pyrrolidinedione | 5.29 | 5.02 |
| 113.133 | C6H12 | alkanes | C14-C33 alkanes | 3.83 | 57.37 |
| 114.090 | C6H11NO | amides | Caprolactam | 3.96 | 15.85 |
| 128.113 | C7H13NO | amides | Formamide, N-cyclohexyl- | 3.98 | 6.39 |
| 129.068 | C7H12O2 | gamma-lactones | Heptalactone, gamma- | 32.17 | 1.80 |
| 130.052 | C9H7N | N-aromatics | Quinoline | 0.00 | 13.49 |
| 131.049 | C9H8O2 | benzofuranones | 1(3H)-Isobenzofuranone, 5-methyl- | 5.02 | 2.15 |
| 140.147 | C9H19NO | amides | Formamide, N,N-dibutyl- | 0.71 | 32.94 |
| 141.165 | C9H18O2 | alkanoic acids | Nonanoic acid | 2.11 | 7.02 |
| 143.100 | C8H14O2 | gamma-lactones | Octalactone, gamma- | 19.72 | 1.53 |
| 144.048 | C10H9N | N-aromatics | Quinoline, 2-methyl- | 1.62 | 2.14 |
| 148.040 | C8H5NO2 | N-aromatics | Phthalimide | 6.03 | 8.21 |
| 149.024 | C8H4O3 | benzofuranones | Phthalic anhydride | 19.55 | 70.04 |
| 157.107 | C9H16O2 | gamma-lactones | Nonalactone, gamma- | 18.07 | 9.52 |
| 163.040 | C9H6O3 | benzofuranones | 4-Methylphthalic anhydride | 35.51 | 19.86 |
| 167.179 | C12H24O | 2-alkanones | 2-Dodecanone | 5.06 | 0.85 |
| 168.072 | C12H9N | N-aromatics | Carbazole | 1.83 | 2.05 |
| 171.126 | C10H18O2 | gamma-lactones | Decalactone, gamma- | 18.05 | 4.74 |
| 173.149 | C10H20O2 | alkanoic acids | n-Decanoic acid | 6.16 | 3.72 |
| 179.086 | C13H8O2 | oxyPAHs | 9H-Fluoren-9-one, 1-hydroxy- | 24.72 | 6.28 |
| 180.088 | C13H9N | N-aromatics | Benzo[f]quinoline | 3.26 | 10.97 |
| 181.099 | C13H8O | oxyPAHs | 9H-Fluoren-9-one | 40.70 | 3.56 |
| 183.083 | C13H10O | oxyPAHs | Benzophenone | 21.35 | 0.44 |
| 185.081 | C12H8S | S-compounds | Dibenzothiophene | 9.23 | 1.12 |
| 185.139 | C11H20O2 | gamma-lactones | Undecalactone, gamma- | 11.50 | 4.63 |
| 193.103 | C15H12 | PAHs | Methyl-phenanthrene-2 | 13.62 | 0.27 |
| 194.100 | C14H11N | N-aromatics | Benzo[f]quinoline, 2-methyl- | 3.30 | 2.06 |
| 195.087 | C14H10O | oxyPAHs | Anthrone-1 | 17.54 | 10.82 |
| 199.043 | - | multiple | Naphtho[1,2-c]furan-1,3-dione; 1,8-Naphthalic anhydride; Dibenzothiophene, 4-methyl- | 5.82 | 6.77 |
| 199.167 | C12H22O2 | gamma-lactones | Dodecalactone, gamma- | 14.30 | 4.31 |
| 201.181 | C12H24O2 | alkanoic acids | Dodecanoic acid | 9.77 | 38.50 |
| 203.087 | C16H10 | PAHs | Fluoranthene | 14.31 | 13.08 |
| 204.097 | C12H13NO2 | N-aromatics | N-n-Butylphthalimide | 4.42 | 9.41 |
| 205.091 | - | multiple | Cyclopenta(def)phenanthrenone; 2-Phenylnaphthalene; 9,10-Anthracenedione, 2- | 20.08 | 12.53 |
| 207.118 | - | multiple | Dimethylphenanthrene-1; Dimethylphenanthrene-2; Dimethylanthracene-1; Dimethylanthracene-2; Dimethylanthracene-3 | 13.07 | 0.23 |
| 209.059 | C14H8O2 | oxyPAHs | Anthraquinone | 17.13 | 29.27 |
| 213.177 | - | multiple | Tridecalactone, delta-; Tridecalactone, gamma-; 6-Methyl-2-tridecanone; 2-Tetradecanone; 3-Tetradecanone; 7H-Benz[de]anthracen-7-one; 11H-Benzo[a]fluoren-11-one | 6.58 | 3.64 |
| 214.084 | C10H15NO2 | N-aromatics | Benzenesulfonamide, N-butyl- | 3.09 | 2.54 |
| 215.192 | C13H26O2 | alkanoic acids | Tridecanoic acid | 6.20 | 13.75 |
| 217.117 | C15H22O2 | aromatic esters | Benzoic acid, 2-ethylhexyl ester | 19.60 | 6.08 |
| 219.050 | C9H14O6 | alkyl esters | Triacetin | 11.89 | 0.34 |
| 227.078 | C18H10 | PAHs | Cyclopenta(cd)pyrene, 3,4-dihydro- | 0.00 | 0.32 |
| 227.197 | C14H26O2 | gamma-lactones | Tetradecalactone, gamma- | 11.79 | 1.20 |
| 227.229 | C15H30O | 2-alkanones | 2-Pentadecanone | 7.28 | 3.62 |

| | | | | | |
|---|---|---|---|---|---|
| 229.146 | - | multiple | Oxybenzone; Benzanthrene; Chrysene; 6,8-Dimethoxy-3,4-dihydro-2H-dibenzofuran-1-one | 13.30 | 7.57 |
| 229.215 | C14H28O2 | alkanoic acids | Tetradecanoic acid | 13.32 | 39.35 |
| 231.129 | - | multiple | 7H-Benz[de]anthracen-7-one; 11H-Benzo[a]fluoren-11-one; Dimethyldibenzothiophene-1; Dimethyldibenzothiophene-2; Dimethyldibenzothiophene-3; Benzyl Benzoate | 7.82 | 1.57 |
| 241.085 | C18H10O2 | oxyPAHs | Benz(A)anthracene-7,12-dione | 4.80 | 0.11 |
| 241.214 | - | multiple | Pentadecalactone, delta-; Pentadecalactone, gamma-; 2-Hexadecanone; 3-Hexadecanone | 21.67 | 1.52 |
| 243.227 | C15H30O2 | alkyl esters | Tetradecanoic acid, methyl ester | 5.96 | 0.59 |
| 245.145 | C16H22O3 | aromatic esters | Homosalate | 7.00 | 19.16 |
| 251.194 | C15H22O3 | aromatic esters | 2-Ethylhexyl salicylate | 30.69 | 40.18 |
| 255.232 | C16H30O2 | gamma-lactones | Hexadecalactone, gamma- | 15.18 | 2.51 |
| 255.259 | C17H34O | 2-alkanones | 2-Heptadecanone | 7.92 | 3.37 |
| 257.247 | C16H32O2 | alkanoic acids | n-Hexadecanoic acid | 79.08 | 150.01 |
| 271.259 | C17H34O2 | alkyl esters | Isopropyl Myristate | 6.48 | 17.04 |
| 279.162 | C16H22O4 | phtalates | Dibutyl phthalate | 13.10 | 42.79 |
| 283.264 | C18H34O2 | gamma-lactones | Octadecalactone, gamma- | 16.97 | 0.12 |
| 299.279 | C19H38O2 | alkyl esters | i-Propyl hexadecanoate | 12.12 | 3.56 |
| 371.352 | C27H46 | hopanes | 17a(H)-22,29,30-trisnorhopane | 2.74 | 0.10 |
| 387.383 | C25H40O4 | phtalates | Phthalic acid, ethyl pentadecyl ester | 2.17 | 0.45 |
| 399.398 | C29H50 | hopanes | 17a(H),21b(H)-30-norhopane | 0.31 | 0.15 |
| 413.413 | C30H52 | hopanes | 17a(H),21b(H)-hopane | 0.45 | 0.10 |
| 427.428 | C31H54 | hopanes | 17a(H),21b(H)-22S-homohopane | 1.07 | 0.10 |

# Chapter 5: Summary and Outlook

The goal of the work that has been described in this thesis was to develop novel analytical approaches for detailed studies on processes of atmospheric organic gases and aerosols including measurements in the laboratory and in the field. The core instrument around which the new applications were built is a PTR-TOF-MS. This instrument allows for online measurements of volatile organic compounds with proton affinities higher than that of water. A significant advantage of the PTR-TOF-MS is its high mass resolution, which allows distinguishing compounds with mass difference below 250 ppm, such as isoprene and furane with molecular weights of 68.063 and 68.026 Da, respectively.

First, a laboratory system to study the impact of air pollution on plant emissions with the PTR-TOF-MS was developed and tested, in collaboration with the Institute for Environmental Biology at Utrecht University. A setup consisting of two plant chambers and a reaction chamber with gas chromatography assisted PTR-TOF-MS as a detection unit was built. The gas chromatography was included in the setup to allow for better identification of isomeric compounds in air samples delivered from the chambers system, which is a great benefit. For example, birch seedlings emit several monoterpenes (all detected at m/z 81.070 and 137.133 Da with PTR-TOF-MS). In case only PTR-TOF-MS was used as a detection unit, we could only characterize the total monoterpene emissions. With the use of gas chromatography we observed that three different monoterpenes (α-pinene, d-limonene and β-phellandrene) were mainly emitted. This is of importance, since different monoterpenes have very different capacities to form SOA in the atmosphere. Moreover, monoterpenes are used by plants for plant-to-ecosystem communication and different monoterpenes are responsible for delivering different messages.

The flexibility of the setup allows using plant chambers of different size and designs. The use of small plant chambers in the setup allows for faster implementation of experiments with young plants that can be grown and measured within a few weeks. Results from a pilot study (not included in this thesis) demonstrate the capacity of the system to investigate environmental issues of high importance, such as the investigation on the discrepancy between the observed and predicted chemical loss of ozone via reactions with plant emissions. The system has also been used to study the impact of pollution and UV-B radiation on plant emissions. The discovered increased plant emissions upon UV-B radiation are

currently further investigated by my colleague Paulien Gankema. Identifying the genes that are responsible for the enhanced emissions will be a part of her PhD thesis. More studies on how plants respond to air pollution are of great interest. In our system air pollution can be simulated by mixing plant emissions and ozone in the reaction chamber. In step 2 another plant (of the same species) is exposed to the polluted air. In such way the complex effects of pollution can be studied, such as changes in the emission capacity or altered chemical communication between the plants.

The work presented in Chapter 2 identified several possible improvements to the system. First, fans in the big plant chambers can be installed to allow for a faster mixing. The current mixing time is 30 min and, even though that was fast enough for the measurements presented in Chapter 2, the faster mixing would lead to quicker stabilization of the system with plants, which would allow for faster experiments. Second, the light intensity in the setup could be increased through, e.g., LEDs (versus currently used TL-D lamps) to allow for higher plant emissions and, consequently, an improved possibility to observe relatively small changes in emissions. Currently observed emissions were low and near to the detection limit. Moreover, LEDs cause lower heating than conventional lamps which is beneficial for the setup, since temperature in the plant chambers will not be changed substantially and no additional temperature control is required. Third, a $NO_x$ source and detector can be installed to control $NO_x$ levels in the reaction chamber so that ozonolysis experiments can be performed either under $NO_x$ or VOC limiting conditions.

As a second analytical achievement, an offline aerosol measurement technique (offline TD-PTR-MS) was developed and validated based on the comparison measurements with the in situ TD-PTR-MS technique during a field study at the Cabauw Experimental Site for Atmospheric Research (CESAR)[2] in winter 2011. The experiments consisted of aerosol sampling on quartz filters using a high volume filter sampler in the field with consecutive analysis of the collected filters in the laboratory using a custom made thermal desorption unit and the PTR-TOF-MS as a detection unit.

The comparison between the in situ and filter measurements revealed that filters sampled for one day were influenced by strong positive filter sampling artifacts

[2] http://www.cesar-observatory.nl/

(50-80% of the organic aerosol mass), which is likely caused by the adsorption of gas phase compounds on the filters due to the high specific surface area of the quartz filters. For filters sampled for two and three days, slightly negative artifacts were observed (7-35% of the organic aerosol mass) which is likely caused by incomplete desorption of aerosols off the filters and/or loss due to chemical reactions on the filters. The big advantage of the offline setup is that it makes application of PTR-TOF-MS much more flexible and logistically simpler. Measurements of filters collected in various locations can be performed relatively quickly, providing useful insights on organic aerosol composition at locations that have not been previously characterized in detail. However, well-controlled filter handling is required to minimize artifacts and to yield comparable results between the filters. It is necessary to store filters almost immediately in the freezer after sampling is finished, and a minimum filter sampling period of two days is advised to minimize the artifacts. For filters sampled for one day the use of backup filters may be the best choice to correct for artifacts associated with the adsorption of semivolatile gas phase compounds. Backup filters are filters located during aerosol sampling behind sampling (front) filters, so that no particles but only vapors are adsorbed on the backup filters. The relatively low associated costs make offline TD-PTR-MS attractive also for student projects. For example, Niels van Elst analyzed filter samples from a ship cruise in across the Atlantic Ocean (S-N traject) and found distinct signatures of pollution as the ship approach the European continent and also in the Southern Atlantic.

Calibration measurements of the offline TD-PTR-MS technique were performed for monocarboxylic acids. The measurements indicated that alkanoic acids with molecular masses ($M_r$) below 290 Da are quantified well, while large losses (62-96% of the mass) were observed for monocarboxylic acids with $M_r$>300 Da, and the double-bond containing monocarboxylic acids with 220 Da<$M_r$<290 Da, respectively. One possible reason for the incomplete detection of these compounds is that they desorb fully only at temperatures above 350 ˚C. Another possibility is that the acid may be thermally decomposed on the filters during the desorption procedure. In order to understand the exact cause of the low detected fraction, it would be useful to carry out measurements with higher desorption temperatures (above 350 ˚C), which may need adjustment of the thermal desorption unit. Future measurements of the double bond-containing acids with $M_r$<220 Da are needed to test the detection efficiency of these acids. A calibration of the setup with various other classes of compounds would be beneficial and is currently done by Theo

Dorst as part of his research project in the master program *Science Education and Communication*.

In a recent study (Holzinger et al., 2013), we showed that in-situ TD-PTR-MS is capable of quantitatively detecting total organic aerosol (OA), and OA components that are typically detected by aerosol mass spectrometry (e.g. hydrocarbon like OA, semivolatile oxygenated OA, and low volatility oxygenated OA). In order to further characterize this technique, in particular its ability to measure individual organic compounds, in-situ TD-PTR-MS was compared to measurements of filter samples collected during the CalNex 2010 campaign with an two-dimensional gas chromatography - time-of-flight mass spectrometry system (GC×GC/TOF-MS). For most compounds with concentrations above 2 ng/m$^3$ a reasonable agreement was observed, and with the exception of alkanes, all compound classes could be detected. This is a very promising result and clearly warrants further exploration of individual TD-PTR-MS signals. Many of the detected ions are probably due to specific compounds that may carry information on sources and processing of OA in the air. This study showed the potential of TD-PTR-MS to monitor aerosol marker compounds for the first time.

In all, the presented development of the systems leads to a better understanding of the chemical composition of organic aerosol and characterization of plant emissions under various conditions. This is of high value for the following three reasons. First, organic aerosol influences the surface temperature directly and indirectly through light scattering and adsorption, and increase of cloud lifetime. Second, aerosol particles are harmful for human beings as they lead to increased morbidity and mortality. Third, organic gases (VOCs) emitted by plants are oxidized in the atmosphere leading to the formation of carbon dioxide and tropospheric ozone. The latter are anthropogenic greenhouses gases and lead to increased surface temperatures on Earth.

# Bibliography

Andreae, M. O., & Crutzen, P. J. (1997). Atmospheric Aerosols: Biogeochemical Sources and Role in Atmospheric Chemistry. *Science*, *276(2)*, 1052-1058.

Aprea, E., Cappellin, L., Gasperi, F., Morisco, F., Lembo, V., Rispo, A., Tortora, R., Vitaglione, P., Caporaso, N., & Biasioli, F. (2014). Application of PTR-TOF-MS to investigate metabolites in exhaled breath of patients affected by coeliac disease under gluten free diet. *Journal of Chromatography. B, Analytical Technologies in the Biomedical and Life Sciences*, *966*, 208–13. doi:10.1016/j.jchromb.2014.02.015.

Arey, J., Atkinson R., & Aschmann, S. M. (1990). Product study of the gas-phase reactions of monoterpenes with the OH radical in the presence of NOx. *Journal of Geophysical Research, 95(D11)*, 18539– 18546.

Aschmann, S.M., Arey, J., & Atkinson, R. (2002). OH radical formation from the gas-phase reactions of O3 with a series of terpenes. *Atmospheric Environment, 36*, 4347-4355.

Atkinson, R. (1997). Gas-phase tropospheric chemistry of volatile organic compounds. 1. Alkanes and alkenes. *Journal of Physical Chemistry Reference Data*, *26*, 215–290.

Atkinson, R., & Arey, J. (2003). Gas-phase tropospheric chemistry of biogenic volatile organic compounds: a review. *Atmospheric Environment, 37(2)*, 197–219.

Beauchamp, J., Wisthaler, A., Hansel, A., Kleist, E., & Miebach, M. (2005). Ozone induced emissions of biogenic VOC from tobacco: relationships between ozone uptake and emission of LOX products Volatile organic compound (VOC) emissions from tobacco. *Plant Cell Environment*, *28*, 1334–1343.

Biasioli, F., Gasperi, F., Yeretzian, C., & Märk, T. D. (2011). PTR-MS monitoring of VOCs and BVOCs in food science and technology. *TrAC Trends in Analytical Chemistry*, *30*(7), 968–977. doi:10.1016/j.trac.2011.03.009.

Boucher, O., Randall, D., Artaxo, P., Bretherton, C., Feingold, G., Forster, P., Kerminen, V.-M., Kondo, Y., Liao, H., Lohmann, U., Rasch, P., Satheesh, S.K., Sherwood, S., Stevens, B. & Zhang, X.Y. (2013). Clouds and Aerosols. In: Climate Change 2013: *The Physical Science Basis. Contribution of Working Group I to the Fifth Assessment Report of the Intergovernmental Panel on Climate Change* [Stocker, T.F., D. Qin, G.-K. Plattner, M. Tignor, S.K. Allen, J. Boschung, A. Nauels, Y. Xia, V. Bex and P.M. Midgley (eds.)]. Cambridge University Press, Cambridge, United Kingdom and New York, NY, USA.

ten Brink, H. M., Plomp, A., Spoelstra, H., & van de Vate, J. F. (1983). A high-resolution electrical mobility aerosol spectrometer (MAS). *Journal of Aerosol Science, 14*, 589–597, doi:10.1016/0021-8502(83)90064-2.

ten Brink, H., Maenhaut, W., Hitzenberger, R., Gnauk, T., Spindler, G., Even, A., Chi, X., Bauer, H., Puxbaum, H., Putaud, J.-P., Tursic, J., & Berner, A. (2004). INTERCOMP2000: the comparability of methods in use in Europe for measuring the carbon content of aerosol. *Atmospheric Environment, 38*, 6507–6519, doi:10.1016/j.atmosenv.2004.08.027.

Cappa, C.D., Lovejoy, E.R., & Ravishankara, A.R. (2008). Evaporation Rates and Vapor Pressures of the Even-Numbered C8-C18 Monocarboxylic Acids. *Journal of Physical Chemistry A, 112*, 3959-3964.

Chan, A.W.H., Isaacman, G., Wilson, K.R., Worton, D.R., Ruehl, C.R., Nah, T., Gentner, D.R., Dallmann, T.E., Kirchstetter, T.W., Harley, R.A., Gilman, J.B., Kuster, W.C., de Gouw, J.A., Offenberg, J.H., Kleindienst, T.E., Lin, Y.H., Rubitschun, C.L., Surratt, J.D., Hayes, P.L., Jimenez, J.L., & Goldstein, A.H. (2013). Detailed chemical characterization of unresolved complex mixtures in atmospheric organics: Insights into emission sources, atmospheric processing, and secondary organic aerosol formation. *Journal of Geophysical Research: Atmospheres*, *118*, 6783–6796, doi:10.1002/jgrd.50533.

Chandramouli, B., Jang, M., & Kamens, R.M. (2003). Gas–particle partitioning of semi-volatile organics on organic aerosols using a predictive activity coefficient model: analysis of the effects of parameter choices on model performance. *Atmospheric Environment, 37,* 853–864.Coutant, R. W., Brown, L., Chuang, J. C., Riggin R.M., & Lewis R.G. (1988). Phase distribution and artifact formation in ambient air sampling for polynuclear aromatic hydrocarbons. *Atmospheric Environment, 22(2),* 403-409.

Cubasch, U., Wuebbles, D., Chen, D., Facchini, M.C., Frame, D., Mahowald, N., & J.-G. Winther. (2013). Introduction. In: Climate Change 2013: The Physical Science Basis. Contribution of Working Group I to the Fifth Assessment Report of the Intergovernmental Panel on Climate Change [Stocker, T.F., Qin, D., Plattner, G.-K., Tignor, M., Allen, S.K., Boschung,J., Nauels, A., Xia,Y., Bex, V., & Midgley, P.M. (eds.)]. *Cambridge University Press*, Cambridge, United Kingdom and New York, NY, USA.

DeCarlo, P.F., Kimmel, J.R., Trimborn, A., Northway, M.J., Jayne, J.T., Aiken, A.C., Gonin, M., Fuhrer, K., Horvath, T., Docherty, K.S., Worsnop, D.R., & Jimenez, J.L. (2006). Field-Deployable, High-Resolution, Time-of-Flight Aerosol Mass Spectrometer. *Analytical Chemistry, 78*, 8281-8289.

Denman, K. L., Brasseur, G., Chidthaisong, A., Ciais, P., Cox, P. M., Dickinson, R. E., Hauglustaine, D., Heinze, C., Holland, E., Jacob, D., Lohmann, U., Ramachandran, S., da Silva Dias, P. L., Wofsy, S. C., & Zhang, X. (2007). Climate Change 2007: The Physical Science Basis. Contribution of Working Group I to the Fourth Assessment Report of the Intergovernmental Panel on Climate Change. *New York: Cambridge University Press*.

Dentener, F. (2003). Interannual variability and trend of CH 4 lifetime as a measure for OH changes in the 1979–1993 time period. *Journal of Geophysical Research, 108(D15),* 4442, doi:10.1029/2002JD002916.

Donahue, N. M., Kroll, J. H., Pandis, S. N., & Robinson, A. L. (2012). A two-dimensional volatility basis set – Part 2: Diagnostics of organic-aerosol evolution. *Atmospheric Chemistry and Physics*, 12(2), 615–634, doi:10.5194/acp-12-615-2012.

Draxler, R.R., & Rolph, G.D. (2013). HYSPLIT (Hybrid single-particle lagrangian integrated trajectory) Model access via NOAA ARL READY Website (http://www.arl.noaa.gov/HYSPLIT.php). NOAA Air Resources Laboratory, College Park, MD.

Falara, V., Akhtar, T. A., Nguyen, T. T. H., Spyropoulou, E. A., Bleeker, P. M., Schauvinhold, I., Matsuba, Y., Bonini, M.E., Schilmiller, A.L., Last, R.L., Schuurink, R.C., & Pichersky, E. (2011). The tomato terpene synthase gene family. *Plant Physiology, 157,* 770–789.

Fehsenfeld, F., Calvert, J., Fall, R., Goldan, P., Guenther, A. B., Hewitt, C. N., Lamb, B., Liu, S., Trainer, M., Westberg, H., & Zimmerman, P. (1992). Emissions of volatile organic compounds from vegetation and the implications for atmospheric chemistry. *Global Biogeochemical Cycles, 6(4),* 389–430.

Ghirardo, A., Koch, K., Taipale, R., Zimmer, I., Schnitzler, J. P., & Rinne, J. (2010). Determination of de novo and pool emissions of terpenes from four common boreal/alpine trees by 13CO2 labelling and PTR-MS analysis. *Plant Cell Environment, 33,* 781–792.

Goldstein, A. H., & Galbally, I. E. (2007). Known and unexplored organic constituents in the Earth's Atmosphere. *Environmental Science and Technology, 41,* 1514-1521.

Goodner, K.L. (2008). Practical retention index models of OV-101, DB-1, DB-5, and DB-Wax for flavor and fragrance compounds. *Food Science and Technology, 41,* 951-958.

de Gouw, J., & Jimenez, J. L. (2009). Organic aerosols in the Earth's atmosphere. *Environmental Science & Technology, 43(20),* 7614–8. doi:10.1021/es9006004.

Graus, M., Müller, M., & Hansel, A. (2010). High resolution PTR-TOF: quantification and formula confirmation of VOC in real time. *Journal of the American Society for Mass Spectrometry, 21(6),* 1037–1044, doi:10.1016/j.jasms.2010.02.006.

Guenther, A., Nicholas, C., Fall, R., Klinger, L., Mckay, W. A., & Scholes, B. (1995). A global model of natural volatile organic compound emissions. *Journal of Geophysical Research, 100*(94), 8873–8892.

Guenther, A., Geron, C., Pierce, T., Lamb, B., Harley, P., & Fall, R. (2000). Natural emissions of non-methane volatile organic compounds, carbon monoxide, and oxides of nitrogen from North America. *Atmospheric Environment, 34,* 2205-2230.

Guenther, A., Karl, T., Harley, P., Wiedinmyer, C., Palmer, P.I., & Geron, C. (2006). Estimates of global terrestrial isoprene emissions using MEGAN (Model of Emissions of Gases and Aerosols from Nature). *Atmospheric Chemistry and Physics, 6,* 3181-3210.

Hakola, H., Rinne, J., & Laurila, T. (1998). The hydrocarbon emission rates of tea-leafed willow (*Salix Phylicifolia*), silver birch (*Betula Pendula*) and European aspen (*Populus Tremula*). *Atmospheric Environment, 32(10),* 1825-1833.

Hallquist, M., Wenger, J. C., Baltensperger, U., Rudich, Y., Simpson, D., Claeys, M., Dommen, J., Donahue, N.M., George, C., Goldstein, A.H., Hamilton, J.F., Herrmann, H., Hoffmann, T., Iinuma, Y., Jang, M., Jenkin, M.E., Jimenez, J.L., Kiendler-Scharr, A., Maenhaut, W., McFiggans, G., Mentel, Th.F., Monod, A., Prevot, A.S.H., Seinfeld, J.H., Surratt, J.D., Szmigielski, R., & Wildt, J. (2009). The formation , properties and impact of secondary organic aerosol : current and emerging issues. *Atmospheric Chemistry and Physics*, *9*, 5155–5236.

Hamilton, J., Webb, P., Lewis, A., Hopkins, J., Smith, S., & Davy, P. (2004). Partially oxidised organic components in urban aerosol using GCXGC-TOF/MS. *Atmospheric Chemistry and Physics Discussions*, *4(2)*, 1393–1423, doi:10.5194/acpd-4-1393-2004.

Harren, F. J. M., & Cristescu, S. M. (2013). Online, real-time detection of volatile emissions from plant tissue. *AoB Plants*, *5*, plt003. doi:10.1093/aobpla/plt003.

Harrison, R. M., & Yin, J. (2000). Particulate matter in the atmosphere: which particle properties are important for its effects on health? *Science of The Total Environment*, *249*, 85–101.

Hartikainen, K., Riikonen, J., Nerg, A., Kivimäenpää, M., Ahonen, V., Tervahauta, A., Kärenlampi, S., Mäenpää, M., Rousi, M., Kontunen-Soppela, S., Oksanen, E., & Holopainen, T. (2012). Impact of elevated temperature and ozone on the emission of volatile organic compounds and gas exchange of silver birch (*Betula pendula* Roth). *Environmental and Experimental Botany*, *84*, 33-43.

Hatakeyama, S., Izumi, K., & Akimoto, H. (1991). Reactions of OH with α-pinene and β-pinene in air: estimate of global CO production from the atmospheric oxidation of terpenes, *Journal of Geophysical Research, 96 (D1)*, 947–958.

Hayes, P. L., Ortega, A. M., Cubison, M. J., Froyd, K. D., Zhao, Y., Cliff, S. S., Hu, W.W., Toohey, D.W., Flynn, J.H., Lefer, B.L., Grossberg, N., Alvarez, S., Rappenglück, B., Taylor, W., Allan, J.D., Holloway, J.S., Gilman, J.B., Kuster, W.C., de Gouw, J.A., Massoli, P., Zhang, X., Liu, J., Weber, R.J., Corrigan, A.L., Russell, L.M., Isaacman, G., Worton, D.R., Kreisberg, N.M., Goldstein, A.H., Thalman, R., Waxman, E.M., Volkamer, R., Y.H.Lin, Surratt, J.D., Kleindienst, T.E., Offenberg, J.H., Dusanter, S., Griffith, S., Stevens, P.S., Brioude, J., Angevine, W.M., & Jimenez, J. L. (2013). Organic aerosol composition and sources in Pasadena, California, during the 2010 CalNex campaign. *Journal of Geophysical Research: Atmospheres*, *118(16)*, 9233–9257. doi:10.1002/jgrd.50530

Holzinger, R., Williams, J., Herrmann, F., Lelieveld, J., Donahue, N. M., & Röckmann, T. (2010a). Aerosol analysis using a Thermal-Desorption Proton-Transfer-Reaction Mass

Spectrometer (TD-PTR-MS): a new approach to study processing of organic aerosols. *Atmospheric Chemistry and Physics*, *10*, 2257–2267, doi:10.5194/acp-10-2257-2010.

Holzinger, R., Kasper-Giebl, A., Staudinger, M., Schauer, G., & Röckmann, T. (2010b). Analysis of the chemical composition of organic aerosol at the Mt. Sonnblick observatory using a novel high mass resolution thermal-desorption proton-transfer-reaction mass-spectrometer (hr-TD-PTR-MS). *Atmospheric Chemistry and Physics*, *10*, 10111–10128, doi:10.5194/acp-10-10111-2010.

Holzinger, R., Goldstein, A. H., Hayes, P. L., Jimenez, J. L., & Timkovsky, J. (2013). Chemical evolution of organic aerosol in Los Angeles during the CalNex 2010 study. *Atmospheric Chemistry and Physics*, *13*, 10125–10141, doi:10.5194/acp-13-10125-2013.

Huffman, J. A., Docherty K. S., Aiken A. C., Cubison M. J., Ulbrich I. M., DeCarlo P. F., Sueper D., Jayne J. T., Worsnop D. R., Ziemann P. J., & Jimenez J. L. (2009). Chemically-resolved aerosol volatility measurements from two megacity field studies. *Atmospheric Chemistry and Physics*, *9*, 7161–7182.

Ibrahim, M. A., Mäenpää, M., Hassinen, V., Kontunen-Soppela, S., Malec, L., Rousi, M., Pietikäinen, L., Tervahauta, A., Kärenlampi, S., Holopainen, J.K., & Oksanen, E.J. (2010). Elevation of night-time temperature increases terpenoid emissions from *Betula pendula* and *Populus tremula. Journal of Experimental Botany, 61(6),* 1583–1595.

Jaoui, M., & Kamens, R. M. (2003). Mass balance of gaseous and particulate products from beta-pinene/O3/air in the absence of light and beta-pinene/NOx/air in the presence of natural sunlight. *Journal of Atmospheric Chemistry, 45(2),* 101–141.

Jayne, J. T., Leard, D. C., Zhang, X. F., Davidovits, P., Smith, K. A., Kolb, C. E., & Worsnop, D. R. (2000). Development of an aerosol mass spectrometer for size and composition analysis of submicron particles. *Aerosol Science and Technology*, *33*, 49–70.

Jimenez, J. L., Canagaratna, M. R., Donahue, N. M., Prevot, a S. H., Zhang, Q., Kroll, J. H., DeCarlo, P.F., Allan, J.D., Coe, H., Ng, N.L., Aiken, A.C., Docherty, K.S., Ulbrich, I.M., Grieshop, A.P., Robinson, A.L., Duplissy, J., Smith, J.D., Wilson, K.R., Lanz, V.A., Hueglin, C., Sun, Y.L., Tian, J., Laaksonen, A., Raatikainen, T., Rautiainen, J., Vaattovaara, P., Ehn, M., Kulmala, M., Tomlinson, J.M., Collins, D.R., Cubison, M.J., Dunlea, E.J., Huffman, J.A., Onasch, T.B., Alfarra, M.R., Williams, P.I., Bower, K., Kondo, Y., Schneider, J., Drewnick, F., Borrmann, S., Weimer, S., Demerjian, K., Salcedo, D., Cottrell, L., Griffin, R., Takami, A., Miyoshi, T., Hatakeyama, S., Shimono, A., Sun, J.Y., Zhang, Y.M. Dzepina, K., Kimmel, J.R., Sueper, D., Jayne, J.T., Herndon, S.C., Trimborn, A.M., Williams, L.R., Wood, E.C., Middlebrook, A.M., Kolb, C.E., Baltensperger, U., & Worsnop, D. R. (2009). Evolution of organic aerosols in the atmosphere. *Science*, *326*, 1525–9. doi:10.1126/science.1180353.

Jordan, A., Haidacher, S., Hanel, G., Hartungen, E., Märk, L., Seehauser, H., Schottkowsky, R., Sulzer P., & Mark, T.D. (2009). A high resolution and high sensitivity

proton-transfer-reaction time-of-flight mass spectrometer (PTR-TOF-MS). *International Journal of Mass Spectrometry, 286(2-3),* 122–128, doi:10.1016/j.ijms.2009.07.005.

Kallio, M., Jussila, M., Rissanen, T., Anttila, P., Hartonen, K., Reissell, A., Vreuls, R., Adahchour, M., & Hyötyläinen, T. (2006). Comprehensive two-dimensional gas chromatography coupled to time-of-flight mass spectrometry in the identification of organic compounds in atmospheric aerosols from coniferous forest. *Journal of Chromatography. A, 1125(2),* 234–43, doi:10.1016/j.chroma.2006.05.050.

Kanakidou, M., Seinfeld, J. H., Pandis, S. N., Barnes, I., Dentener, F. J., Facchini, M. C., Van Dingenen, R., Ervens, B., Nenes, a., Nielsen, C. J., Swietlicki, E., Putaud, J. P., Balkanski, Y., Fuzzi, S., Horth, J., Moortgat, G. K., Winterhalter, R., Myhre, C. E. L., Tsigaridis, K., Vignati, E., Stephanou, E. G., & Wilson, J. (2005). Organic aerosol and global climate modelling: a review. *Atmospheric Chemistry and Physics*, *5*, 1053–1123, doi:10.5194/acp-5-1053-2005.

Karl, T., Harley, P., Guenther, A., Rasmussen, R., Baker, B., Jardine, K., & Nemitz, E. (2005). The bi-directional exchange of oxygenated VOCs between a loblolly pine (Pinus taeda) plantation and the atmosphere. *Atmospheric Chemistry and Physics*, *5*, 3015–3031.

Karl, T., Harley, P., Emmons, L., Thornton, B., Guenther, A., Basu, C., Turnipseed, A., & Jardine, K. (2010). Efficient atmospheric cleansing of oxidized organic trace gases by vegetation. *Science, 330(6005),* 816–819.

Kawamura, K., & Sakaguchi, F. (1999). Molecular distributions of water soluble dicarboxylic acids in marine aerosols over the Pacific Ocean including tropics. *Journal of Geophysical Research, 104*, 3501–3509.

Kegge, W., & Pierik, R. (2009). Biogenic volatile organic compounds and plant competition, *Trends in Plant Science, 15(3),* 126-132.

Kegge, W., Weldegergis, B.T., Soler, R., Vergeer-Van Eijk, M., Dicke, M., Voesenek, L.A.C.J., & Pierik, R. (2013). Canopy light cues affect emission of constitutive and methyl jasmonate-induced volatile organic compounds in Arabidopsis thaliana, *New Phytologist, 200 (3),* 861-874.

Kirchstetter, T. W., Corrigan, C. E., & Novakov, T. (2001). Laboratory and field investigation of the adsorption of gaseous organic compounds onto quartz filters. *Atmospheric Environment, 35*, 1663–1671.

Kirschke, S., Bousquet, P., Ciais, P., Saunois, M., Canadell, J. G., Dlugokencky, E. J., Bergamaschi, P., Bergmann, D., Blake, D.R., Bruhwiler, L., Cameron-Smith, P., Castaldi, S., Chevallier, F., Feng, L., Fraser, A., Heimann, M., Hodson, E.L., Houweling, S., Josse, B., Fraser, P.J., Krummel, P.B., Lamarque, J.-F., Langenfelds, R.L., Le Quéré, C., Naik, V., O'Doherty, S., Palmer, P.I., Pison, I., Plummer, D., Poulter, B., Prinn, R.J., Rigby, M., Ringeval, B., Santini, M., Schmidt, M., Shindell, D.T., Simpson, I.J., Spahni, R., Steele,

L.P., Strode, S.A., Sudo, K., Szopa, S., van der Werf, G.R., Voulgarakis, A., van Weele, M., Weiss, R.F., Williams, J.E., & Zeng, G. (2013). Three decades of global methane sources and sinks. *Nature Geoscience, 6(10),* 813–823, doi:10.1038/ngeo1955.

König, G., Brunda, M., Puxbaum, H., Hewitt, C. N., Duckham, S. C., & Rudolph, J. (1995). Relative contribution of oxygenated hydrocarbons to the total biogenic VOC emissions of selected mid-European agricultural and natural plant species. *Atmospheric Environment, 29(8),* 861–874.

Kulmala, M. (2003). How particles nucleate and grow, *Science, 302,* 1000–1001.

Lambe, A. T., Chacon-Madrid, H. J., Nguyen, N. T., Weitkamp, E. a., Kreisberg, N. M., Hering, S. V., Goldstein, A. H., Donahue, N. M., & Robinson, A. L. (2010). Organic aerosol speciation: intercomparison of Thermal Desorption Aerosol GC/MS (TAG) and filter-based techniques. *Aerosol Science and Technology, 44*, 141–151, doi:10.1080/02786820903447206.

Larsen, Bo.R., Di Bella, D., Glasius, M., Winterhalter, R., Jensen, N. R., & Hjorth, J. (2001). Gas-Phase OH Oxidation of Monoterpenes: Gaseous and Particulate Products. *Journal of Atmospheric Chemistry, 38,* 231–276.

Leblanc, D.C. (2004). Statistics - Concepts and Applications for Science, 189, *Jones and Bartlett,* Sudbury, MA.

Lee, A., Goldstein, A. H., Kroll, J. H., Ng, N. L., Varutbangkul, V., Flagan, R. C., & Seinfeld, J. H. (2006). Gas-phase products and secondary aerosol yields from the photooxidation of 16 different terpenes. *Journal of Geophysical Research, 111,* D17305.

Legrand, M., & De Angelis, M. (1996). Light carboxylic acids in Greenland ice : A record of past forest fires and vegetation emissions from the boreal zone. *Journal of Geophysical Research, 101 (D2),* 4129–4145.

Lindinger, W., Hansel, A., & Jordan, A. (1998). On-line monitoring of volatile organic compounds at pptv levels by means of Proton-Transfer-Reaction Mass Spectrometry (PTR-MS). Medical applications, food control and environmental research. *International Journal of Mass Spectrometry and Ion Processes, 173,* 191-241.

Lipsky, E. M., & Robinson, A. L. (2006). Effects of dilution on fine particle mass and partitioning of semivolatile organics in diesel exhaust and wood smoke. *Environmental Science and Technology, 40*, 155–162.

Lopez-Hilfiker, F. D., Mohr, C., Ehn, M., Rubach, F., Kleist, E., Wildt, J., Mentel, Th. F., Lutz, A., Hallquist, M., Worsnop, D., & Thornton, J. A. (2014). A novel method for online analysis of gas and particle composition: description and evaluation of a Filter Inlet for Gases and AEROsols (FIGAERO). *Atmospheric Measurement Techniques, 7*, 983–1001.

Mader, B. T., & Pankow, J. F. (2001). Gas/solid partitioning of semivolatile organic compounds (SOCs) to air filters. 3. An analysis of gas adsorption artifacts in measurements of atmospheric SOCs and organic carbon (OC) when using teflon membrane filters and quartz fiber filters. *Environmental Science and Technology, 35(17),* 3422–3432.

McDow, S.R., & Hunzicker, J.J. (1990). Vapor adsorption artifact in the sampling of organic aerosol: face velocity effects. *Atmospheric Environment, 24A(10),* 2563-2571.

Mentel, T. F., Wildt, J., Kiendler-Scharr, A., Kleist, E., Tillmann, R., Dal Maso, M., Fisseha, R., Hohaus, Th., Spahn, H., Uerlings, R., Wegener, R., Griffiths, P.T., Dinar, E., Rudich, Y., & Wahner, A. (2009). Photochemical production of aerosols from real plant emissions. *Atmospheric Chemistry and Physics, 9,* 4387–4406.

Montzka, S. S, Krol, M., Dlugokencky, E., Hall, B., Jöckel, P., & Lelieveld, J. (2011). Small interannual variability of global atmospheric hydroxyl. *Science, 331,* 67–9, doi:10.1126/science.1197640.

Myhre, G., Shindell, D., Bréon, F.-M., Collins, W., Fuglestvedt, J., Huang, J., Koch, D., Lamarque, J.-F., Lee, D., Mendoza, B., Nakajima, T., Robock, A., Stephens, G., Takemura, T., & Zhang, H. (2013). Anthropogenic and Natural Radiative Forcing. In: Climate Change 2013: The Physical Science Basis. Contribution of Working Group I to the Fifth Assessment Report of the Intergovernmental Panel on Climate Change [Stocker, T.F., Qin, D., Plattner, G.-K., Tignor, M., Allen, S.K., Boschung, J., Nauels, A., Xia, Y., Bex, V., & Midgley, P.M. (eds.)]. Cambridge University Press, Cambridge, United Kingdom and New York, NY, USA.

Nel, A. (2005). Atmosphere. Air pollution-related illness: effects of particles. *Science, 308,* 804–6, doi:10.1126/science.1108752.

Niinemets, Ü. (2009). Mild versus severe stress and BVOCs: thresholds, priming and consequences. *Trends in Plant Science, 15(3),* 145-153.

Orlando, J.J., Noziere, B., Tyndall, G.S., Orzechowska, G.E., Paulson, S.E., & Rudich, Y. (2000). Product studies of the OH- and ozone-initiated oxidation of some monoterpenes. *Journal of Geophysical Research, 105 (D9),* 11561–11572.

Park, J.-H., Goldstein, A. H., Timkovsky, J., Fares, S., Weber, R., Karlik, J., & Holzinger, R. (2013). Active atmosphere-ecosystem exchange of the vast majority of detected volatile organic compounds. *Science, 341,* 643–7, doi:10.1126/science.1235053.

van Poecke, R.M.P., Posthumus, M. A., & Dicke, M. (2001). Herbivore-induced volatile production by Arabidopsis thaliana leads to attraction of the parasitoid Cotesia rubecula: chemical, behavioral, and gene-expression analysis. *Journal of Chemical Ecology, 27(10),* 1911–1928.

Pope, C.A., & Dockery, D. W. (2006). Health Effects of Fine Particulate Air Pollution : Lines that Connect. *Journal of Air and Waste Management Association, 56*, 709–742.

Prinn, R., Cunnold, D., Simmonds, P., Alyea, F., Boldi, R., Crawford, A., & Fraser, P. (1992). Global Average Concentration and Trend for Hydroxyl Radicals Deduced From ALE / GAGE Trichloroethane (Methyl Chloroform) Data for 1978-1990. *Journal of Geophysical Research, 97 (D2)*, 2445–2461.

Riess, U., Tegtbur, U., Fauck, C., Fuhrmann, F., Markewitz, D., & Salthammer, T. (2010). Experimental setup and analytical methods for the non-invasive determination of volatile organic compounds, formaldehyde and NOx in exhaled human breath. *Analytica Chimica Acta*, 669(1-2), 53–62, doi:10.1016/j.aca.2010.04.049.

Riipinen, I., Pierce, J. R., Yli-Juuti, T., Nieminen, T., Häkkinen, S., Ehn, M., Junninen, H., Lehtipalo, K., Petaja, T., Slowik, J., Chang, R., Shantz, N.C., Abbatt, J., Leaitch, W. R., Kerminen, V.-M., Worsnop, D. R., Pandis, S. N., Donahue, N. M., & Kulmala, M. (2011). Organic condensation: a vital link connecting aerosol formation to cloud condensation nuclei (CCN) concentrations. *Atmospheric Chemistry and Physics, 11(8)*, 3865–3878.

Rolph, G.D. (2013). Real-time environmental applications and Display system (READY) website (http://www.ready.noaa.gov), NOAA Air Resources Laboratory, College Park, MD.

Romano, A., Fischer, L., Herbig, J., Campbell-Sills, H., Coulon, J., Lucas, P., Cappellin, L., & Biasioli, F. (2014). Wine analysis by FastGC proton-transfer reaction-time-of-flight-mass spectrometry. *International Journal of Mass Spectrometry*, *369*, 81–86, doi:10.1016/j.ijms.2014.06.006.

Sahu, L. K. (2012). Volatile organic compounds and their measurements in the troposphere. *Current Science, 102(12)*, 1645-1649.

Schauer, C., Niessner, R., & Pöschl, U. (2003). Polycyclic aromatic hydrocarbons in urban air particulate matter: decadal and seasonal trends, chemical degradation, and sampling artifacts. *Environmental Science and Technology*, *37*, 2861–2868.

Schripp, T., Etienne, S., Fauck, C., Fuhrmann, F., Märk, L., & Salthammer, T. (2014). Application of proton-transfer-reaction-mass-spectrometry for Indoor Air Quality research. *Indoor Air*, *24(2)*, 178–89, doi:10.1111/ina.12061.

Schripp, T., Fauck, C., & Salthammer, T. (2010). Interferences in the determination of formaldehyde via PTR-MS: What do we learn from m/z 31? *International Journal of Mass Spectrometry*, *289(2-3)*, 170–172, doi:10.1016/j.ijms.2009.11.001.

Shorees, B., Atkinson, R., & Arey, J. (1991). Product formation from the gas-phase reactions of OH radicals and O3 with β-Phellandrene. *International Journal of Chemical Kinetics*, *23*, 897-906.

Sihabut, T., Ray, J., Northcross, A., & McDow, S. R. (2005). Sampling artifact estimates for alkanes, hopanes, and aliphatic carboxylic acids. *Atmospheric Environment*, *39*(37), 6945–6956. doi:10.1016/j.atmosenv.2005.02.053.

Subramanian, R., Khlystov, A. Y., Cabada, J. C., & Robinson, A. L. (2004). Positive and negative artifacts in particulate organic carbon measurements with denuded and undenuded sampler configurations. *Aerosol Science and Technology, 38(S1),* 27–48, doi:10.1080/02786820390229354.

Subramanian, R., Donahue, N. M., Bernardo-Bricker, A., Rogge, W. F., & Robinson, A. L. (2007). Insights into the primary-secondary and regional-local contributions to organic aerosol and PM2.5 mass in Pittsburgh, Pennsylvania. *Atmospheric Environment, 41*, 7414-7433.

Summerfelt, S.T., & Hochheimer, J.N. (1997). Review of ozone processes and applications as an oxidizing agent in aquaculture. *The Progressive Fish-Culturist, 59*, 94-105.

Timkovsky, J., Dusek, U., Henzing, J.S., Kuipers, T.L., Röckmann, T., & Holzinger, R. (2015). Offline thermal-desorption proton-transfer-reaction mass spectrometry to study composition of organic aerosol. *Journal of Aerosol Science*, 79, 1-14, doi: 10.1016/j.jaerosci.2014.08.010.

Turpin, J., & Huntzicker, J. J. (1994). Investigation of organic aerosol sampling in the Los Angeles basin. *Atmospheric Environment, 28(19),* 3061-3071.

Turpin, B. J., Saxena, P., & Andrews, E. (2000). Measuring and simulating particulate organics in the atmosphere: problems and prospects. *Atmospheric Environment, 34(18),* 2983–3013, doi:10.1016/S1352-2310(99)00501-4.

Ulbrich, I. M., Canagaratna, M. R., Zhang, Q., Worsnop, D. R., & Jimenez, J. L. (2009). Interpretation of organic components from Positive Matrix Factorization of aerosol mass spectrometric data. *Atmospheric Chemistry and Physics, 9(9),* 2891–2918, doi:10.5194/acp-9-2891-2009.

Veres, P. R., Roberts, J. M., Cochran, A. K., Gilman, J. B., Kuster, W. C., Holloway, J. S., Graus, M., Flynn, J., Lefer, B., Warneke, C., & de Gouw, J. (2011). Evidence of rapid production of organic acids in an urban air mass. *Geophysical Research Letters, 38(17),* L17807, doi:10.1029/2011GL048420.

Viana, M., Chi, X., Maenhaut, W., Cafmeyer, J., Querol, X., Alastuey, A., Mikuška, P., & Večeřa, Z. (2006). Influence of sampling artefacts on measured PM, OC, and EC levels in carbonaceous aerosols in an urban area. *Aerosol Science and Technology*, *40*, 107–117, doi:10.1080/02786820500484388.

Viana, M., Maenhaut, W., ten Brink, H. M., Chi, X., Weijers, E., Querol, X., Alastuey, A., Mikuška, P., & Večeřa, Z. (2007). Comparative analysis of organic and elemental carbon concentrations in carbonaceous aerosols in three European cities. *Atmospheric Environment*, *41*, 5972–5983, doi:10.1016/j.atmosenv.2007.03.035.

Vogel, A. L., Äijälä, M., Brüggemann, M., Ehn, M., Junninen, H., Petäjä, T., Worsnop, D.R., Kulmala, M., Williams, J., & Hoffmann, T. (2013). Online atmospheric pressure

chemical ionization ion trap mass spectrometry (APCI-IT-MSn) for measuring organic acids in concentrated bulk aerosol – a laboratory and field study. *Atmospheric Measurement Techniques, 6(2),* 431–443, doi:10.5194/amt-6-431-2013.

Volk, H.E., & Hertz-Picciotto, I. (2013). Traffic-related air pollution, particulate matter, and autism. *JAMA Psychiatry, 70(1),* 71-77, doi: 10.1001/jamapsychiatry.2013.266.

Watson, J. G., Chow, J. C., Chen, L.-W. A., & Frank, N. H. (2009). Methods to assess carbonaceous aerosol sampling artifacts for IMPROVE and other long-term networks. *Journal of the Air and Waste Management Association, 59*, 898–911, doi:10.3155/1047-3289.59.8.898.

Weber, R. J., Orsini, D., Daun, Y., Lee, Y.-N., Klotz, P. J., & Brechtel, F. (2001). A Particle-into-Liquid Collector for Rapid Measurement of Aerosol Bulk Chemical Composition. *Aerosol Science and Technology*, *35*, 718–727, doi:10.1080/02786820152546761.

Weiner, I.B., & Craighead, W.E. (2010). Corsini Encyclopedia of Psychology, 1723, Hoboken, NJ, Wiley.

Wiedensohler, A., Birmili, W., Nowak, A., Sonntag, A., Weinhold, K., Merkel, M., Wehner, B., Tuch, T., Pfeifer, S., Fiebig, M., Fjäraa, A. M., Asmi, E., Sellegri, K., Depuy, R., Venzac, H., Villani, P., Laj, P., Aalto, P., Ogren, J. A., Swietlicki, E., Williams, P., Roldin, P., Quincey, P., Hüglin, C., Fierz-Schmidhauser, R., Gysel, M., Weingartner, E., Riccobono, F., Santos, S., Grüning, C., Faloon, K., Beddows, D., Harrison, R., Monahan, C., Jennings, S. G., O'Dowd, C. D., Marinoni, A., Horn, H.-G., Keck, L., Jiang, J., Scheckman, J., McMurry, P. H., Deng, Z., Zhao, C. S., Moerman, M., Henzing, B., de Leeuw, G., Löschau, G., & Bastian, S. (2012). Mobility particle size spectrometers: harmonization of technical standards and data structure to facilitate high quality long-term observations of atmospheric particle number size distributions. *Atmospheric Measurement Techniques, 5*, 657-685, doi:10.5194/amt-5-657-2012.

Williams, B. J., Goldstein, A. H., Kreisberg, N. M., & Hering, S. V. (2006). An in situ instrument for speciated organic composition of atmospheric aerosols: Thermal Desorption Aerosol GC/MS-FID (TAG). *Aerosol Science and Technology, 40*, 627–638, doi:10.1080/02786820600754631.

Williams, B. J., Goldstein, A. H., Kreisberg, N. M., & Hering, S. V. (2010). In situ measurements of gas/particle-phase transitions for atmospheric semivolatile organic compounds. *Proceedings of the National Academy of Sciences, 107(15),* 6676–81, doi:10.1073/pnas.0911858107.

Williams, B. J., Jayne, J. T., Lambe, A. T., Hohaus, T., Kimmel, J. R., Sueper, D., Brooks, W., Williams, L.R., Trimborn, A.M., Martinez, R.E., Hayes, P.L., Jimenez, J.L., Kreisberg, N.M., Hering, S.V., Worton, D.R., Goldstein, A.H., & Worsnop, D. R. (2014). The First Combined Thermal Desorption Aerosol Gas Chromatograph—Aerosol Mass Spectrometer

(TAG-AMS). *Aerosol Science and Technology, 48(4),* 358–370, doi:10.1080/02786826.2013.875114

Wisthaler, A., Jensen, N.R., Winterhalter, R., Lindinger, W., & Hjorth, J. (2001). Measurements of acetone and other gas phase product yields from the OH-initiated oxidation of terpenes by proton-transfer-reaction mass spectrometry (PTR-MS), *Atmospheric Environment, 35,* 6181–6191.

Worton, D. R., Kreisberg, N. M., Isaacman, G., Teng, A. P., McNeish, C., Górecki, T., Hering, S.V., & Goldstein, A. H. (2012). Thermal Desorption Comprehensive Two-Dimensional Gas Chromatography: An Improved Instrument for In-Situ Speciated Measurements of Organic Aerosols. *Aerosol Science and Technology, 46(4),* 380–393, doi:10.1080/02786826.2011.634452.

Yatavelli, R. L. N., & Thornton, J. A. (2010). Particulate organic matter detection using a Micro-Orifice Volatilization Impactor Coupled to a Chemical Ionization Mass Spectrometer (MOVI-CIMS). *Aerosol Science and Technology, 44,* 61–74, doi:10.1080/02786820903380233.

Yatavelli, R. L. N., Stark, H., Thompson, S. L., Kimmel, J. R., Cubison, M. J., Day, D. A., Campuzano-Jost, P., Palm, B.B., Hodzic, A., Thornton, J.A. Jayne, J.T., Worsnop, D.R., & Jimenez, J. L. (2014). Semicontinuous measurements of gas–particle partitioning of organic acids in a ponderosa pine forest using a MOVI-HRToF-CIMS. *Atmospheric Chemistry and Physics, 14(3),* 1527–1546, doi:10.5194/acp-14-1527-2014.

Yu, J. Z., Xu, J., & Yang, H. (2002). Charring characteristics of atmospheric organic particulate matter in thermal analysis. *Environmental Science and Technology, 36,* 754–761.

Zhao, J., & Zhang, R. Y. (2004). Proton transfer reaction rate constants between hydronium ion (H3O(+)) and volatile organic compounds. *Atmospheric Environment, 38,* 2177–2185.

Zhao, Y., Kreisberg, N. M., Worton, D. R., Isaacman, G., Gentner, D.R., Chan, A.W.H., Weber, R.J., Liu, S., Day, D.A., Russell, L.M., Hering, S.V., & Goldstein, A.H. (2013). Sources of organic aerosol investigated using organic compounds as tracers measured during CalNex in Bakersfield. *Journal of Geophysical Research, 118(11),* 11388–11398, doi:10.1002/jgrd.50825.

# List of publications

**Timkovsky, J.**, Gankema, P., Pierik, R., & Holzinger, R. (2014). A plant chamber system with downstream reaction chamber to study the effects of pollution on biogenic emissions. *Environmental Science: Processes and Impacts*, 16, 2301-2312, doi: 10.1039/C4EM00214H.

**Timkovsky, J.**, Dusek, U., Henzing, J.S., Kuipers, T.L., Röckmann, T., & Holzinger, R. (2015). Offline thermal-desorption proton-transfer-reaction mass spectrometry to study composition of organic aerosol. *Journal of Aerosol Science*, 79, 1-14, doi: 10.1016/j.jaerosci.2014.08.010.

**Timkovsky, J.**, Chan, A.W.H., Dorst, T., Goldstein, A.H., Oyama, B., & Holzinger, R. Organic aerosol composition measurements with advanced offline and in-situ techniques during the CalNex campaign. Manuscript submitted to *Atmospheric Measurement Techniques*, 2014.

Park, J.-H., Goldstein, A. H., **Timkovsky, J.**, Fares, S., Weber, R., Karlik, J., & Holzinger, R. (2013). Eddy covariance emission and deposition flux measurements using proton transfer reaction – time of flight – mass spectrometry (PTR-TOF-MS): comparison with PTR-MS measured vertical gradients and fluxes. *Atmospheric Chemistry and Physics*, *13*, 1439–1456, doi: 10.5194/acp-13-1439-2013.

Holzinger, R., Goldstein, A. H., Hayes, P. L., Jimenez, J. L., & **Timkovsky, J.** (2013). Chemical evolution of organic aerosol in Los Angeles during the CalNex 2010 study. *Atmospheric Chemistry and Physics*, *13*, 10125–10141, doi:10.5194/acp-13-10125-2013.

Park, J.-H., Goldstein, A. H., **Timkovsky, J.**, Fares, S., Weber, R., Karlik, J., & Holzinger, R. (2013). Active atmosphere-ecosystem exchange of the vast majority of detected volatile organic compounds. *Science*, *341*, 643–7, doi:10.1126/science.1235053.

# Acknowledgements

Now I would like to give my many thanks to my colleagues, family and friends.

First, I would like, of course, to thank my daily supervisor Rupert Holzinger. Rupert, thank you very much for your time and help. It was always possible to just step by your office and get your valuable advice or help. I appreciate it very much. I am also very thankful to you for giving me a possibility to work on various interesting projects including the field campaigns in cool locations! Next, I wanna thank Thomas for his always valuable and sharp input and comments on my presentations and articles. I also wanna thank Uli for her valuable input and comments on my research. Of course, I wanna thank Paulien for our collaboration during which I learnt a lot about teamwork.

I wanna thank my office mates Ivan, Sylvia, Adriaan, Carlos, Markella, Melchior, Anwar and Marco. It's been nice and fun to share the office with you and I think we learnt some good stuff from each other. Even though now it's the time to say goodbye to a well-known sleeping bag, I hope new tradition will appear in the office ☺. Adriaan, I keep good memories of push-ups in the office. A tradition 'woord van de dag', which appeared in our office, helped me to learn better dutch and in general I am very grateful to my dutch colleagues who patiently were helping me to improve my dutch!

I am also very grateful and pleased to have worked in such a nice group of scientists and would like to thank my colleagues and friends: Sony, Elena, Célia, Narcisa, Guillaume, Magdalena, Dorota, Marion, Arjan, Sudhanshu, Abhijit, Bia, Sourish, Elena J., Laura, Thijs, Mark, Dewi, Abdel, Lisa, and many others. It's been a lot of fun hanging out with you, discussing various interesting issues, sporting, having nice parties, BBQs and outdoor activities. If I needed any help, it was always possible to ask you. Thank you for this, I appreciate it very much. Ik wil hartelijk Carina, Yvonne en Sandra danken wie altijd heel behulpzaam zijn. Michel, Henk en Carina, hartelijk dank voor de hulp in het lab! I am also very grateful to the scientists from other laboratories and countries for our fruitful collaboration: Ronald Pierik, Bas Henzing, Jeong-Hoo Park, Allen Goldstein, Arthur Chan, and many others.

Дорогие мама и папа! Спасибо вам большое за то сколько сил, тепла и мудрости вы в меня вложили. Низкий вам поклон. Конечно, я бы не достиг всего этого если бы не вы! Солнышко, я не буду здесь много писать. Ты просто сделала мою жизнь прекрасной и наполенной смыслом! Лана и Антон, Игорь, спасибо что вы у меня есть и готовы придти на помощь в трудную минуту! Спасибо семье Лиды за поддержку и внимание.

Спасибо моим русским голландским друзьям Дане и Ире, Мише и Жене, Эдику, Глебу и Даше, Саше и Яне и многим другим за отличное время проведенное вместе, интересные обсуждения, хождение под парусом и, в целом, прекрасный отдых от работы. I am also very grateful to my great international friends: Cata & Adriaan, Alouette & Michal, Christiana & Fanis and many others. It’s been being great having such wonderful friends=family! ☺

## Curriculum Vitae

Joseph Timkovsky was born on July 5, 1987 in Minsk, Belarus. At the age of 13 he became interested in chemistry and, therefore, he entered the Lyceum of Belarusian State University where he studied from 2002 to 2004 in a chemistry class. Studying there and participating at international chemistry Olympiads allowed Joseph to enter Chemistry Department at Moscow State University where he studied from 2004 till 2009. In 2007 Joseph followed a summer internship at Cambridge University, UK when he discovered an area of chemistry which particularly attracted him: atmospheric chemistry. To pursue his interest, he started performing research at the Laboratory of Gas Impurities in the Atmosphere at Obukhov Institute of Atmospheric Physics in Moscow, Russia in fall 2007. To broaden his knowledge in atmospheric chemistry and gain more international experience, Joseph spent his summer 2008 doing an internship at National Oceanic and Atmospheric Administration (NOAA) in Boulder, the US. Joseph wrote his Master thesis at Obukhov Institute of Atmospheric Physics and defended it *cum laude* in 2009. Next, he decided to pursue PhD degree in atmospheric chemistry and, therefore, he joined a group of Atmospheric Physics and Chemistry at Utrecht University, the Netherlands under the supervision of Dr. Rupert Holzinger. Joseph's hobbies include sailing, spending time with friends, reading and sporting.